PHD

The fracture behaviour of PMMA in liquid environments.

Hakeem, M. I.

Award date:
1980

Awarding institution:
University of Bath

THE FRACTURE BEHAVIOUR OF PMMA IN LIQUID ENVIRONMENTS

Submitted by

M. I. HAKEEM

for the degree of Ph.D.
of the University of Bath
1980.

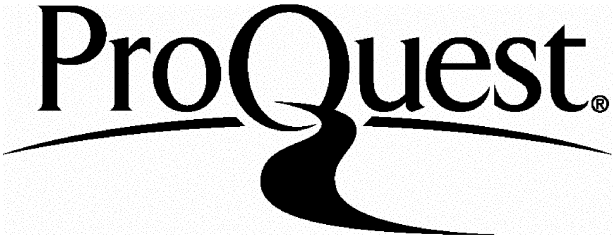

To my Parents, and

Brothers Joseph and Victor.

ACKNOWLEDGEMENTS

I would like to express first and foremost my gratitude to my parents for their support and encouragement during the period of this work for which I am indebted.

I also wish to express my gratitude to Mr. M. G. Phillips for his supervision, help and enthusiasm, without which it would not have been possible to pursue this research.

My thanks also to the School of Materials Science for financing the research, and to Professor Bryan Harris for allowing the use of the School facilities.

I am indebted to all the technical staff for their valuable advice and help in this work, and to Dr. K. A. Edge of the School of Engineering for his contribution to the computational work.

Sincere thanks are also extended to fellow students and colleagues in the School of Materials Science for their help and interest during the course of this work. Lastly, but not least, my thanks must also go to Sally Waldegrave whose patient and efficient typing enables this thesis to be presented.

ABSTRACT

This thesis contains a study which has been conducted using fracture mechanics parameters to describe crack and craze growth behaviour in PMMA under the influence of liquid environment.

The text of this work is divided into two main parts:

Part I has two component chapters; Chapter 1 contains a general introduction to environmental fracture in polymers. Chapter 2 outlines the basis of fracture mechanics concepts used in the analysis of results, and contains a literature review on the failure behaviour of PMMA in dry and wet environment. The survey includes results from dead load tests and monotonically increasing displacement conditions.

Part II contains the work which has been undertaken to investigate the environmental fracture of PMMA. This part is subdivided into four phases.

Phase I describes an effective method which is successfully used to monitor craze growth in PMMA under the influence of dead load and methanol environment. In the same chapter (3) the results together with the discussion are given.

Phase II gives results obtained from crack propagation tests in PMMA in air and liquid environments. These tests are performed under monotonically increasing load-point displacement conditions using

the double torsion technique which is described in Chapter 4. Chapter 5 contains the experimental results and shows that in dry tests, crack propagation is stable with characteristic K_c and crack speed values. To the contrary, tests performed in methanol have developed unstable cracking which is identified with a sequence of rapid jumps.

Phase III follows here where the mechanism which constitutes these jumps is determined. This is done with the aid of the K/v relationship obtained during a crack jump. The linear compliance analysis for the test piece geometry in Chapter 6, together with an experimental technique developed to measure rapid load drops, given in Chapter 7, provide the basis for the measurement of the K/v values.

In Phase IV a mathematical model is proposed in Chapter 8, which successfully identifies the various stages which occur during the fracture of PMMA both dry and in methanol. A thorough fractographic study is carried out in Chapter 9 in support and completion of the model, with further evidence given from acoustic emission results, shown in Chapter 10. As an alternative environmental condition, fracture tests are performed in distilled water and crack propagation results are given in Chapter 11. These have shown similar crack jumping mechanism to that in methanol.

NOTATION

U_e	Elastic strain energy.
U_s	Free surface energy.
A_s	Crack surface area.
σ_f	Fracture stress.
γ	Specific surface energy of the crack surface.
a	Crack length.
E	Young's modulus.
γ_p	Plastic energy.
G	Energy release rate.
G_c	Critical energy release rate (fracture toughness).
C	Specimen compliance.
Q	Characterising force.
P	Applied load.
y	Displacement of the loading points.

K	Stress intensity factor.
θ, r	Polar co-ordinates with the origin at the crack tip.
σ	Applied stress.
Y^2	Finite plate correction factor.
ν	Poisson's ratio.
K_i	Stress intensity at crack initiation.
K_c	Stress intensity for stable propagation.
K_a	Stress intensity at crack arrest.
K_o	Initial stress intensity factor.
$\dot{a}$	Crack speed.
v	Crack front velocity.
σ_y	Yield stress.
w	Thickness of SEN specimen.
b	Width of specimen.

$2L$	Length of span.
Δ_{Total}	Total deflection in specimen.
$\Delta_{no\ crack}$	Deflection in specimen with no crack.
Δ_{crack}	Deflection due to the crack in specimen.
E^*	Reduced modulus.
$V_2\left(\frac{a}{w}\right)$	Geometry factor.
t	Time.
t_o	Initial time.
t_f	Failure time.
x	Craze length.
v_a	Steady state craze growth velocity.
b_c	Crack width.
h	Thickness of double torsion test piece.
ρ	Distance between loading points.

Z	Machine cross-head speed.
ϕ	Crack velocity correction factor.
P_c	Instantaneous load.
P_i	Load initiation.
P_a	Load arrest.
α	Angle of twist.
M	Twisting moment.
A and B	Constants.

CONTENTS

PART 1

LITERATURE REVIEW

CHAPTER 1: INTRODUCTION

CHAPTER 2: PREVIOUS WORK ON CRACK PROPAGATION

CHAPTER 1 INTRODUCTION

1.1 Outline of the project

The main object of this project was to examine the potential of fracture mechanics parameters and test methods in describing the fracture behaviour of a brittle polymer (PMMA) in a hostile liquid environment (Methanol).

The general intention was to apply test method and procedures where crack propagation in a polymer can be monitored under dead-load and monotonically increasing displacement conditions.

In the event, unstable "slip stick" behaviour was observed in PMMA specimens immersed in methanol, a phenomenon unexpected at the time. Since considerable interest has been reported in the literature in the phenomena of crack initiation and arrest under conditions where cracking proceeds by the "stick slip" mode, attention was focussed towards the analysis of what constitutes this jumping behaviour. In the process a technique was developed for measurements of rapid or catastrophic crack propagation.

The project was later extended to cover the effect of distilled water on PMMA cracking behaviour.

1.2 Environmental fracture in polymers

1.2.1 General characteristics of environmental fracture

In engineering it is now recognised that fracture strengths in materials are considerably lower than predicted theoretically, due to flaws or microcracks acting as stress raisers in a loaded specimen. These stress-cracks, whether internal or external, are usually caused by tensile stress less than the short-time mechanical strength of the material (1), and their initiation may be hastened in the presence of a suitable environment. Such an environmental attack in polymers can be divided into two main categories:-

(a) Environmental stress-cracking (E.S.C.): This is a purely physical phenomenon where the environment plays no chemical part and does not physically change the polymer material beyond the development of macroscopically brittle-appearing cracks initiated on the polymer surface. When failure occurs in the polymer, the brittle fracture surface has distinctive pattern of ribs and hackles (2), reminiscent of fracture surface in glass (3).

Principal variables which effect E.S.C. behaviour are molecular weight, molecular weight distribution, crystallinity, and the chemical nature, viscosity, surface tension properties of the environmental cracking agents. Published work on E.S.C. in polyolefins and the influence of these variables can be found in a good review by Howard (4).

(b) Stress or solvent crazing phenomena: The ability of certain liquids to penetrate a brittle polymer causes swelling and hence a softening effect. When the softened material is stressed, flaws or crazes are formed and consequently the polymeric material fails under a stress level lower than its normal strength. This is known as solvent crazing and usually occurs in amorphous thermoplastics such as PMMA and polycarbonate.

Its major influencing variables appear to be much the same as for environmental stress cracking except for a different relative order of importance. Here the stress level and solvent power assume a greater significance than the influence of molecular weight, molecular weight distribution and crystallinity.

1.2.2 Previous work on environmental fracture in brittle polymers

Environmental attack in glassy polymers such as PMMA causes rapid initiation of microcracks or crazes, which promotes failure of the material.

Early investigations into the nature of these crazes were carried out in dry conditions using flexural tests and the mechanism of stress crazing was considered similar to solvent stress crazing (5). Crazes which appeared in the absence of the environment were shown to be formed under tensile rather than compressive stresses (6). It was also noted that in addition to applied stresses, residual stresses or strains, left during resin and specimen preparation, can cause

crazing (7), and increase the severity when external loads are applied. Beside needing stresses for their initiation, crazes were shown to require sites from which to initiate. Probable factors to initiate sites have been reported by Maxwell and Rahm (8) and by Nielsen (9). Inhomogeneities and flaws or stress concentration such as voids, scratches, impurities or other external defects are often observed to determine craze sites.

Regarding crazes in glassy polymers due to the presence of both stress and solvent, the early studies by Bernier and Kambour (10) were concentrated on chemical factors such as "solubility parameter" which cause the environment to promote cracking or crazing. However, about the same time Andrews and Bevan (11) introduced the fracture mechanics approach to the subject and devised an energy criterion for craze initiation. They used notched specimens immersed in hostile environments such as methanol and ethanol. Under these conditions when a stress was applied crazes were observed to grow consistently from the tip of the notch into the bulk of the material.

Recently a thorough study of craze growth in brittle polymers was carried out using the concepts of fracture mechanics (48). A full discussion is presented in section 2.3.

CHAPTER 2 PREVIOUS WORK ON CRACK PROPAGATION

2.1 Fracture mechanics concepts

2.1.1 The Griffith approach

The fracture strengths of brittle materials are found to be well below their theoretical values which are believed to be in the order of one tenth of the Young's modulus (12). This fall in strength was recognised as early as 1920 by A. A. Griffith (13). Griffith (1921) working on glass as a model for a brittle material, found an appreciable difference between the theoretical tensile strength and the experimental value. His conclusion was that glass is not a perfectly homogeneous material but contains flaws which act as localised stress raisers and cause successive bond breakage. This lead him to propose a theory to predict the tensile strength of these flawed bodies. His basic premise was that unstable fracture would occur if an increment of crack growth resulted in more stored energy being released than is absorbed by the creation of new surface.

i.e. condition for fracture is given by

$$\frac{\partial U_e}{\partial A} \geqslant \frac{\partial U_s}{\partial A_s} \qquad (2.1)$$

where U_e is the elastic strain energy

U_s is the free surface energy

A_s is the crack surface area

This lead him to a critical stress value σ_f for a specimen of unit width containing an elliptical centre crack of length 2a subjected to plane stress loading figure 2.1 given by an equation of the form

$$\sigma_f = \sqrt{\frac{2E\gamma}{\Pi a}} \qquad (2.2)$$

where E = Young's modulus of the material

γ is the specific surface energy of the crack surface

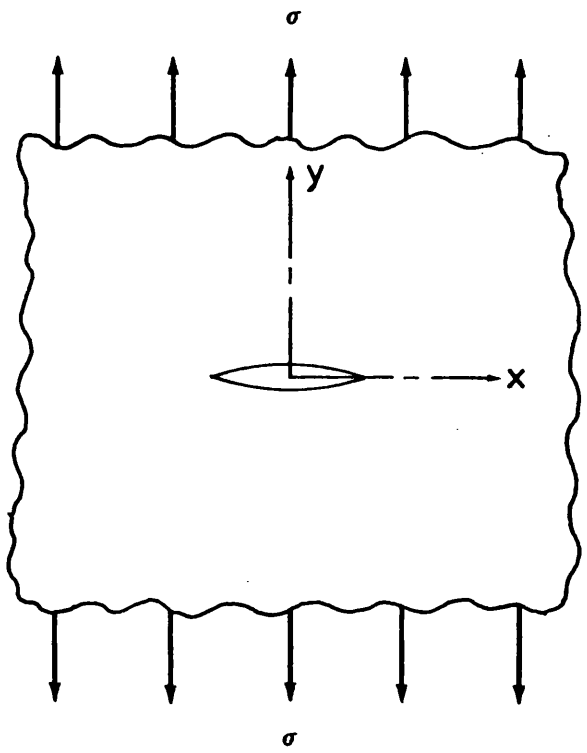

Figure 2.1 Infinite plate with elliptical centre crack

This energy approach has been applied to many brittle materials such as some metals and ceramics. In the early 1960's Berry applied it to the fracture of amorphous glassy polymers, such as PMMA (14) and polystyrene (15). The value of γ was worked out for these materials from fitting equation (2.2) to a plot of σ_f against a or directly from the slope of the plot of σ_f against $a^{-\frac{1}{2}}$, E is determined from a separate experiment.

2.1.2 Application to materials which show plastic deformation

The energy approach as devised by Griffith considers γ to be a surface energy. However γ values measured from fracture experiments for many materials have indicated that other energy-absorbing processes are involved, since these values are much greater than γ values obtained by surface energy measurement. Orowan (16) noted that plastic deformation at the crack tip is the main contributing source and is approximately three orders of magnitude greater than the surface energy. This lead Irwin (17) and Orowan (18) to modify the original Griffith formulae so that plastic deformation prior to failure could be accounted for by the theory. The modified version of equation (2.2) is

$$\sigma_f = \sqrt{\frac{2E\,\gamma_p}{\pi a}} \qquad (2.3)$$

where γ_p is the energy absorbed by plastic deformation in the creation of unit area of fracture surface.

2.1.3 Strain energy release rate as a fracture criterion

Irwin (19) extended the Griffith approach by proposing that the strain energy release rate could be regarded as a force for crack extension. This force, he denoted by G (after Griffith) would have a critical value G_c when a crack starts to propagate

$$\therefore \quad -\frac{\partial U_e}{\partial a} \text{ (for unit width of crack front)} = G$$

and the fracture criterion

$$G = G_c$$

where G_c is known as the fracture toughness.

During fracture two surfaces are formed, hence the relationship between G_c and the surface work can be expressed as

$$G_c = 2\gamma_p$$

as such Irwin (19) considered the new modified Griffith criterion equation (2.3) as a means to evaluate the strain energy release rate at the point of fracture, i.e. G_c, using the expression

$$\sigma_f = \sqrt{\frac{EG_c}{\pi a}} \qquad (2.4)$$

Evaluation of the energy release rate by a different means for different loading conditions and geometries was latter proposed by Irwin and Kies (20). They (21) were the first to note that the strain energy in an elastic body U_e could be presented in the form

$$U_e = \frac{Q^2 C}{2} \qquad (2.5)$$

where Q = characterising force

C = specimen compliance

The compliance C is given by $C = \frac{y}{P}$

P is the load and y the relative displacement of the loading points.

From the above strain energy expression, it immediately follows that the strain energy release rate with respect to crack extension is given by

$$\frac{\partial U_e}{\partial a} = \frac{1}{2} Q^2 \left(\frac{\partial C}{\partial a}\right) \qquad (2.6)$$

Irwin and Kies (20) suggested that measuring the compliance of the specimen with various crack lengths, would lead to the corresponding value of $\frac{\partial C}{\partial a}$. A fracture test could then be interpreted by evaluating $\frac{\partial U_e}{\partial a}$ at fracture using the fracture load and the value of

$\frac{\partial C}{\partial a}$ for the appropriate crack length. On the basis of this result a considerable amount of work was carried out to determine the compliance of various specimen shapes. See for example Day (22) and Srawley et al (23).

2.1.4 Stress intensity factor as a fracture criterion

Irwin (19) (1957) produced an alternative interpretation of fracture phenomena by the introduction of the K concept, known as the stress intensity factor. Using the solution for an elastic sheet with central through thickness crack obtained by Westergaard (24) in 1939, he derived an expression for the stresses in the vicinity of the crack tip of a centrally notched plate of infinite width shown in figure 2.2. This is given as

$$\sigma_{ij} = K (2\Pi r)^{-\frac{1}{2}} f(\theta) \qquad (2.7)$$

where r and θ are polar co-ordinates with an origin at the crack tip, i and j are orthogonal co-ordinates of stress directions, $f(\theta)$ is dependent upon the particular stress component but not on geometry or applied load.

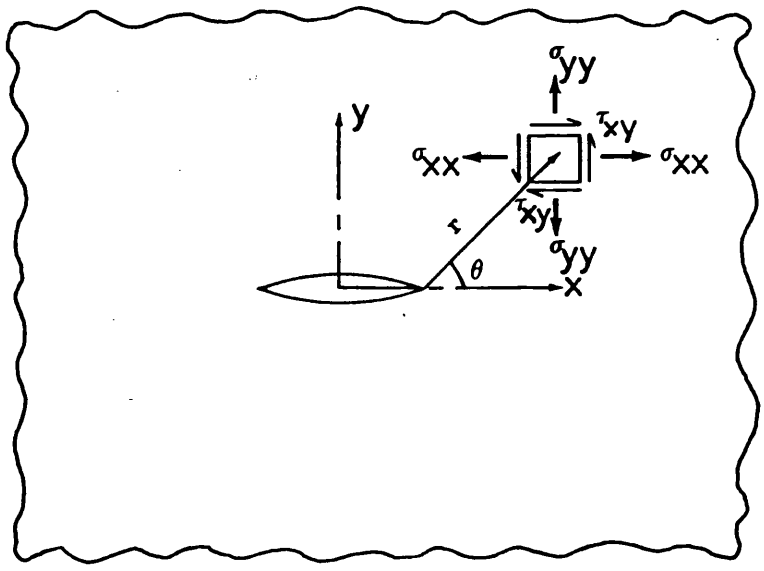

Figure 2.2 Infinite plate with elliptical centre crack (stress intensity criterion)

Modes of failure:

When crack propagation occurs, three modes of failure can be envisaged and these are shown in figure 2.3

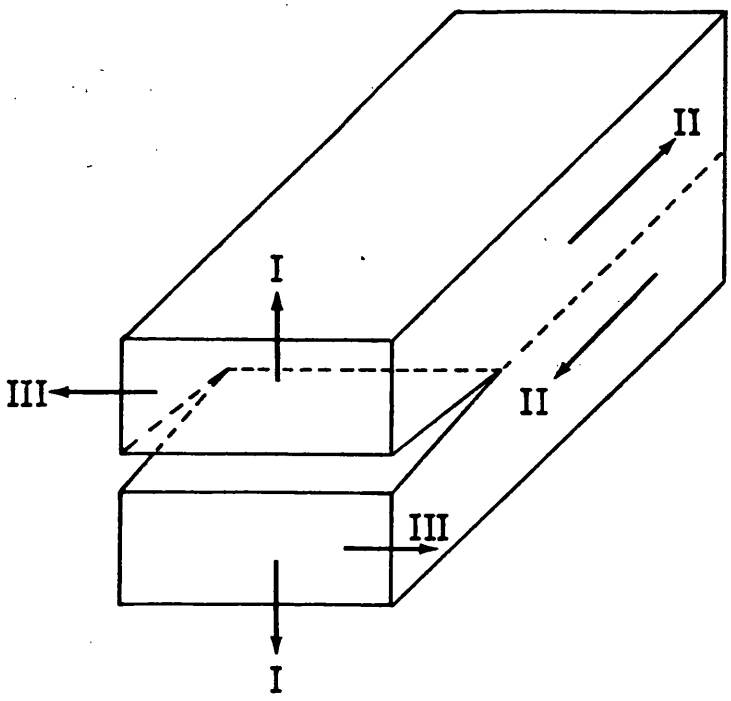

Figure 2.3 Three modes of fracture

Mode I (opening mode) corresponds to the fracture surfaces separating normal to each other.

Mode II (sliding mode) corresponds to mutual shearing of the crack walls in a direction normal to the crack front.

Mode III (tearing mode) corresponds to mutual shearing parallel to the crack front.

With the knowledge of this Irwin presented his results as follows:

Mode I

$$\sigma_{xx} = \frac{K_I}{(2\pi r)^{\frac{1}{2}}} \cos\frac{\theta}{2}\left[1 - \sin\frac{\theta}{2}\sin\frac{3\theta}{2}\right]$$

$$\sigma_{yy} = \frac{K_I}{(2\pi r)^{\frac{1}{2}}} \cos\frac{\theta}{2}\left[1 + \sin\frac{\theta}{2}\sin\frac{3\theta}{2}\right]$$

$$\sigma_{xy} = \frac{K_I}{(2\pi r)^{\frac{1}{2}}} \sin\frac{\theta}{2}\cos\frac{\theta}{2}\cos\frac{3\theta}{2}$$

Mode II

$$\sigma_{xx} = \frac{-K_{II}}{(2\pi r)^{\frac{1}{2}}} \sin\frac{\theta}{2}\left[2 + \cos\frac{\theta}{2}\cos\frac{3\theta}{2}\right]$$

$$\sigma_{yy} = \frac{K_{II}}{(2\pi r)^{\frac{1}{2}}} \sin\frac{\theta}{2}\cos\frac{\theta}{2}\cos\frac{3\theta}{2}$$

$$\sigma_{xy} = \frac{K_{II}}{(2\pi r)^{\frac{1}{2}}} \cos\frac{\theta}{2}\left[1 - \sin\frac{\theta}{2}\sin\frac{3\theta}{2}\right]$$

Mode III

$$\sigma_{zx} = \frac{-K_{III}}{(2\pi r)^{\frac{1}{2}}} \sin\frac{\theta}{2}$$

$$\sigma_{zy} = \frac{K_{III}}{(2\pi r)^{\frac{1}{2}}} \cos\frac{\theta}{2}$$

The constants K are stress intensity factors, defined by the condition that the appropriate stress (σ_{yy} for mode I, σ_{xy} for mode II, σ_{zy} for mode III) ahead of the crack (i.e. $\theta = 0$) is $K\,(2\pi r)^{-\frac{1}{2}}$.

Hence the solution is

$$\sigma_{yy} = K\,(2\pi r)^{-\frac{1}{2}} \qquad (2.8)$$

From the stress distribution analysis ahead of the crack tip (25), figure 2.4, the tensile stress σ_{yy} is given as

$$\sigma_{yy} = \frac{\sigma_{app}}{\left[1-\frac{a^2}{x^2}\right]^{\frac{1}{2}}} = \frac{\sigma_{app}}{\left[\frac{x^2-a^2}{x^2}\right]^{\frac{1}{2}}} \qquad (2.9)$$

where σ_{app} = applied stress

$2a$ = crack length

x = distance from the origin, at the midpoint of the crack.

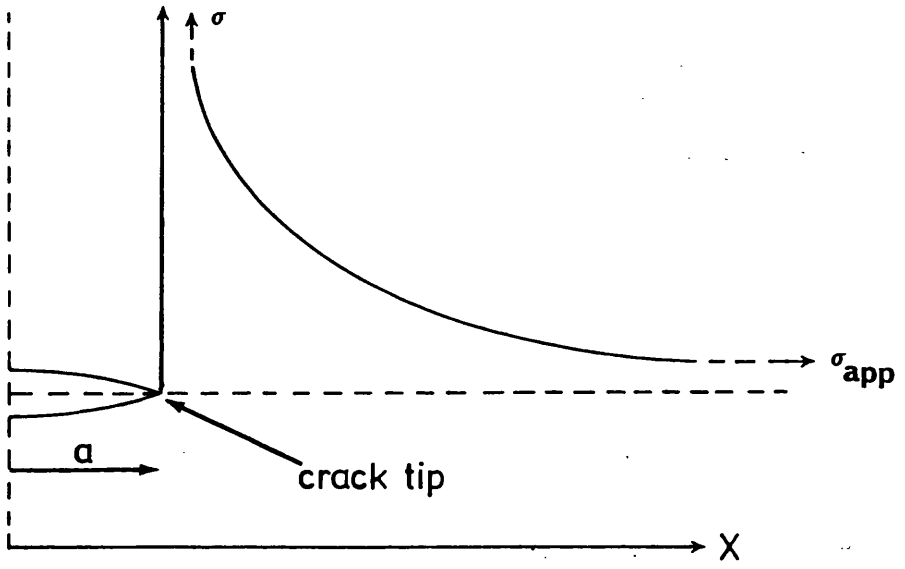

Figure 2.4 Schematic diagram of tensile stress distribution ahead of a sharp, through-thickness crack of length 2a in an infinite body.

To express in terms of r, for comparison with Irwin's equation (2.8) write $x = r + a$.

Therefore equation (2.9) can be expressed as

$$\sigma_{yy} = \frac{\sigma_{app}}{\left[\frac{(r+a)^2-a^2}{(r+a)^2}\right]^{\frac{1}{2}}} = \frac{\sigma_{app}}{\left[\frac{(2a+r)r}{(a+r)^2}\right]^{\frac{1}{2}}} \approx \frac{\sigma_{app}}{\left[\frac{2r}{a}\right]^{\frac{1}{2}}} \qquad (2.10)$$

Inserting the value of σ_{yy} from equation (2.8) in equation (2.10) gives

$$K\,(2\pi r)^{-\frac{1}{2}} = \frac{\sigma_{app}}{\left(\frac{2r}{a}\right)^{\frac{1}{2}}} \qquad (2.11)$$

$$K = \frac{\sigma_{app}\,(2\pi r)^{\frac{1}{2}}}{\left(\frac{2r}{a}\right)^{\frac{1}{2}}}$$

$$K^2 = \sigma_{app}^2\,\pi a \qquad (2.12)$$

where σ is the applied stress and 2a is the crack length.

When specimens of finite width are used, correction factors are introduced to allow for either bending effects or the presence of the free edges. The solution for K is then given by

$$K^2 = \sigma^2 Y^2 a \qquad (2.13)$$

where Y^2 is the finite plate correction factor.

Solutions for Y^2 for various specimen shapes and loading conditions can be found in Paris and Sih (26) (1965) and Brown and Srawley (27) (1966).

2.1.5 Relation between K and G

Irwin (19) noted there was a simple relationship between this factor and his previous concept G, provided that the latter is regarded as elastic energy released per unit extension of the crack thus:-

equation (2.4) gives $\sigma = \sqrt{\frac{EG}{\pi a}}$

and equation (2.12) gives $K^2 = \pi\sigma^2 a$

therefore $K^2 = EG$ for plane stress (2.14)

and $K^2 = \frac{EG}{(1-\nu^2)}$ for plane strain (2.15)

2.1.6 Stability of crack propagation

The Griffith criterion refers to a specimen geometry which fails catastrophically when crack spreading starts and fracture surface energy is inferred from failure stress. In engineering structures appreciable crack growth may precede catastrophic failure, and this growth referred to as "sub-critical", contradicts the strict Griffith failure criterion. Because of its importance, many investigators were concerned with tests and techniques where controlled crack

propagation in brittle polymers could be achieved. Obreimoff (28) (1930) was the first to study such a behaviour. He wedged open a crack in mica, and evaluated the local work of cracking from simple bending theory. Benbow and Roesler (29) (1956) extended Obreimoff's method to deal with high polymers. They spread cracks in glass by indenting the glass with the end of a steel cylinder and evaluated the work from the load to spread the crack and from elasticity theory.

Nowadays the most commonly used test specimens for promoting controlled crack propagation are the double torsion test piece and certain geometries of tapered double cantilever beam specimens. From these techniques "sub-critical" cracking was investigated thoroughly, and a new terminology for the stress intensity factor was introduced.

K_c is now accepted as the stress intensity to promote stable crack propagation at a constant crack velocity v. Whereas K_{Ic} expresses the instability criterion where the crack tip rapidly accelerates, i.e. catastrophic failure. Both K_c and K_{Ic} are dependent on test piece geometry, environment and condition around the crack tip.

The author believes that the above terminology could be misleading since the mode of failure "I" is the same in each case.

From the three modes, Mode I is by far the most pertinent to crack propagation in brittle solids, it gives the most conservative estimate of material strength. Therefore the mode of failure is understood as Mode I and as such

K_i will represent the stress intensity factor at crack initiation

K_c stress intensity for stable crack propagation and

K_a stress intensity at crack arrest.

Broutman and McGarry (30) employing the double cantilever beam test geometry found that crack propagation was usually stable in brittle thermoplastics. In double torsion tests this is shown by a constant speed and load over a length of crack growth (cf figure 5.2(a) page 79 from the present work). However propagation tended to be unstable in thermosets and crack jumping was observed. (Figure 5.6(a) page 87 shows a representative load deflection curve.)

The instability of thermosetting materials e.g. epoxies and polyesters has been investigated thoroughly and was considered to be influenced by the following variables:-

(a) Strain rate (i.e. cross-head speed of the machine) (31, 32, 33).
(b) The amount and type of curing agent and the state of cure (34).
(c) The presence of liquid environment (31, 32).
(d) Temperature of testing (32, 33, 35).

A good review on the subject is given by R. J. Young (36).

As regards thermoplastic material e.g. PMMA, controlled crack propagation tests on dry PMMA have demonstrated that the material

exhibits stable cracking behaviour at cross-head displacement rates which give crack velocities less than 100 mm sec^{-1}. Above this velocity instability sets in (37, 38, 39). On the other hand the introduction of liquid environment to the crack tip leads to unstable crack-propagation at cross-head displacement rates which would otherwise result in stable behaviour (29, 39, 40).

Mai and Atkins (41, 42) pointed out that the criterion of stability depends on two factors: One varies with the type of test-piece and is called the geometric stability factor and the other, which depends upon the material is $\frac{dG}{d\dot{a}}$ which is the rate of change of the fracture toughness with crack velocity. They showed that continuous propagation will take place when $\frac{dG}{d\dot{a}}$ is positive. When it is negative propagation will become unstable even in specimens which should promote stable crack growth. Gledhill et al (35) however argues that the decrease of the specific work of fracture with crack speed i.e. $\frac{dG}{d\dot{a}}$, is not the cause but rather the consequence of "stick-slip" or unstable cracking.

2.2 Previous work on crack propagation in dry PMMA

Since the introduction of the Griffith - Irwin criterion, many attempts have been made to apply it to glassy polymers in order to correlate and explain their fracture behaviour. Many such attempts were performed on the transparent brittle polymer (PMMA) - using the Griffith approach to evaluate the "surface work" γ_p by different test methods. A summary of the published results is given in table 2.5

Table 2.5. Fracture toughness values for PMMA in air (Quoted in reference (43))

Author(s)	Test method	$\dot{a}$ (mm/sec)	$\gamma_p \times 10^2$ (Joules/m^2)	$K_{(I)c}^{(calc)}$ (MN/m$^{3/2}$)
Benbow and Roesler (1957) (29)	PC(c)	$\sim 10^{-2}$	4.9	{1.69}†
Benbow (1961) (105)	CNC(c)	10^{-2}	4.2	{1.56}
Berry (1961) (14)	SEN	Instability	3.0	{1.12}
Berry (1963)(94)	PC	10^{-3}	1.4	(0.76)†
van den Boogaart (1966) (95)	PC	$\sim 10^{-3}$	1.65	(0.83)
Broutman and McGarry (1965) (30)	PC	1.25	1.25	(0.99)
Broutman and Kobayashi (96)	TC	1.25	2.0	(1.26)
Davidge and Tappin (1968) (97)	B	Instability	(3.65)	1.94
Olear and Erdogan (1968) (98)	CN	Instability	(1.39)	1.19
Key, Katz and Parker (1968) (99)	SEN	Instability	(1.15-2.7)	1.09-1.66
Kies (1953) (100)	SEN	Instability	6.15	{1.19}
Svennson (1961) (101)	CNC(c)	$\sim 10^{-2}$	4.5	{1.16}
Vincent and Gotham (1966) (102)	SEN	6.8×10^{-2}		
	PC,I	4.3×10^{1}	1.5-3.4	{0.93-1.61}
Williams, Radon, and	SEN,DEN			
Turner (1968) (1) (38)	B	2.5×10^{-3}**	(2.2-3.5)	1.13-1.43
Williams, Radon, and	SEN,DEN,			
Turner (1968)(2) (38)	B	Instability	(2.11-3.0)	1.48-1.75
Irwin and Kies (1954) (21)	CN	Instability	4.4	{1.6 }
Fujishiro (1971) (103)	PC	$\sim 10^{-2}$	0.923	(0.63)
Higuchi (1965) (104)	DEN	Instability	3.6	{1.7 }

†( ) = Converted value - using "derived" E (via Williams {1972})
{ } = Converted value - using quoted E
** "Apparent" speed
CNC = centre notch cleavage
PC = parallel cleavage
TC = tapered cleavage
SEN = single edge notch
(c) = with compression
CN = centre notched
I = impact
B = bending
DEN = double edge notch.

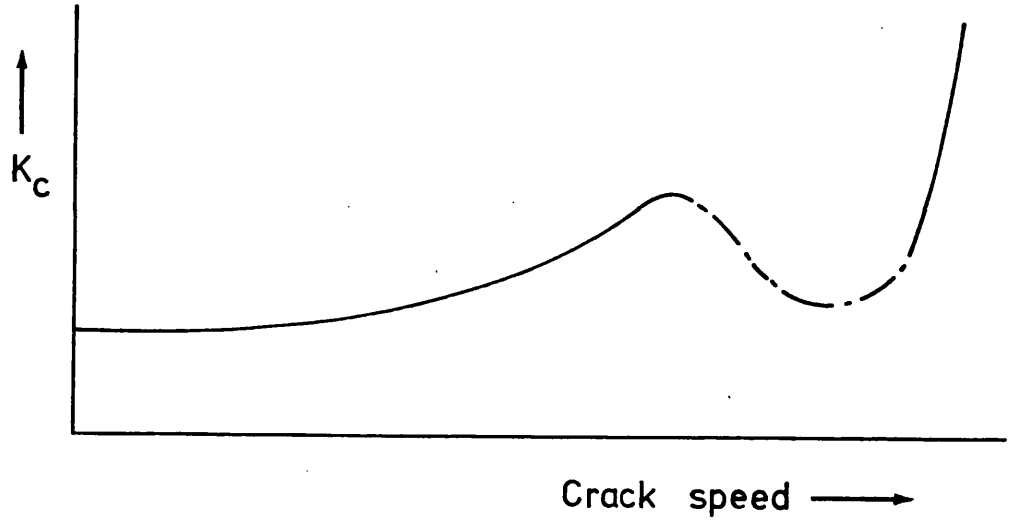

Figure 2.6 Schematic representation of K_c versus crack speed curve - PMMA in air.

taken from the work of Marshall and Williams (43). At first sight, the results appear to be inconsistent. However when they were correlated as a function of crack speed (i.e. K vs v curve), they have been shown to follow a consistent pattern (43).

For PMMA fractured in air, Marshall et al (37) found that the supposed constant value for K_c is in fact dependent on the crack speed and its value rises as the crack speed is increased. Although Marshall's measurements were in the low speed region v < 50 mm/sec, a similar relationship between K_c/crack speed for high speed failure was also found valid by Green (44) and Cotterell (45).

A schematic diagram for PMMA K/v curve is shown in figure 2.6. Such K(v) curves have nowadays been accepted as a means to characterize polymer fracture properties.

2.3 Fracture mecahnics applied to environmental fracture

Crazing in glassy organic polymers is now accepted to be the precursor of fracture. The presence of crazes in the material presents a potential danger because of the possibilities of void coalescence within the craze which can eventually result in crack growth.

Glassy polymers e.g. PMMA, which are brittle and do crack readily in air, grow crazes when subjected to environmental attack. These crazes usually resemble cracks because of the low refractive index

of the structure, and higher magnification microscopy is often necessary to differentiate the two. Crack and craze growth in polymers is of major importance in the exploitation of polymers, and the concepts and parameters of fracture mechanics which have been adopted successfully in the description of crack propagation in PMMA in air were also used to investigate craze growth behaviour in the presence of environment.

The bulk of these studies concentrated on tests where the applied load was kept constant, and will be dealt with first, later however conditions of monotonically increasing load (or displacement) which are also relevant to this research will be looked into.

2.3.1 Dead load tests. Results.

Early investigators concerned with the environmental mechanism, proposed that craze initiation was based on a critical stress (46) and a critcal strain (10) criterion. Hence craze growth in polymers under the combined influence of stress and solvents was reported to be stress dependent (46). This proved to be inconsistent and when the fracture mechanics concepts were introduced instead, to describe craze initiation phenomena, the following were reported.

Craze initiation and growth:

Methanol crazes initiating from the crack tip in polymer samples were dependent on the initial stress intensity factor K (48, 49) and have two distinct types of growth behaviour, one leading to craze arrest

and the other to final fracture depending on the magnitude of K_o (48, 49, 50). In the former the craze growth rate decreased until the craze came to arrest, whereas in the latter case the growth rate initially decreased but then eventually became constant.

Fluid flow into a craze:

The flow mechanism of the environment into a craze at the crack tip has been postulated to influence craze growth behaviour (49). Marshall et al (48) and Kramer et al (49) proposed models for fluid flow in the craze to predict growth kinetics. These models were based upon two types of fluid flow behaviour, restricted (end flow) and unrestricted (side flow) and tests were designed to demonstrate them.

In the unrestricted tests, specimens were immersed entirely in the methanol, whereas for restricted flow, specimen sides were sealed with grease, and the craze fed with methanol, only through the crack. Williams et al (51) in their model have shown that initial growth at high stress intensity values was controlled by hydrodynamic transport of liquid through the porous craze to the craze tip, while at low K values growth was controlled by the relaxation of the stress in the craze fibrils. A similar model for the latter case has been proposed by Veheulpen et al (52) for craze growth in air. It was also suggested by Marshall et al (48) that the driving force for flow in the craze is atmospheric pressure. Kambour (53), however, argues that both fibrils and voids in the craze have small diameters and therefore one would expect flow to be driven by capillarity.

This was supported by Kramer et al (49) and a new model for hydrodynamic flow in the craze was presented.

Cessation of craze growth:

The tendency for crazes to cease at the lower values of stress intensity K_o for dead load type experiments was the concern of many research workers and various criteria for this feature have been proposed. Kambour (53) has suggested that craze growth ceases because the polymer becomes oriented by the competing process of plastic shear flow ahead of the craze. Graham et al (54) have advanced the hypothesis that the craze stops when it reaches a certain length "x" predicted by the Dugdale model (55). The Dugdale model envisages a flat elliptical hole in an infinite plate, subjected at infinity to a tensile stress normal to the plane of the crack. At the crack tips a yielded zone of the length "x" is of such a length that the stress at the end of it is finite, figure 2.7.

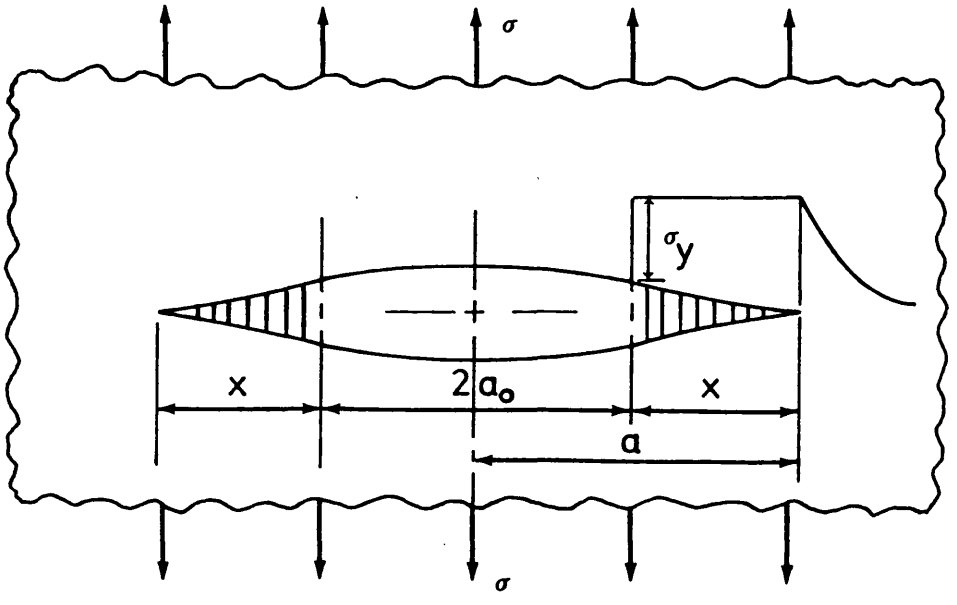

Figure 2.7 Dugdale model at the crack tip.

For a plate with a central crack of length 2a, Dugdale's model gives the zone size "x" as

$$x = a_o \left[\sec (\pi\sigma/2\sigma_y) - 1 \right] \qquad (2.16)$$

$$\text{or } \frac{a_o}{a} = \frac{2}{\pi} \cos^{-1}\left(\frac{\sigma}{\sigma_y}\right) \qquad (2.17)$$

Andrews and Bevan (56) have proposed that growth ceases when the strain energy release rate of the craze falls below a critical value, the minimum plastic work and surface energy that must be supplied to generate a craze.

The proposals of Graham et al (54) and Andrews et al (56) were both dismissed by Kramer et al (57) who observed that

(1) the strain energy release rate for a craze increased with increasing craze length, an increase which they have attributed to the work done behind the craze tip, for example, in the deformation of fibrils extending across the craze from one surface to the other;

(2) the stresses in the craze are not approaching the constant value expected from the Dugdale model. They later proposed in another publication (49), that the solvent craze is preceded by a short length of dry craze, and the craze stops when the fibril volume fraction in the solvent section becomes so large that fluid transport through this zone becomes negligible.

2.3.2. Monotonically increasing loads. Test Results.

Environmental fracture of PMMA under monotonically increasing load (or displacement) was rarely reported in the literature except for the published work by Mai (40), who adopted the method in an attempt to determine K(v) curves in presence of liquid environments. However, the results showed that the presence of liquid, e.g. carbon-tetrachloride at the crack tip caused immediate crack arrest and the fracture load increased followed by instability. This made it difficult to assess the fracture toughness of the material and measure its corresponding propagation velocity.

Mai, concerned to achieve continuous cracking, used specimens and techniques which promote stable cracking in monotonically increasing displacement experiments (40). From these tests he reported that the fracture toughness in an environment compared to that in air, is a function of crack velocity as illustrated in figure 2.8. In the low velocity range ($a < 10^{-5}$m sec^{-1}) the fracture toughness in a liquid is lower than in air, whereas in the high crack speed range ($a > 10^{-5}$m sec^{-1}) the fracture toughness is greater than in air. The explanation given was that in the former case, the crack grows with the solvent induced craze structure and thus needs less energy for its propagation, while in the latter additional work other than that necessary for cracking unit area of material is required to rupture and regenerate craze cavities near the affected crack tip region. This suggests that the environmental mechanisms in the last case is a strengthening rather than a weakening effect.

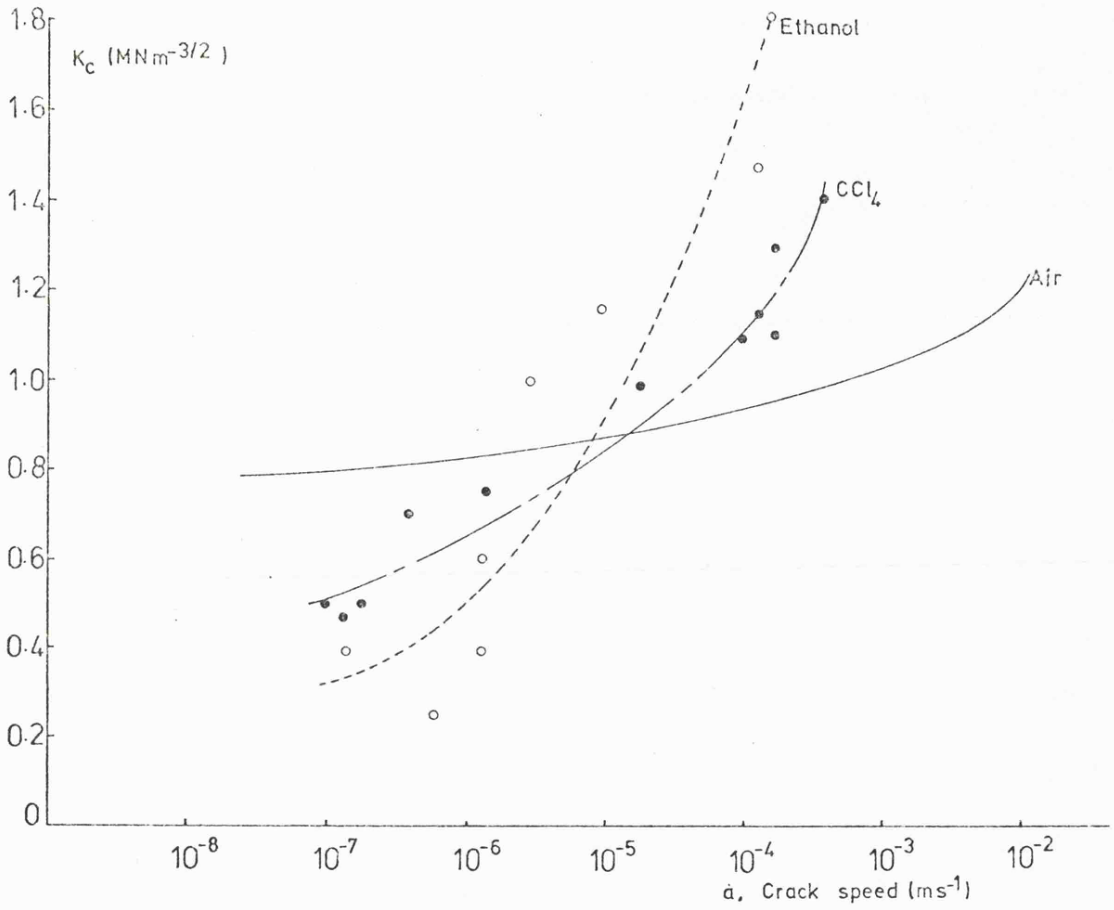

Figure 2·8 Variation of fracture toughness with crack speed in air, ethanol and carbon tetrachloride (after reference 40)

2.4 Summary

Environmental cracking of rigid polymers such as PMMA, proceeds by initiation and growth of a craze-like zone of cavitation which breaks down to form a crack. The fracture mechanics successfully used in studying crack growth in dry conditions, provided a useful frame work for interpreting and systematising the results of environmental crack growth studies.

In dry conditions for PMMA, fracture tests were performed by assuming the existence of a critical stress intensity factor $K_c(\dot{a})$, or equivalently a value of fracture toughness $G_c(\dot{a}) = \frac{K^2_c(\dot{a})}{E}$ that is an increasing function of crack velocity $\dot{a}$.

Experimental values of K_c were plotted as a function of $\log_{10} \dot{a}$ with the intention that a unique curve should be obtained regardless of specimen geometry or the initial crack length or loading. By integrating this curve, time-to-failure for the material could be predicted. The result is shown in figure 2.6. The curve is nearly horizontal at low crack growth rates, indicating that for a practical purpose there is a threshold K below which measureable slow crack growth does not occur.

With the introduction of liquid environment to PMMA, the effect on the threshold K seemed to vary with the type of loading conditions (K here is the stress intensity for craze growth).

Under dead-load conditions, samples of PMMA in the presence of liquid environment have shown a fall in strength with a lower K value than in air. This was explained by the diffusion of liquid into the craze, effectively plasticizing the fibrils. The depression of glass transition temperature Tg in the fibrils enhances the drawing of craze fibrils from the craze surface as well as producing increased fibril rupture. As a result rapid failure occurs.

Contrary to the above, environmental fracture tests in PMMA performed under monotonically increasing load have shown a strengthening effect. Larger K was required to produce a high å than is required in air as is shown in figure 2.8. Probably at higher values of K bundles of crazes are formed at the crack tip which do not form to the same extent in air due to the incubation time for air craze nucleation. These crazes cause bluntness of the crack tip. Indeed it was reported by Mai (40) that K_{Ic}, the K value for unstable (and very rapid) crack propagation is reached in the presence of a blunt crack and is usually larger in various liquid environments than in air.

With these two environment mechanisms in mind, the author set up an investigation to study these crazes and cracks with particular reference to factors which could influence their growth behaviour. This was performed as follows :

In constant load conditions, previous results were to be corroborated using an independent technique to those reported in the literature for monitoring craze growth.

A thorough examination of environmental fracture under monotonically increasing displacement was to be carried out with particular attention focussed on the observed instability behaviour and its after effects.

Later however it became apparent that PMMA double torsion test-pieces shaped to promote stable crack propagation, if immersed in methanol would give consistent jumping behaviour. The study was then extended to include the cause and mechanism of these jumps, aided by K_c and å measurements made during the jump. Since fracture surfaces provide vital information about the nature and mechanism of failure, a thorough study was to be carried out on the surfaces produced by the two loading conditions.

PART II

EXPERIMENTAL PROGRAMME

PHASE I

CHAPTER 3: DEAD LOAD TESTS

EXPERIMENTAL PROGRAMME

Dead load tests were performed in an attempt to find a correlation between failure time and applied stress intensity factor derived from the applied load and specimen dimensions. The results were to cover dry and immersed samples.

Single-edge-notched specimens (SEN) were preferred because the methanol crazes grew consistently from the tips of the starter cracks. Following the work of Marshall, subcritical crack propagation was observed in methanol tests, hence attempts were made to find a (K,v) relationship for PMMA in methanol using an improved technique where v is determined directly from measurements of load-point displacement rate.

Double torsion tests were performed to investigate the fracture behaviour of PMMA both dry and immersed, under monotonically increasing displacement rate conditions (these tests will be described by the term "Instron type").

Once again the aim was to obtain (K,v) curves. The double torsion specimens were used in preference to SEN, as they are geometrically more stable.

PHASE I

CHAPTER 3 DEAD LOAD TESTS

3.1 Bend tests. Three point loading.

3.1.1 Apparatus

A diagram of the loading apparatus is shown in figure 3.1. A rectangular SEN specimen was mounted on two rigid round supports and loaded using a single lever arm which provided a load multiplication factor of 5. To ensure vertical loading, a semiellipse was milled on the lever arm and rested on a sharp wedge machined on the top of the loading pin which also had a V wedge on its lower end (see side diagram).

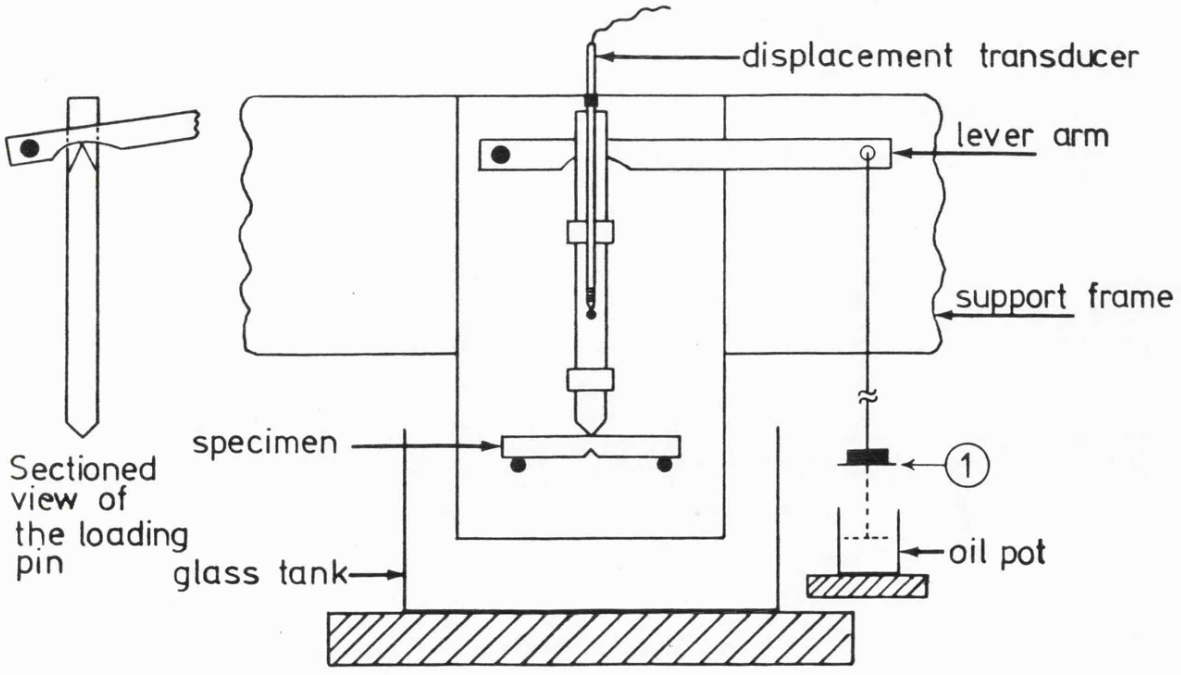

Figure 3.1 Three-point loading technique

The dead load was maintained throughout a test, and for environmental tests, specimens were surrounded by glass tanks containing the liquid environment.

To perform multiple tests, five such rigs were used, and were mounted inside an environmental cabinet for temperature control. The top pan (1) shown in the diagram held the applied load while the bottom one shown as dotted lines was immersed in an oil pot acting as a damper to prevent disturbances in the system when fracture occurred in one sample. Initially dial gauges were used to measure the deflection in the centre of the specimens at time intervals. However this proved ineffective since continuous monitoring of crack growth was required. Consequently displacement transducers were used instead. The outputs from the transducers were passed to a data logger, where all necessary information of deflection as a function of time was automatically monitored and collected on a punched tape. The processing of this information to derive plots of crack length as a function of time is discussed later. A number of samples were tested over a range of load values which was chosen such that the upper limit was to give immediate failure (see section 3.2.1).

Calibration of the applied load:

This was necessary since the weight of the lever and hanger as well as friction between metal joints must be considered in the determination of precise applied load.

A strain gauge load cell (Tycho type JP 250) was mounted vertically under the pin and weights were added on the pan. The force exerted on the load cell was measured from the cell output voltage. Using a procedure of progressively loading and then unloading, a calibration curve of actual force applied versus the weight hung on the lever arm was obtained (figure 3.2).

This shows a linear relationship with an intercept of ≃ 3N on the y-axis, which is the force exerted by the weight of both lever arm and hanger.

Calibration of the displacement transducers:

Sangamo transducers of type A.G were used. These were internally calibrated and have a linear stroke displacement of ± 2.5 mm. Using a rig with a fixed micrometer their linearity was re-checked. A linear curve of transducer voltage output versus micrometer displacement was obtained (figure 3.3).

3.1.2 Specimen preparation and dimensions

Specimens of the dimensions 50mm x 6mm x 6mm, were cut from clear acrylic sheet. They were notched and pre-cracked to produce cracks the lengths of which were within the range (0.45-0.55)W (figure 3.4).

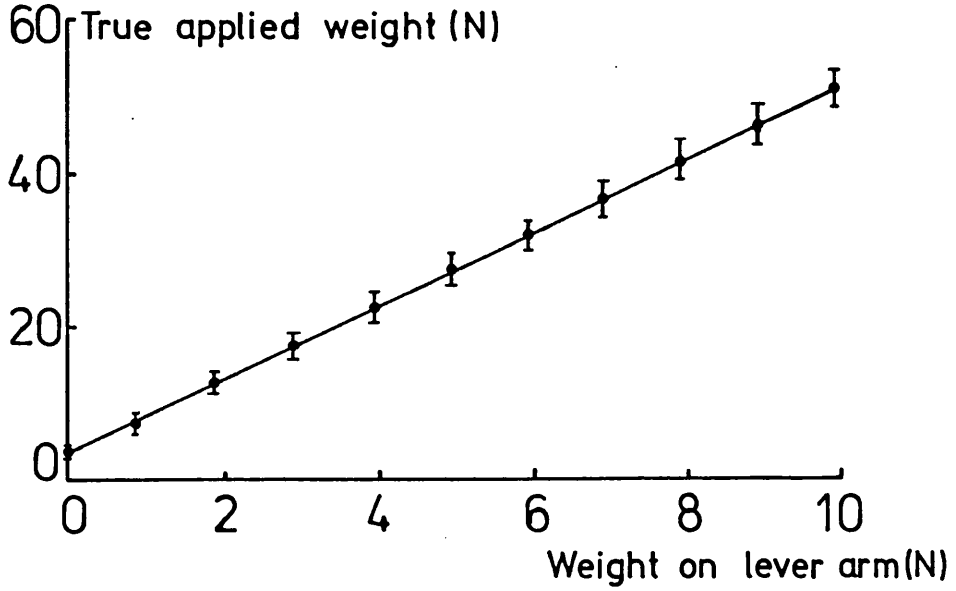

Figure 3.2 Calibration curve (True force exerted on a specimen vs weight hung on lever arm).

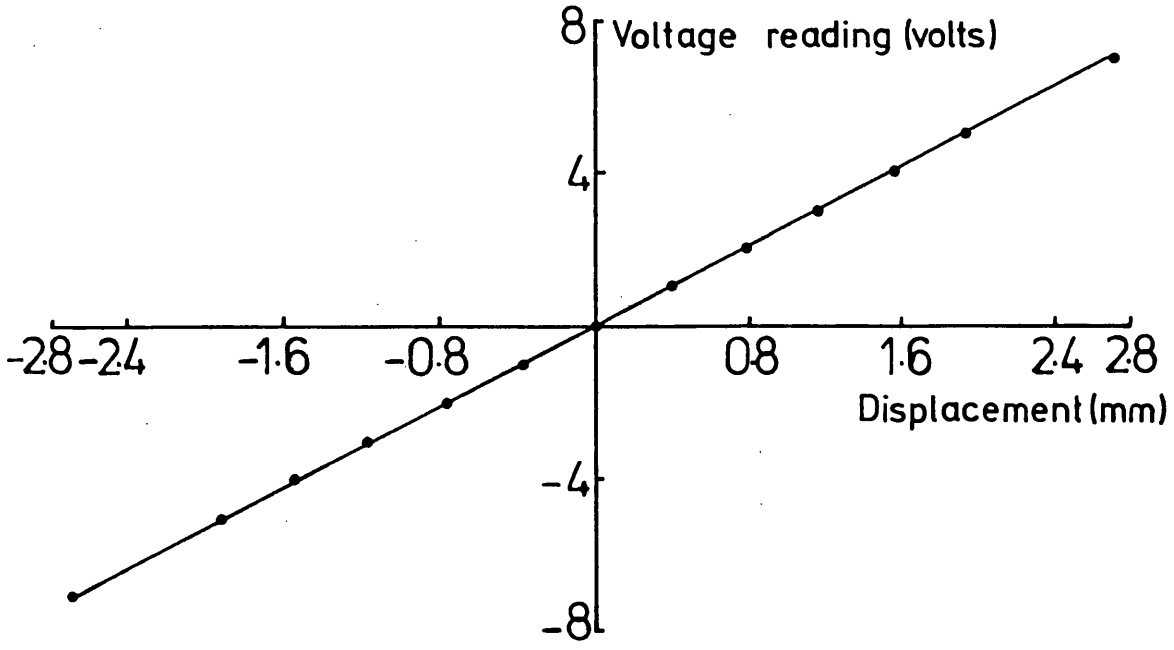

Figure 3.3 Calibration curve (Transducer voltage output vs micrometer displacement).

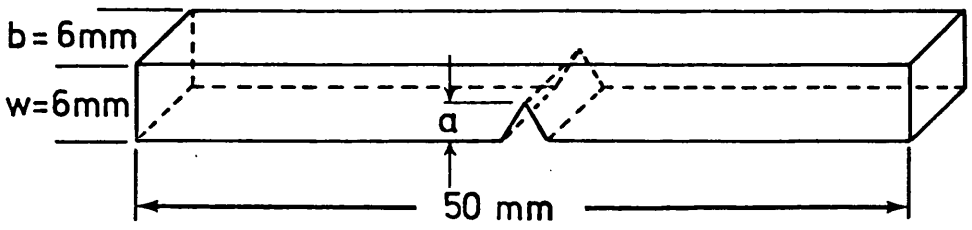

Figure 3.4 SEN specimen geometry

The sharp cracks were introduced in the specimens using the technique developed by Marshall et al (37). Initially a vee notch was milled in the specimen to control the initiation of the sharp crack. Then a Stanley blade fitted to the Vickers hardness machine via an adaptor was pressed into the notch root of the sample held in a vice on the machine table. A natural starter crack was thus formed ahead of the blade.

3.1.3 Choice of material and environments

PMMA was chosen as the test material because considerable knowledge of its behaviour in various conditions had been reported previously (37, 38, 58). It is a brittle polymer where the concepts of fracture mechanics can be applied successfully, also it is a transparent material and crack propagation can be easily monitored.

Material conditioning:

Samples were used in the as-received condition. Pre-conditioning such as annealing was found not to be required since the prepared samples under polarized light showed no appreciable internal stresses. Also a control test was performed where under the same conditions, an annealed specimen showed no difference in fracture behaviour with a non-annealed one.

Methanol was chosen initially as the most suitable environment since it does not severely craze the PMMA surface. However, the fracture behaviour of PMMA in distilled water was also investigated.

3.1.4 Analysis for crack propagation measurement

Using an analysis developed from the results of Tada et al (59), displacement measurements made on the SEN specimens during dead load tests, were used to monitor crack propagation.

This section deals with this analysis and gives the general outline to a computer program designed to process the data.

Analysis:

Consider a SEN specimen under 3-point loading, this is shown in figure 3.5.

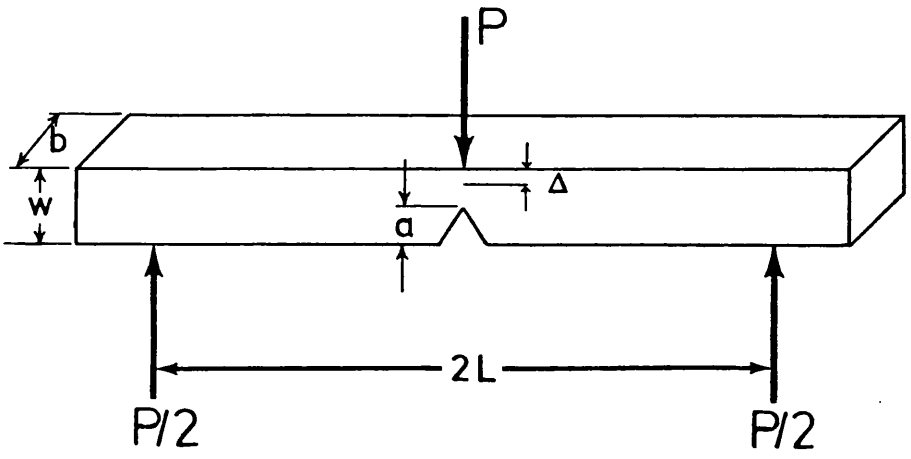

Figure 3.5 SEN specimen under three-point loading.

Reference (59) defines the additional load point displacement due to a crack as follows:

$$\Delta_{Total} = \Delta_{crack} + \Delta_{no\ crack} \qquad (3.1)$$

where Δ_{Total} = Total deflection in specimen

$\Delta_{no\ crack}$ = Deflection with no crack in specimen

Δ_{crack} = Deflection due to the crack in specimen

From the beam theory

$$\Delta_{no\ crack} = \frac{P(2L)^3}{4Ebw^3} \qquad (3.2)$$

where P = applied load

w = specimen thickness

b = specimen width

E = modulus of material

2L = span length

Hence $\Delta_{no\ crack}$ can be determined from the experimental conditions.

Δ_{Total} is measured as a function of time during the experiment. Therefore equation (3.1) gives Δ_{crack} as a function of time. To express crack length as a function of time, we make use of the relationship given in reference (59) where

$$\Delta_{crack} = \frac{\sigma}{E^*} (2L) V_2\left(\frac{a}{w}\right) \qquad (3.3)$$

where $E^* = E$ plane stress

$= \frac{E}{(1-\nu^2)}$ plane strain

The stress $\sigma = \frac{3}{2} \frac{P(2L)}{bw^2}$ for 3-point loading (3.4)

and $V_2\left(\frac{a}{w}\right)$, a geometry factor, is a polynomial in the "reduced crack length" $\left(\frac{a}{w}\right)$.

Eliminating Δ_{crack} between (3.1) and (3.3)

$$\frac{\sigma}{E^*} (2L) V_2\left(\frac{a}{w}\right) = (\Delta_{Total} - \Delta_{no\ crack}) \qquad (3.5)$$

rearranging:

$$V_2\left(\frac{a}{w}\right) = \frac{E^*}{\sigma(2L)} (\Delta_{Total} - \Delta_{no\ crack}) \qquad (3.6)$$

reference (59) gives the following empirical formula to evaluate $V_2\left(\frac{a}{w}\right)$

$$V_2\left(\frac{a}{w}\right) = \left[\frac{(a/w)}{1-(a/w)}\right]^2 \left[5.58 - 19.57\left(\frac{a}{w}\right) + 36.82\left(\frac{a}{w}\right)^2 - 34.94\left(\frac{a}{w}\right)^3 + 12.77\left(\frac{a}{w}\right)^4\right] \qquad (3.7)$$

This formula has better than 1% accuracy for any $\left(\frac{a}{w}\right)$ for $\frac{2L}{w} = 4$.

Having determined $V_2\left(\frac{a}{w}\right)$ by measurement it is possible in principle to solve the polynomial equation (3.7) for $\left(\frac{a}{w}\right)$ and hence determine the crack length. In practice this was done numerically by creating a look-up table.

Using equation (3.6) and (3.7), a program was designed to evaluate the crack length "a" from the specimen deflection at any time "t".

The flow diagram shown in Figure 3.6 outlines the main procedure of one test:-

Values of $\left(\frac{a}{w}\right)$ at intervals of 0.02 substituted in equation (3.7) produced equivalent values of $V_2\left(\frac{a}{w}\right)$. Both $\left(\frac{a}{w}\right)$ and $V_2\left(\frac{a}{w}\right)$ were stored in block 2 in the diagram.

In block 1 the following were stored:-

(a) $\Delta_{\text{no crack}}$ evaluated from equation (3.2).

(b) $\frac{E^*}{\sigma(2L)}$ using equation (3.4) for the σ value.

(c) w the specimen thickness.

(d) Values of Δ_{Total} and time read from the experimental punched tape.

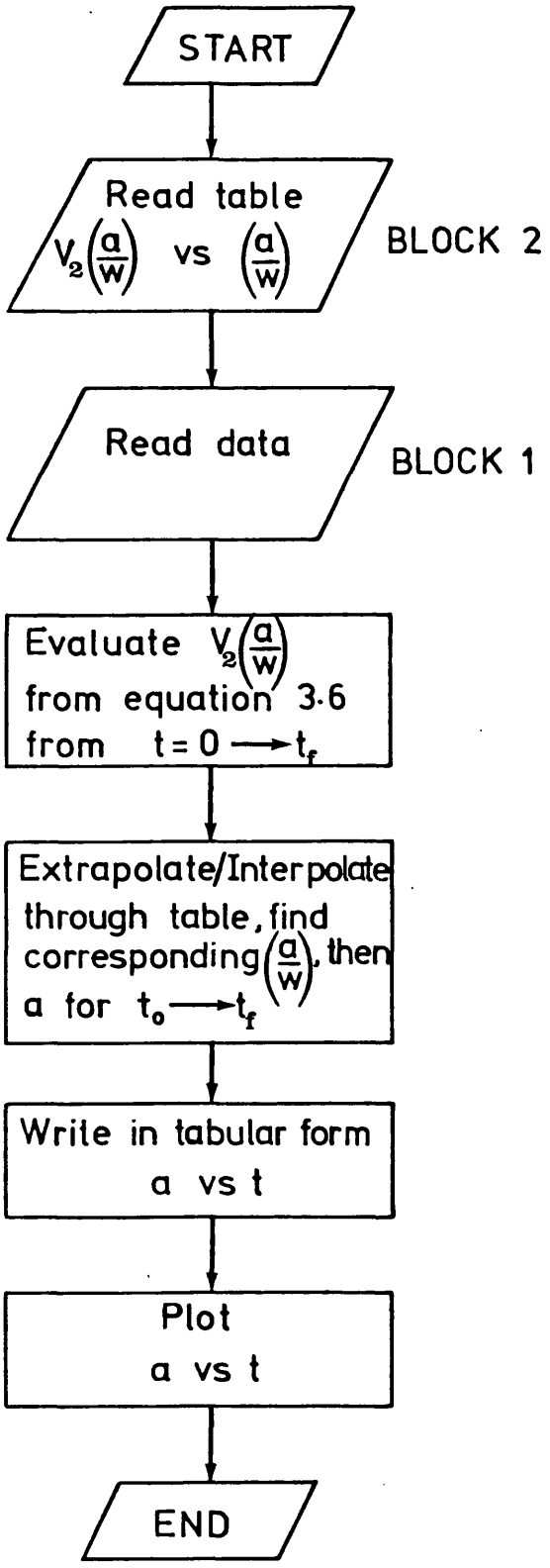

Figure 3.6 Flow diagram to evaluate crack length in SEN specimen from displacement measurement .

The values of Δ_{Total} substituted in equation (3.6) with the corresponding constants $\Delta_{no\ crack}$ and $\frac{E^*}{\sigma(2L)}$, produced equivalent values for $V_2\left(\frac{a}{w}\right)$ at times $t_o \longrightarrow t_f$

t_o = starting time

t_f = failure time

These $V_2\left(\frac{a}{w}\right)$ values were referred to the look-up table in block 2 and the nearest corresponding $\left(\frac{a}{w}\right)$ values were found for $t_o \longrightarrow t_f$. Using the value of w, the corresponding values of crack length "a" vs time "t" were also obtained.

Finally a plot routine operated and a graph of crack length against the time was the end product. These are shown in Section 3.3. The program is capable of handling up to five tests performed at the same time.

3.2 Fracture of PMMA - in Air

3.2.1 Experimental

The load required to give immediate fracture for samples and test conditions employed was found by performing 3-point bend tests in a universal testing machine. This was 7.5 kg f corresponding to K_o = 1.45 $MNm^{-\frac{3}{2}}$, which represented the upper value used for the dead load tests. The experimental procedure consisted of (1) mounting the samples (2) adjusting the transducer to zero followed by (3) load application.

3.2.2 Results and Discussion

SEN specimens tested in air under the above conditions failed to provide crack growth results. At the upper value of K_o (1.45 $MNm^{-\frac{3}{2}}$), samples in air showed immediate failure, whereas at lower values of K_o in the order of 1.0 $MNm^{-\frac{3}{2}}$ or less, specimens were able to withstand the load for days without crack growth. Crack propagation if and when it occurred was unstable in that the crack accelerated continuously to failure, running out of the material almost instantly. A mechanism identical to the one at high K_o. Consequently the crack velocity was found to be extremely difficult to measure. Because of this problem the SEN geometry was abandoned for the dry tests and the double torsion technique was later considered and applied.

Under the combined action of the stress and liquid environment, glassy polymers e.g. PMMA were known from the literature to initiate

silvery like cracks known as crazes. These crazes in SEN specimens were reported to grow inward from the surfaces of the polymer in a stable manner such that measurement of the variation of craze length with time was possible. Therefore it was appropriate here to adopt the system of deflection measurements in studying and identifying the growth behaviour of these crazes.

3.3 Fracture of PMMA - in Methanol

3.3.1 Experimental

SEN specimens immersed in methanol in glass tanks were loaded under dead load conditions figure 3.1. Crazes initiated from the tip of the induced crack and their growth was monitored by following the deflection in the centre of the specimen under a specified load. Tests were performed at room temperature ≃ 293K on a number of samples over a range of load values (11 — 52.5)N, corresponding to values of initial stress intensity factor K_o in the range 0.22 $MNm^{-\frac{3}{2}}$ to 1.11 $MNm^{-\frac{3}{2}}$.

K_o is calculated by using the initial crack length in conjunction with the stress intensity expression derived by Brown and Srawley (27) for SEN specimen, using boundary collocation method. The equation is given as

$$K = \frac{3P(2L)}{2b\, w^{3/2}} \left[1.93\left(\frac{a}{w}\right)^{\frac{1}{2}} - 3.07\left(\frac{a}{w}\right)^{3/2} + 14.53\left(\frac{a}{w}\right)^{5/2} - 25.11\left(\frac{a}{w}\right)^{7/2} + 25.80\left(\frac{a}{w}\right)^{9/2}\right] \qquad (3.8)$$

where a = crack length

$2L$ = length of span

P = applied load

3.3.2 Results and Discussion

Craze initiation and growth:

Under dead load conditions, methanol crazes grown on SEN specimens were followed through the specimen deflections. These deflection measurements were monitored by a data logger and analysed with the aid of a computer program. Plots of craze length versus time over a range of K_o values were obtained. These were studied and the growth pattern observed showed two distinct types, both functions of the initial stress intensity factor.

An output example from the computer illustrating the type of growth is shown in figures 3.7 and 3.8.

Figure 3.7 shows growth which occurs at K_o values > 0.46 $MNm^{-\frac{3}{2}}$. After an initial rapid growth, the craze velocity decreases to a constant (steady-state) growth velocity which is maintained until the craze has almost reached the other edge of the specimen at this point the craze accelerates to failure. In the diagram, the growth behaviour is similar for the same K_o values. The slight displacement in the curves is due to difference in the initial crack length, if this is accounted for, the curves would fall in an almost identical path.

The other type of growth shown in figure 3.8 occurs at low K_o values $\simeq$ 0.25 $MNm^{-\frac{3}{2}}$ where the craze propagation seems to occur in jumps.

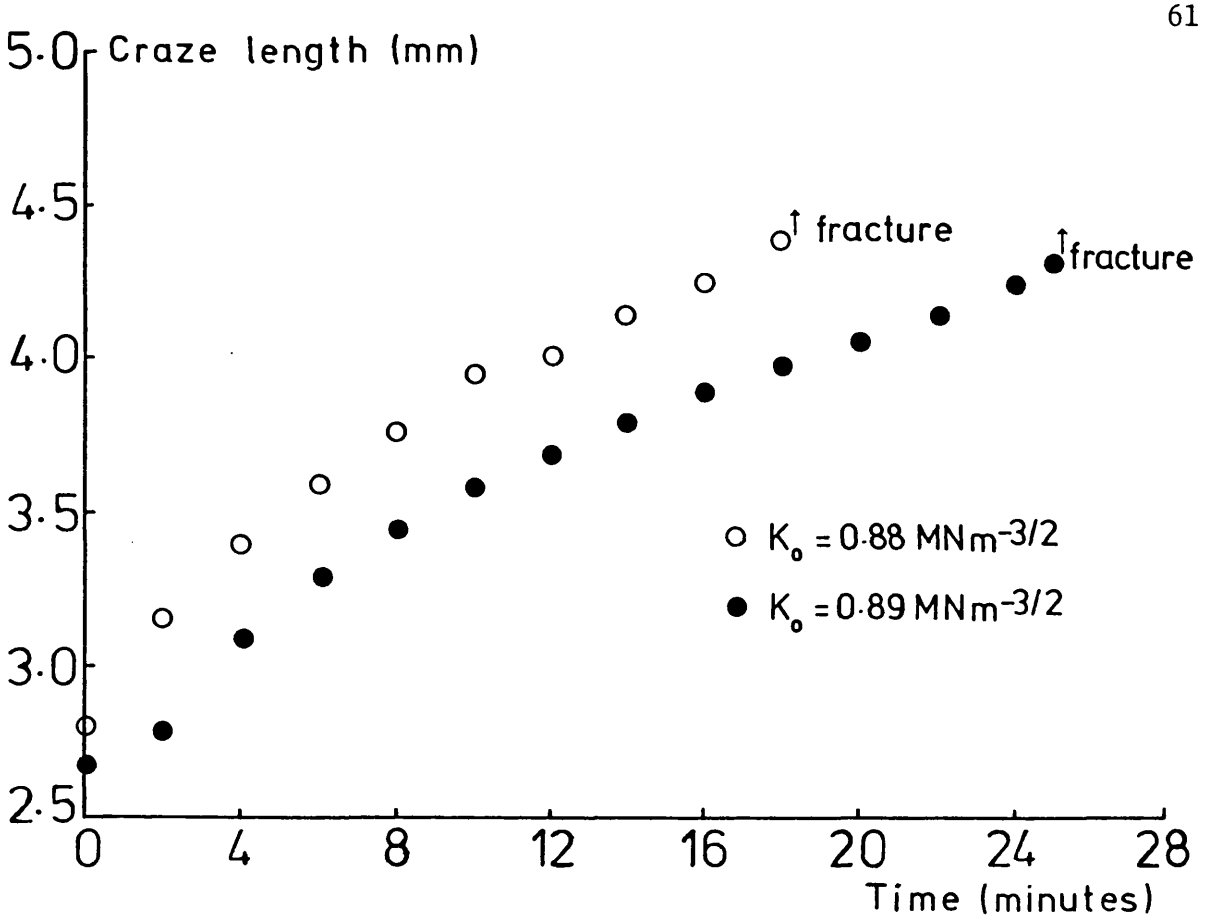

Figure 3·7 Continuous craze growth.

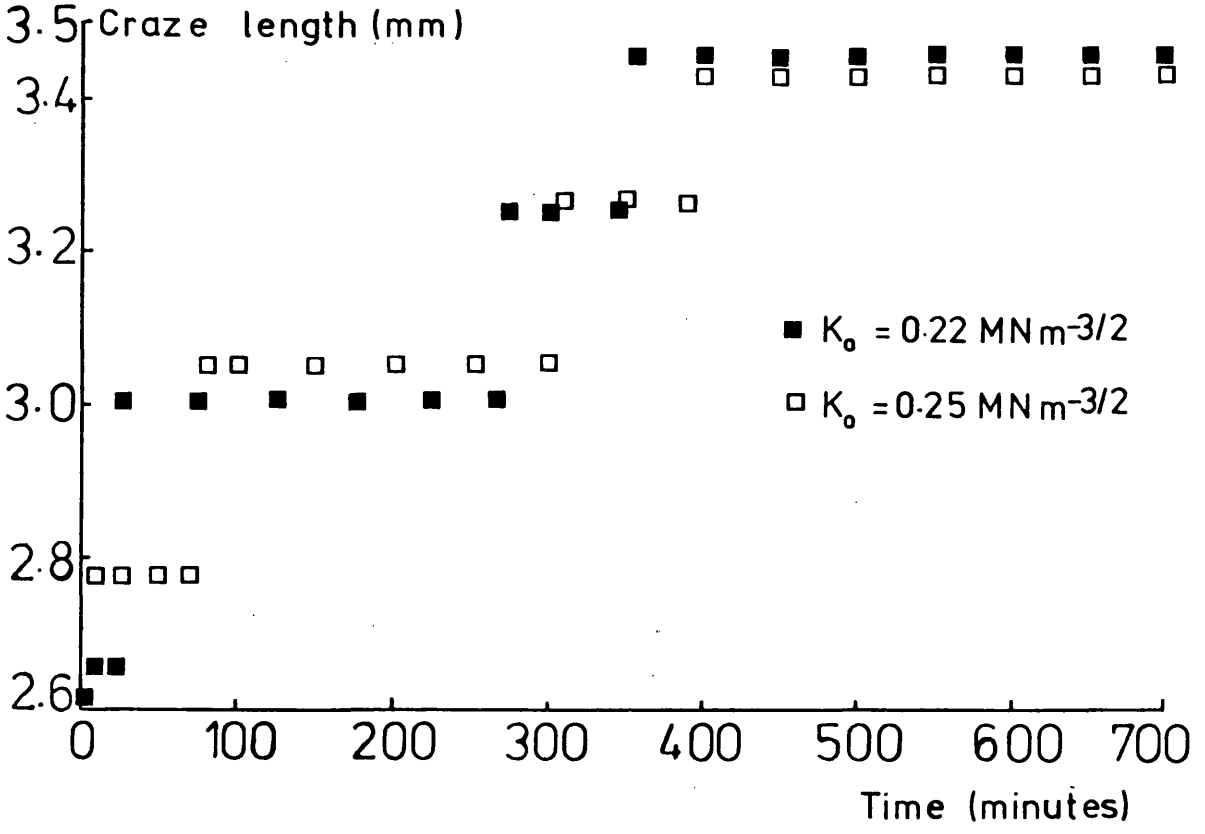

Figure 3·8 Discontinuous craze growth.

In the figure the craze length is shown to remain constant for a time and then a sudden increase in craze length is recorded. Several of these steps were recorded during these tests.

Marshall et al (48) have reported the former type of growth and added that both initiation and growth are dependent on K_o. This is in agreement with the present work as demonstrated in figure 3.9. The high K_o values (1.03 and 1.06) $MNm^{-\frac{3}{2}}$ provided rapid initiation and growth followed by sudden failure. Whereas at low K_o values (0.46 and 0.72) $MNm^{-\frac{3}{2}}$, craze initiation was followed by a long period of steady state growth before the craze accelerated to failure.

When the steady state growth velocities v_a measured from the slope of the craze length/time curves, are plotted against the corresponding K_o values, the correlation between K_o and v_a is also found similar to Marshall's (84) as shown in figure 3.10. These confirm that satisfactory measurement of craze length from the deflection in SEN bend specimens can be achieved.

Regarding craze growth rates at lower values of K_o ($\simeq 0.25$ $MNm^{-\frac{3}{2}}$) they were reported (48, 49, 50) to decrease until growth ceased altogether. In this work this was found not to be the case if enough time was allowed, as clearly demonstrated in figure 3.8. Hereafter a period of $\simeq$ 1 hour with no movements, further craze growth in the form of tiny jumps were observed. The explanation could lie in the mobility of the fluid. Craze growth in liquid environments requires the ability of the fluid to diffuse into the

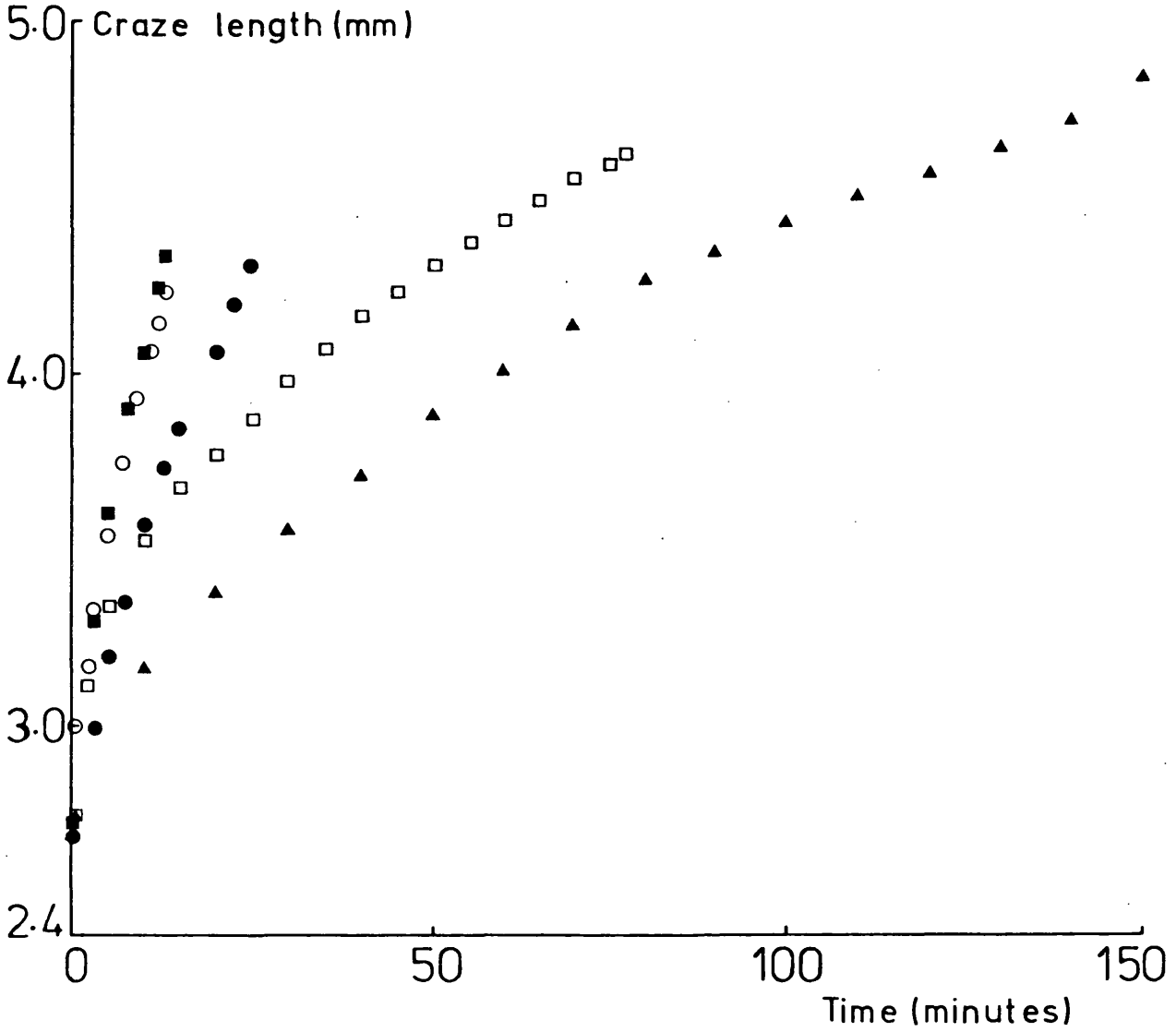

Figure 3.9 Variation of craze length with time
■ K_0=1.06 MNm$^{-3/2}$, ○ K_0=1.03 MNm$^{-3/2}$,
● K_0=0.89 MNm$^{-3/2}$, □ K_0=0.72 MNm$^{-3/2}$, ▲ K_0=0.46 MNm$^{-3/2}$

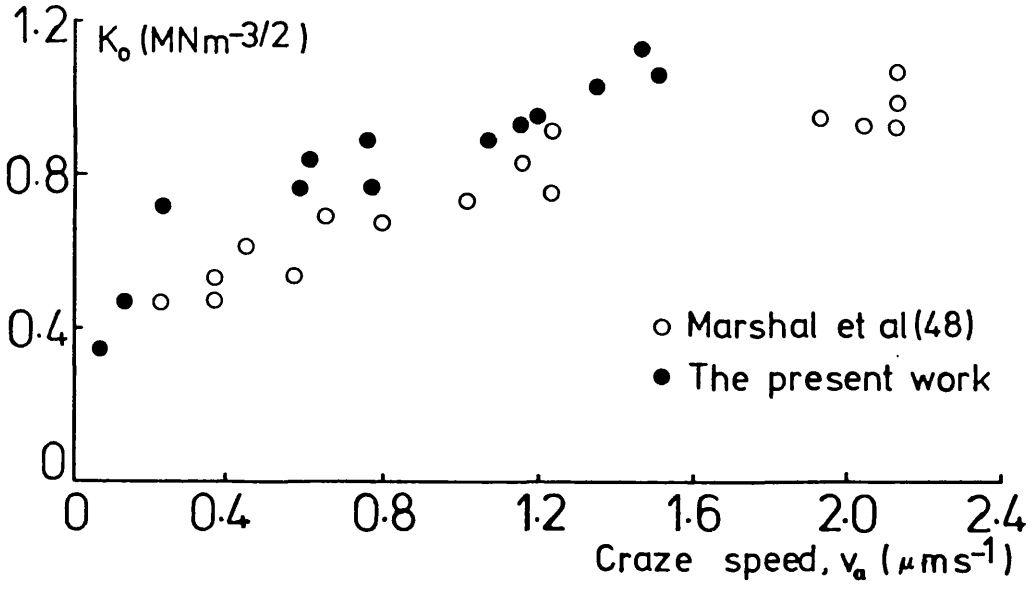

Figure 3.10 Variation of craze speed with initial stress intensity factor.

craze structure. The diffusion rates of liquids in polymers are usually enhanced by the local hydrostatic tension stress field near the craze surface. Therefore, whereas a decrease in high K_o values show a reduction of growth rates, lower K_o should not necessarily lead to zero growth. In this condition, the growth of the already initiated crazes will depend mainly on the rate of diffusion of the solvent and longer time is usually required for growth to occur.

In specimens where growth lead to final failure, failure time is shown as a function of K_o in figure 3.11. The pattern seems identical to the well known static fatigue behaviour of glass in liquids (60).

It is also instructive to compare K_o/t_f results for the all dry PMMA samples reported by Beaumont et al (39), with those obtained by the author in the presence of methanol. This gives a better idea of the effect of methanol on the overall strength performance of PMMA. Figure 3.11 contains both sets of results, and the most striking feature was that although failure is hastened by the presence of methanol at low stress intensity factor, there was a tendency towards an increase in the life expectancy of the polymer in methanol at higher stresses. A possible explanation is that, higher stresses rapidly initiate sharp cracks which in air lead to speedy failure, i.e. Griffith type failure. However, with the presence of methanol, crazes which appear at the crack tip share part of the stored elastic energy and failure is delayed.

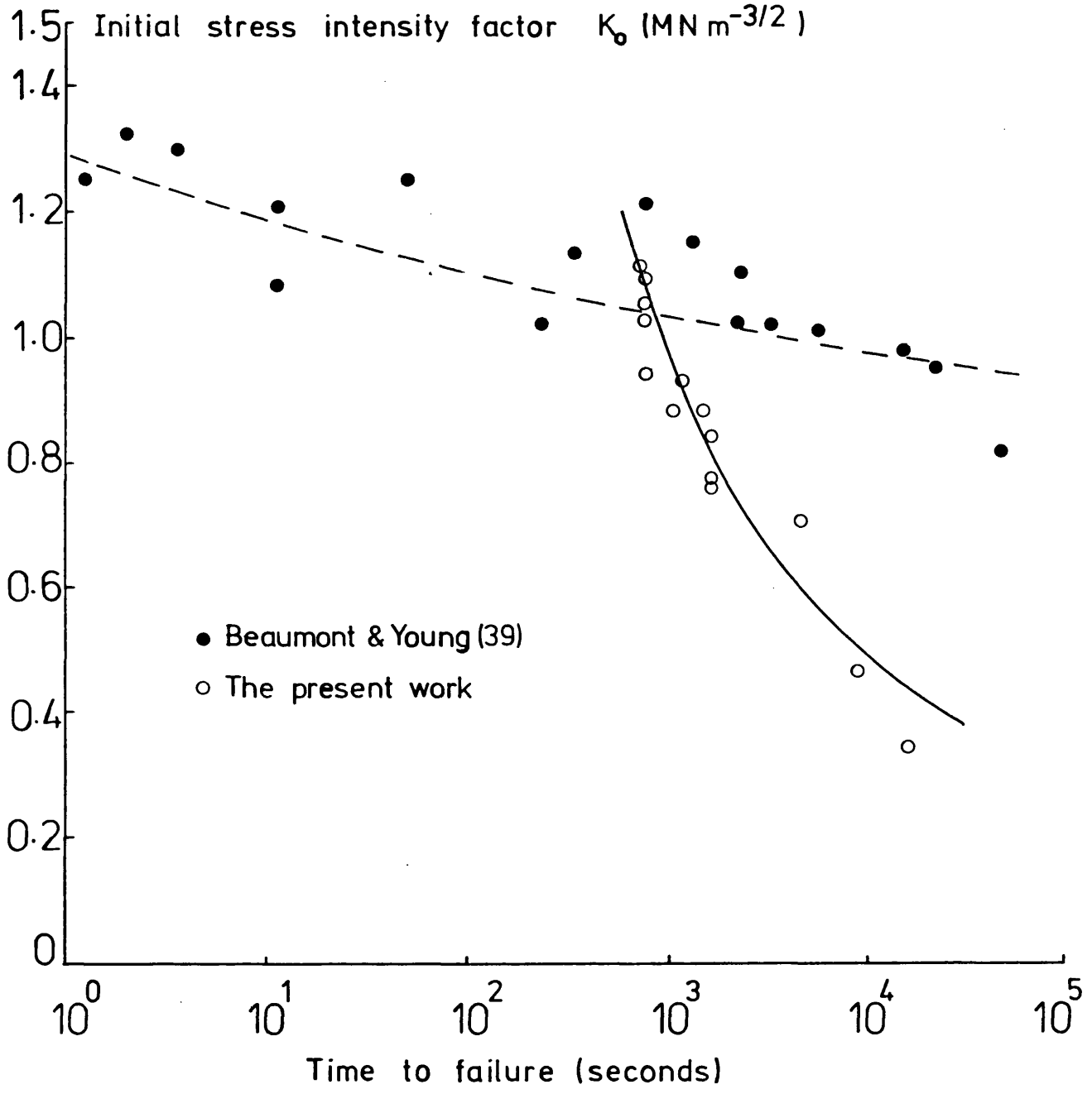

Figure 3.11 Time-to-failure data as a function of initial stress intensity factor. (● in air, ○ in methanol).

3.3.3 Fracture surface appearance

Samples of stressed PMMA immersed in methanol have shown crazes which initiate at the tip of the induced notch and grow perpendicular to the maximum tensile stress. The type of growth observed showed variations in behaviour from rapid failure to apparent arrest depending on the initial stress intensity factor K_o. A fractographic study is adopted here to identify these craze growth with the fracture surface. The method employed for fracture surface examination was to coat the surface with gold; this gave better contrast when the surfaces were examined under the Vickers projection microscope.

It would appear from the fracture surfaces shown in figures 3.12, 3.13 and 3.14, that crack growth in these samples is in two distinct regions. A rough surface close to the notch tip is followed by a smooth surface. In terms of growth behaviour, multiplane crazes grown in notched PMMA specimens were considered by Atkins (61) to produce rough surfaces and introduce a measure of crack stability during propagation, whereas smooth surface represents the transition to unstable cracking with the release of a large amount of strain energy.

The difference in shape and size of these regions was identified with the stress intensity value K_o.

At high growth rates obtained at K_o of the order 1.11 MN $m^{-3/2}$, the fracture surface in figure 3.12 has shown crazes which initiated at

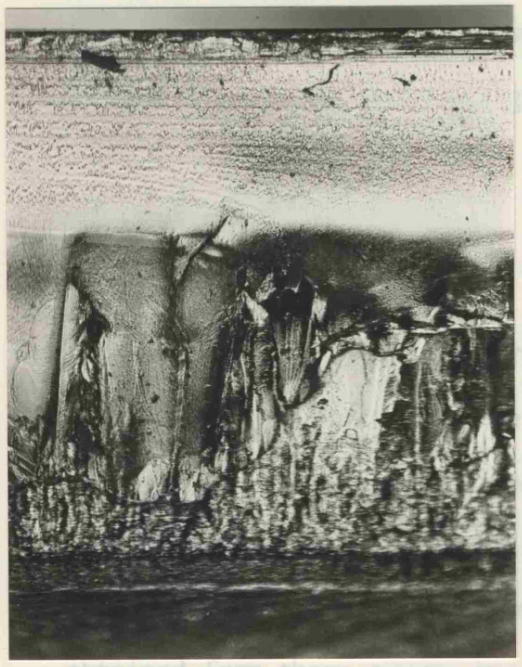

Figure 3.12 Fracture surface X22. Specimen immersed in methanol under dead load equivalent to $K_o = 1.11\ MNm^{-3/2}$

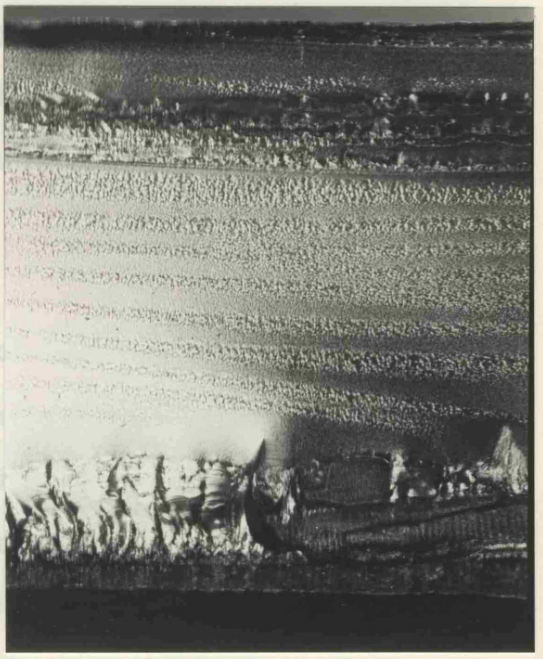

Figure 3.13 Fracture surface X22. Specimen immersed in methanol under dead load equivalent to $K_o = 0.22\ MNm^{-3/2}$

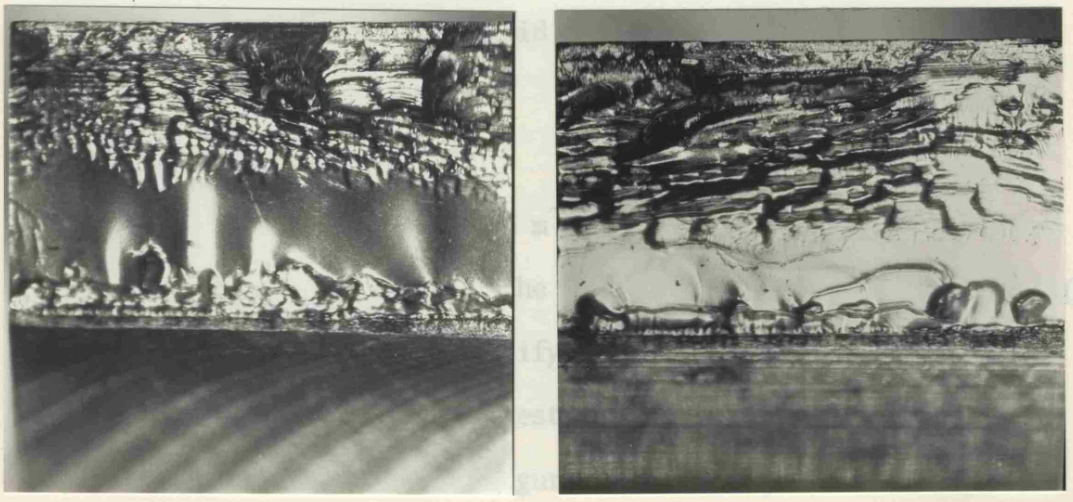

(a) (b)

Figure 3.14 Fracture surface X12. Specimen immersed in methanol under dead load equivalent to
(a) $K_o = 0.46\ MNm^{-3/2}$ (b) $K_o = 0.34\ MNm^{-3/2}$

the crack tip and propagated stably into the specimen to the same length as given by the craze growth curve. Eventually the crack ran out of material and rapid failure followed as shown by the smooth surface.

At the low K_o values of the order of 0.25 MN $m^{-3/2}$, similar methanol crazes were initiated from the same site as shown in figure 3.13. Concerning the craze jumping behaviour recorded on the (a vs t) curves, see figure 3.8, no evidence could be observed on the fracture surface to identify these jumps. However, the total craze length obtained from these curves was of the same magnitude as those measured on the surface. In figure 3.13 the smooth surface following the crazed region, which is associated with rapid fracture, is as a result of the specimen being broken for surface examination. It is instructive here to compare the similarity between this zone and that which is obtained during rapid failure at high growth rates, figure 3.12.

At intermediate K_o value (0.46 MN $m^{-3/2}$), a mirror surface separating the crazed zone was observed on the fracture surface, see figure 3.14(a). Initially this region could identify a rapid transition to unstable propagation. Several specimens tested under identical conditions have produced the same effect, figures 3.14 (a,b), and an examination of craze length/time curves showed no discontinuities, thus indicating stable growth in that region. The mirror surface could represent a portion of the craze which gradually grew from the grainy surface and propagated stably in dry conditions. Further crazing was the

result of methanol penetration through this craze to the tip where further roughening occurred. This mechanism could presumably be restricted to the intermediate K_o values since initiation of a craze in this fashion at higher K_o would have lead to immediate failure.

3.4 Conclusion

The analysis using displacement measurements to study crack/craze growth behaviour, provided a basis for a more convenient and efficient technique in examining the environmental effect on the polymer "PMMA" under dead load conditions. The results derived from the experiments, i.e. craze length vs time curves, were similar to those obtained by the direct and laborious method where craze length measurements were made with the aid of a cathetometer. This confirmed the application of the system adopted.

The results of craze growth were analysed using the initial stress intensity factor K_o as a controlling parameter. In this way two distinct growth patterns have been observed, both functions of K_o.

At higher values of K_o, craze initiation at the notch tip proceeded by steady state growth where the craze speed had a tendency to increase with the increase in K_o. With lower K_o values, the craze growth rate decreased to apparent arrest, however, subsequent small jumps were recorded until the termination of the test.

A fractographic study was used in an attempt to identify these growth behaviour with the fracture surface markings.

In view of the fact that no K/v data could be obtained in dry conditions and since very little had been reported on the environmental fracture of PMMA under increasing load-point displacements, the double torsion technique was considered and introduced to the programme.

PHASE II

DOUBLE-TORSION TESTS. INSTRON TYPE.

CHAPTER 4: DOUBLE TORSION TEST

CHAPTER 5: TESTS AT CONSTANT CROSS-HEAD SPEED

PHASE II DOUBLE-TORSION TESTS. INSTRON TYPE.

CHAPTER 4 DOUBLE TORSION TEST

4.1 Apparatus and test technique

A diagram of the apparatus is shown in figure 4.1. The test is based on a technique suggested by Outwater (62) and developed by Kies and Clark (63). The specimen is a rectangular plate resting on two parallel stainless steel rollers, mounted on the Instron base to provide a rigid platform. The load is applied vertically at the notched end by two little rollers attached via an adaptor to the Instron load cell, mounted on the moving crosshead. As the load-point moves downwards, the two halves of the specimens are subjected to equal torque, forcing the starter crack to initiate and then propagate along the length of the specimen, directed by machined side grooves on both faces. Crack propagation under these conditions has been shown by Evans (64) to be mode I.

For environmental tests, specimens are mounted in a stainless steel tank filled with the appropriate liquid.

4.2 Specimen dimensions and preparation

Double torsion test pieces were cut from 6mm thick ICI "Perspex" acrylic sheet to the same dimensions as those used by G. P. Marshall

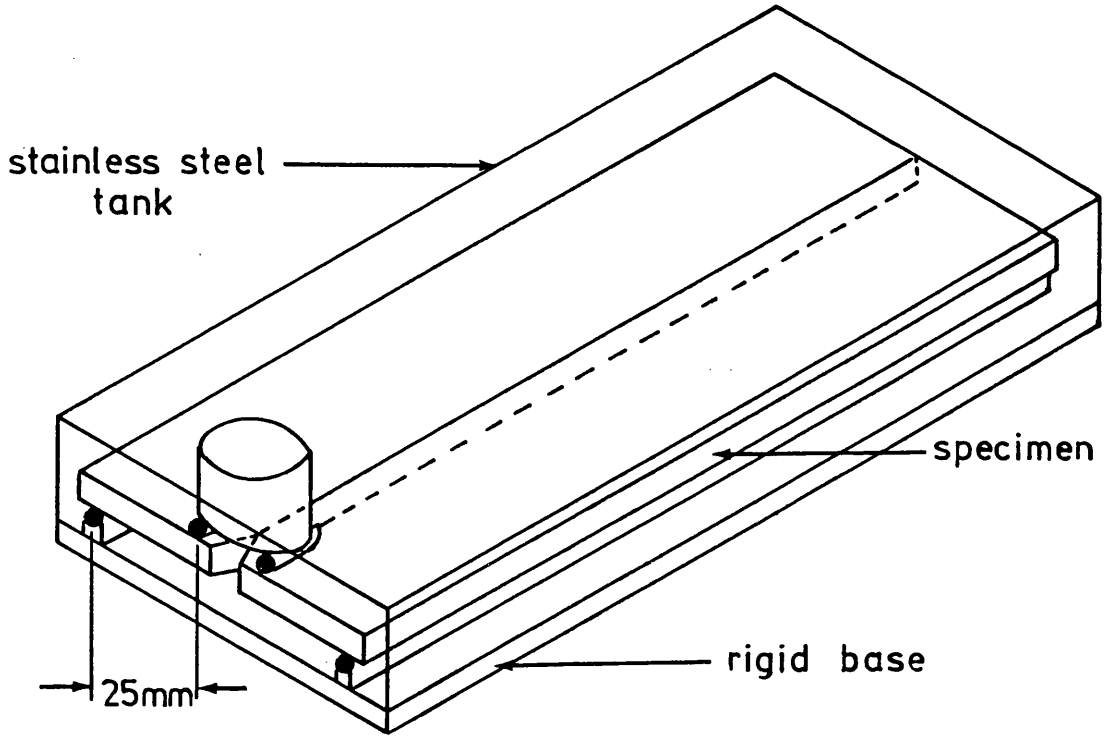

Figure 4.1 Double torsion technique.

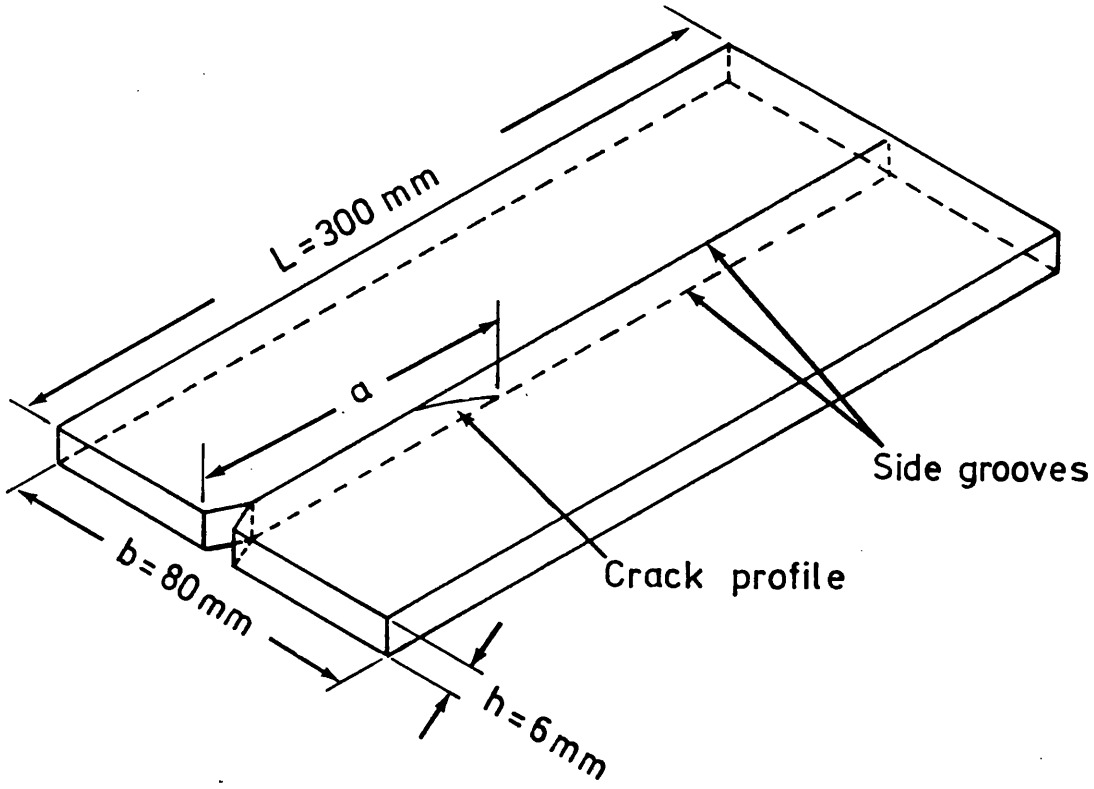

Figure 4.2 Specimen dimensions.

et al (65) i.e. 80mm wide, with central grooves on both sides of the sample (1mm deep x 0.1mm wide) to control the crack. Figure 4.2.

From the double torsion test piece analysis presented in the next section, it has been shown that the crack driving force is independent of crack length. However, there is a departure from this ideal situation, an "end effect" in the region ≈ 1 plate width from each end (66). To allow for this, the specimens were chosen of length 300mm allowing ≈ 150mm of crack path where the double torsion analysis holds.

The width of the groove was also found to be critical if crack wandering was to be prevented. The final chosen value of about 0.1mm was found to give satisfactory results. Starter cracks in the specimens were again initiated using the Vickers hardness machine technique (37). Finally the moment arm employed to bend the sample was 25mm. See figure 4.1.

4.3 Double torsion test piece analysis

The test piece analysis is given in appendix 1, and shows the following results:

By the general compliance method (21), the following expression for the stress intensity factor was obtained

$$K^2 = \left(\frac{P^2}{2b_c}\right)\left(E\,\frac{dC}{da}\right) \qquad (4.1)$$

where K = stress intensity factor

b_c = crack width

P = applied load

E = modulus of the material

C = specimen compliance

An approximate analysis for the specimen compliance (67) gave the following

$$C = \left[\frac{6(1+\nu)\rho^2 a}{Ebh^3}\right] + C_o \qquad (4.2)$$

where C_o = specimen compliance for a = 0

ρ = distance between loading points

b = width of the plate

h = thickness of the plate

ν = poisson's ratio

$$\therefore \quad \frac{dC}{da} = \frac{6(1+\nu)\rho^2}{Ebh^3} = B \qquad (4.3)$$

$$\text{and} \quad \frac{EdC}{da} = \frac{6(1+\nu)\rho^2}{bh^3} \qquad (4.4)$$

Hence the stress intensity factor in equation (4.1) was expressed as

$$K^2 = \frac{P^2}{2b_c}\,\frac{6(1+\nu)\rho^2}{bh^3} \qquad (4.5)$$

$$K = P\sqrt{\frac{3}{b_c}\frac{(1+\nu)\rho^2}{bh^3}} = AP \qquad (4.6)$$

where A is a constant.

From the above points the double torsion test piece shows the following properties:

(a) The compliance C is linearly related to the crack length "a" i.e. $\frac{dC}{da}$ is constant equation (4.3).

(b) Stress intensity K is independent of crack length and proportional to the applied load, equation (4.6). The proportionality constant "A" depends upon specimen dimensions only.

(c) Crack speed $\frac{da}{dt}$ is directly proportional to the time rate of change of compliance $\frac{dC}{dt}$. Therefore differentiating equation (4.2).

$$\frac{dC}{dt} = \left[\frac{6(1+\nu)\rho^2}{Ebh^3}\right]\frac{da}{dt} = B\frac{da}{dt} \qquad (4.7)$$

where the constant B depends upon specimen dimensions and modulus.

CHAPTER 5 TESTS AT CONSTANT CROSS-HEAD SPEED

5.1 Tests in air

5.1.1 Introduction

The determination of K/v data using SEN specimens was difficult because the value of K varied rapidly with crack length and therefore the crack velocity v changed rapidly. In the past to overcome this problem other techniques such as the parallel and tapered cleavage tests were often employed. These methods although used successfully on polymers (37) often required great practical attention and supervision and were found to be time consuming. A more convenient configuration was found, that of the double torsion shown in the previous section, with a constant compliance characteristic. The technique was employed in this work for determining the crack speed data and studying the crack propagation behaviour in dry conditions. The results achieved were used as a control for environmental fracture results.

5.1.2 Experimental procedure

The apparatus used was a double torsion rig designed to be fitted on an Instron universal testing machine model 1122. (See photograph 5.1.)

The cross-head on the Instron was moved downward forcing the crack to propagate along the length of the specimen starting at the end

where the load is applied. Tests were carried out on PMMA samples prepared representing 3 orientations with respect to the long direction of a single cast sheet. Some tests were performed on samples coated with vaseline to study the effect of the jelly on the fracture behaviour, since vaseline coating was applied during environmental tests to prevent surface crazing.

Tests were carried out at room temperature ≃ 293 K and at various cross-head speeds, in order to determine the relationship between K and v.

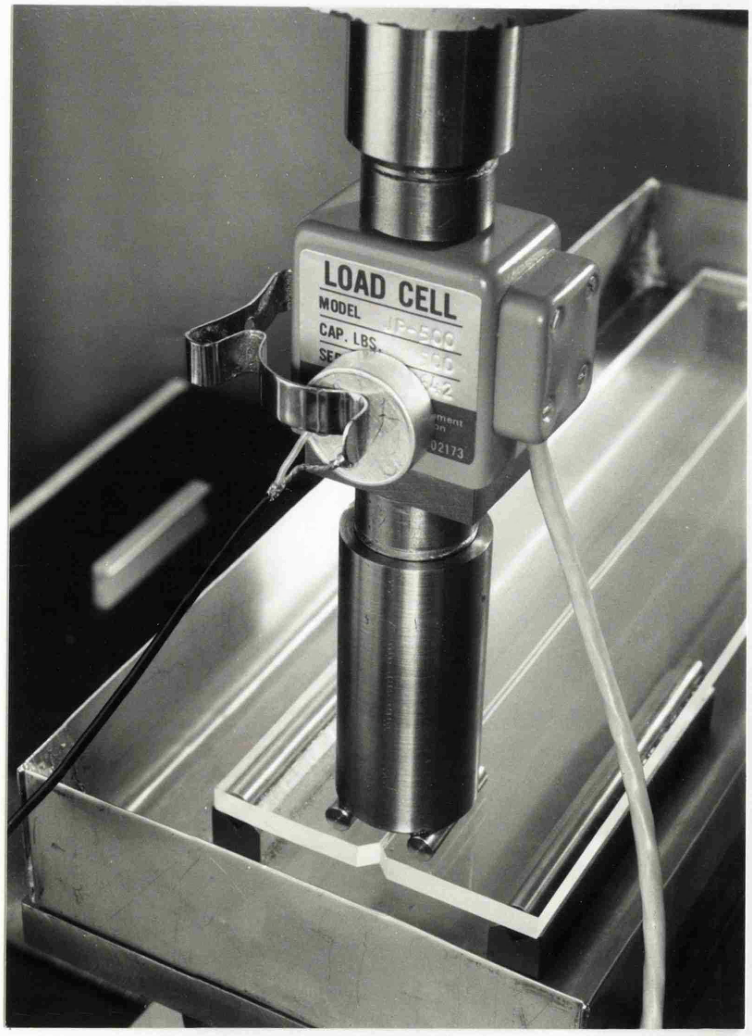

Figure 5.1 Double torsion rig.

5.1.3 Results and discussion

Under constant displacement rate, the load displacement curve (see figure 5.2(a)) showed that after an initial transient which is dependent on the nature of the pre-starter crack, stable crack propagation occurred at constant load P_c corresponding to the stress intensity value K_c.

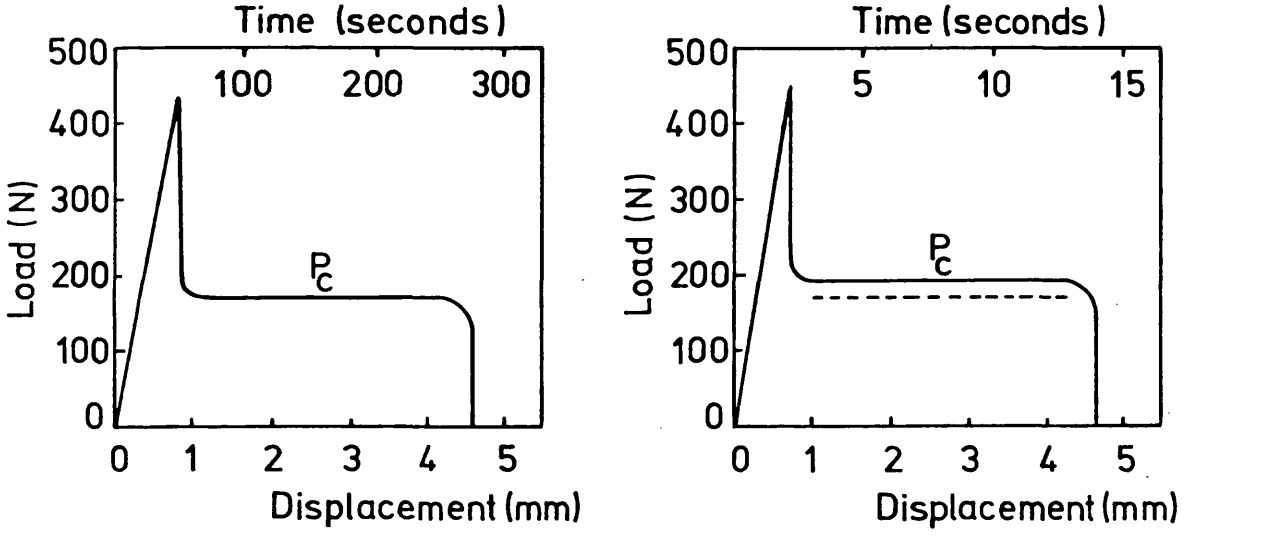

(a) Cross-head speed 1mm/min.

(b) Continuous line cross-head speed 20 mm/min., dotted line cross-head speed 1 mm/min.

Figure 5.2 Load-time (or load-displacement) curves for double torsion test, PMMA in air.

Stable propagation at constant load in a double torsion test is known to comprise propagation at constant crack speed. Equation (4.7) shows

$$\frac{da}{dt} = \frac{1}{B}\frac{dC}{dt}$$

where $$B = \left[\frac{6(1+\nu)\rho^2}{Ebh^3}\right]$$

since $$C = \frac{Y}{P}$$ then for constant load

$$\left(\frac{dC}{dt}\right)_{P_{const}} = \frac{1}{P}\frac{dy}{dt}$$

$$\left(\frac{dC}{dt}\right)_{P_{const}} = \frac{Z}{P} \qquad (4.8)$$

where Z is the machine cross-head speed

$$\therefore \frac{da}{dt} = \frac{Z}{BP} = \text{constant} \qquad (4.9)$$

The influence of cross-head speed on stable crack propagation is shown in figure 5.2(b). The constant value at which load settles during crack propagation increases as cross-head rate increases, and since K_c is directly proportional to P_c equation (4.6) then K_c also increased.

Values of $\frac{da}{dt}$ have been determined independently from equation (4.9) and by direct timing of the crack front past marks scribed on the specimen surface.

A statistical analysis performed on velocity results showed no significant difference between measured and calculated values. The mean value for both methods with the corresponding K_c are shown for two cross-head speeds in table 5.3.

Number of Samples	Cross-head Speed mm/min	K_c MN $m^{-3/2}$	v(measured) m/sec	v(calculated) m/sec
7	1	1.06±0.02	(1.75±0.06) $x10^{-4}$	(1.79±0.06) $x10^{-4}$
7	20	1.15±0.02	(3.87±0.17) $x10^{-3}$	(4.05±0.22) $x10^{-3}$

Table 5.3 Results of K_c and crack velocity (v) from dry tests.

From the tabulated results, it appears that, as has previously been reported (37), K_c showed only a slight increase with increase in cross-head speed, whereas the velocity v markedly increased. The K_c values were also in good agreement with published K_c obtained using other techniques (37). This confirms the theory of A. G. Evans that in a double torsion for brittle material, cracking occurs by mode I opening (64).

In establishing the technique, variables such as orientation, and the presence of absence of a coating of petroleum jelly on the specimen showed no significance in relation to K_c/v value as shown from the results in table 5.4. Also the behaviour of crack propagation

*Specimen Orientation	Specimens free of vaseline cross-head speed 1 mm/min		Vaseline coated specimens cross-head speed 1 mm/min	
	K_c $MNm^{-3/2}$	v m/sec	K_c $MNm^{-3/2}$	v m/sec
0^o	1.04	1.85×10^{-4}	1.06	1.77×10^{-4}
45^o	1.07	1.79×10^{-4}	1.07	1.77×10^{-4}
90^o	1.07	1.76×10^{-4}	1.09	1.70×10^{-4}

Table 5.4 Stress intensity (K_c) with corresponding crack velocity (v) for PMMA in air.

*Orientation with respect to the long axis of the original cast sheet.

remained the same (i.e. stable) when these conditions were considered.

When equation (4.9) is used to evaluate $\frac{da}{dt}$, the value of B must be determined. This is given by the slope of the compliance crack length curve (refer to equation 4.3).

The compliance / crack length curves shown in figure 5.5 for two cross-head speeds (1mm/min. and 20mm/min.) clearly indicates that the rate of change in compliance with crack length $\frac{dC}{da}$ i.e. B, remains constant for all samples of the same dimensions at the same machine speed, but changes with the change in cross-head speed. It is therefore necessary to use a value of "B" appropriate to the cross-head speed employed.

The crack front velocity v is related to $\frac{da}{dt}$ by a factor ϕ known as the crack velocity correction factor (see appendix 2).

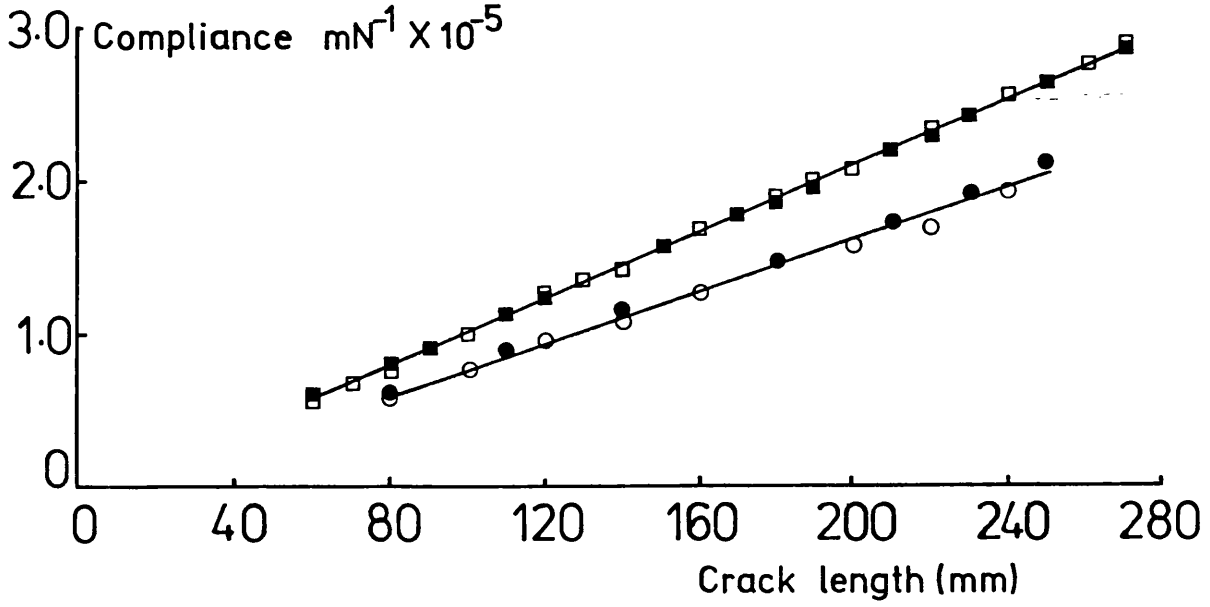

Figure 5.5 Compliance as a function of crack length (dry tests) at cross-head speeds of □■ 1mm/min and ○● 20 mm/min.

5.2 Tests in Methanol

5.2.1 Introduction

Previous work on environmental fracture of polymers was mainly concerned with the initiation and propagation of crazes under essentially constant load conditions (11, 48-50), while relatively little is known about the environmental fracture behaviour of polymers subjected to monotonically increasing loads (or displacements).

Under dead load conditions most organic solvents were found to initiate crazes in the stressed polymer which could lead to delayed failure at stresses well below their fracture stress in air (48). Recently however Mai (40) performed tests under increasing displacement conditions and showed that stable crack propagation on dry PMMA samples was hindered as soon as carbontetrachloride was introduced at the crack tip. The propagating crack was found to arrest and the new fracture load considerably increased followed by unstable cracking. His finding was in good agreement with earlier observations made by Benbow et al (29), who were investigating the effect of water absorption on the specific energy for cracking PMMA under increasing displacement, and recently by Beaumont and Young (39) on the effect of water on PMMA. Their explanation was that water plasticizes the crack tip effectively blunting out the propagating crack by absorbing the stored elastic strain energy in the specimen that would otherwise have dissipated as fracture surface energy. Hence the increase in toughness.

Mai (40) in his work was more concerned with achieving stable propagation in liquid environments, to evaluate the fracture toughness as a function of crack velocity, rather than this transformation from the stable to unstable crack behaviour.

The present work on the fracture of PMMA in methanol lead the author to propose that a polymer/liquid system may be used as a model for studying the relationship between stable and unstable crack propagation, with the advantage that either type of behaviour may be produced at will.

This section deals with the experimental procedure adopted and the results obtained, while a proposed model for a polymer/liquid system is presented in Chapter 8. Tests which were performed on dry PMMA were used as a control.

5.2.2 Experimental

Tests were performed on double torsion specimens, immersed in a bath of methanol, bolted to the Instron base (see photograph 5.1). Prior to immersion in methanol, the samples were coated with a layer of grease to prevent any surface crazing.

The influence of cross-head speed on the fracture behaviour of PMMA in methanol was investigated by performing tests over a range of cross-head speeds, from 0.05 to 50 mm/min..

5.2.3 Results and discussion

A vaseline coated specimen immersed in methanol subjected to a constant strain rate, showed very consistent crack-jumping behaviour. A representative load-deflection curve is shown in figure 5.6(a). The diagram shows that the load increases to a critical value P_i, then a sudden burst is observed where the crack has jumped forward, and the load has dropped to a lower value P_a. The load at this point remains momentarily constant before it starts to climb up again. The initial peak is found to vary markedly in height from sample to sample and evidently reflects again the quality of the pre-formed crack. Thereafter the second and subsequent peaks show only slight variation.

Stress intensity values K_i and K_a are evaluated from P_i and P_a respectively using equation (4.6) derived from the double torsion test piece analysis. For 50 peaks observed over 16 samples representing three orientations tested at a constant cross-head speed (1.0 mm/min.) variance analysis showed the absence of any trend in K_i with sample orientation or with successive peaks in the same test. With respect to K_a, there was no significant effect of orientation but a tendency was observed for the higher values to be recorded after second or third peaks in the same test.

The mean values for K_i and K_a are given in table 5.7.

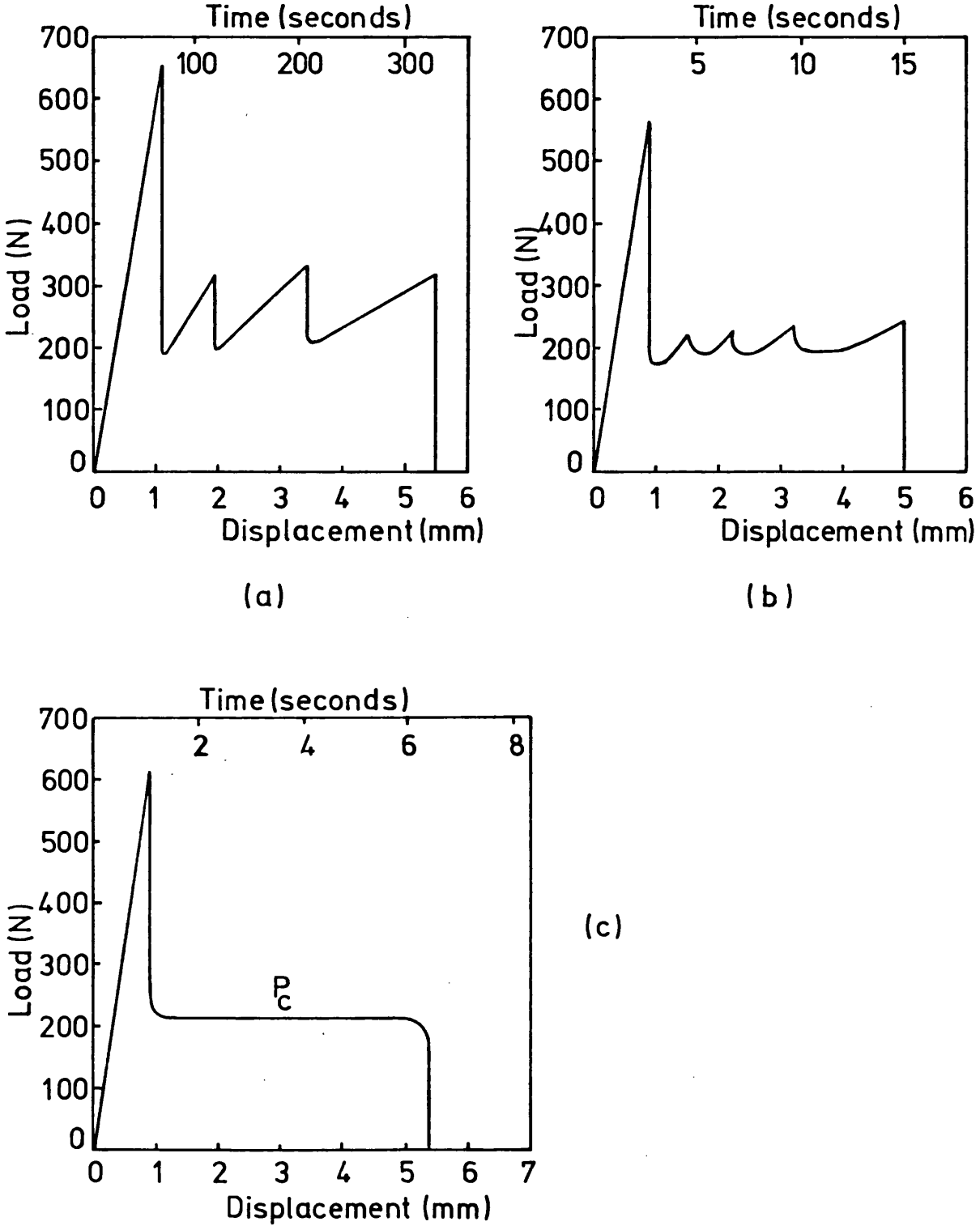

Figure 5.6 Load-time (or load-displacement) curves for grease coated PMMA specimens in methanol.
(a) Cross-head speed 1 mm/min.
(b) Cross-head speed 20 mm/min.
(c) Cross-head speed 50 mm/min.

*Specimen Orientation	K_i $MNm^{-3/2}$	K_a $MNm^{-3/2}$
0^o	1.85 ± 0.11	1.21 ± 0.05
45^o	1.87 ± 0.09	1.23 ± 0.03
90^o	1.81 ± 0.09	1.21 ± 0.05

Table 5.7 Tests in methanol, specimens coated with vaseline, cross-head speed 1 mm/min.

*Orientation with respect to the long axis of the original cast sheet.

It should be noted here that K_c for stable crack propagation in air is comparable with the apparent arrest value for unstable crack propagation while K_i is appreciably higher. Compare figures 5.2(a) and 5.6(a).

Investigation into the effect of cross-head speeds has shown that with the increase in cross-head speed, the crack jumps are initiated at lower P_i values, and followed by a slightly higher load arrest values figure 5.6(b). K_i and K_a values calculated over a range of cross-head speeds are shown in table 5.8 and plotted in figure 5.9.

The results show a significant reduction in the value of K_i as the cross-head speed is increased, while values of K_a are not distinguishable from figures at lower speeds.

From the K vs cross-head speed figure 5.9, if the straight line for K_i is extrapolated to its intersection with the K_a line, crack propagation

Number of Samples	Cross-head Speed mm/min	K_i $MNm^{-3/2}$	K_a $MNm^{-3/2}$
8	0.5	1.80 ± 0.11	1.17 ± 0.03
17	1.0	1.84 ± 0.10	1.21 ± 0.05
6	2.0	1.77 ± 0.09	1.20 ± 0.06
5	5.0	1.79 ± 0.08	1.17 ± 0.03
4	20.0	1.59 ± 0.13	1.23 ± 0.04

Table 5.8 Results from tests on vaseline coated specimens in methanol.

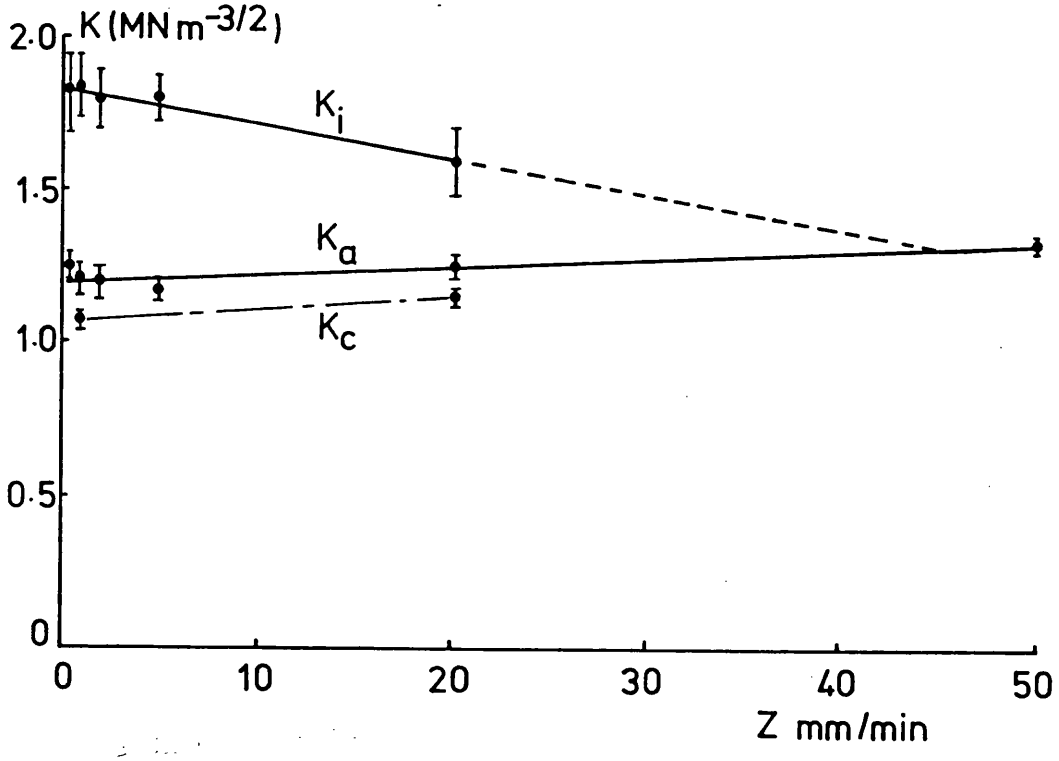

Figure 5.9 Stress intensity vs cross-head speed.
—— Test in methanol.
—·— Test in air.

will eventually be stable. A similar converging shape was demonstrated by Yamini and Young(32) in the fracture study of epoxy resin. In the PMMA/methanol system, figure 5.9 predicts a cross-head speed value of ≃ 45 mm/min. for stable cracking. On the 1122 Instron machine the nearest available cross-head speeds are 20 and 50 mm/min. Double torsion tests performed on the vaseline coated specimen at the 50 mm/min. cross-head speed have indeed shown as predicted, stable crack propagation behaviour under a constant load P_c = 22.2 Kg f equivalent to the stress intensity value K_c = 1.32 $MNm^{-\frac{3}{2}}$ for a crack velocity v = 8.7 x 10^{-3} m/sec. The load time curve is shown in figure 5.6(c).

For the remaining test pieces the difference between K_i and K_a characterized the amount of jumping. With large difference at low cross-head speeds the crack propagated by means of large jumps. The length of these jumps becomes smaller as the displacement rate increases until the cross-head displacement rate of ≃ 50 mm/min. is reached when the propagation became quasi-static and K_i is equivalent to K_c in air.

Similar behaviour has been reported in epoxy resins under dry conditions (32), but it seems to be contrary to the environmental behaviour of PMMA reported by Mai (40), where an increase in cross-head speed caused an increase in K_i figure 2.8. In a publication in the journal of Materials Science (68), Mai explained that the discrepancy was caused by the difference in definition of K_i.

In reference (40) K_i represents values of craze initiation at the point of contact between environment and crack tip i.e. during plasticization, whereas K_i in the present work represents values at crack initiation with the crack breaking out of the plasticized region.

The basic requirement for unstable crack propagation has been stated (41) to be that the specific work of fracture R decreases with increasing crack speed $\dot{a}$ i.e. $\frac{dR}{d\dot{a}} < 0$. In equivalent terms $\frac{dK_c}{d\dot{a}}$ must be negative. PMMA is known from the present work and elsewhere (37) to show an increase of K_c with crack speed, at least up to 0.1 $msec^{-1}$ so that $\frac{dK_c}{d\dot{a}}$ must be inherently positive. It would seem then that the observation of crack jumping behaviour of PMMA in methanol must be attributed exclusively to the effect of the environment, probably through some such mechanism as has been proposed by Gurney and Hunt (69) whereby the crack is arrested by blunting of the tip in material plasticized by the environment. Crack jumping involves the breaking out of the crack into the virgin material under conditions where $K > K_c$ since additional work other than that of creating new surfaces of material is required to overcome the plasticized region at the crack tip.

The above explanation seems feasible, however nothing was reported in the literature prior to this investigation (70) on what follows the crack jump. It appears from the results reported in this section that total failure is not imminent, but the methanol flows towards the fast running crack tip awaiting conditions where once more the

crack can be arrested. As a result stick-slip behaviour prevails, until the crack runs out of material.

To obtain a better understanding of the initiation and arrest mechanism under the above condition, the next stage in the project is set to perform an analysis on the sequence of events constituting these jumps. This was achieved from the (K,$\dot{a}$) relationship obtained during the jump together with a close study of the different zones leading to arrest.

PHASE III

UNSTABLE CRACK PROPAGATION

CHAPTER 6: STUDY OF LOAD DROP IN DOUBLE TORSION TESTS

CHAPTER 7: CAPTURE OF LOAD TRANSIENTS

PHASE III UNSTABLE CRACK PROPAGATION

CHAPTER 6 STUDY OF LOAD DROP IN DOUBLE TORSION TESTS

6.1 Introduction

In the previous section having established that the transition from stable to unstable crack propagation in PMMA specimens is due to the presence of methanol, the question arises of the mechanism which constitutes this behaviour. The relationship between K and the crack velocity during stick-slip propagation may give some help in this direction.

In double-torsion tests, characteristic load-displacement curves were obtained in the study of crack stability. When propagation is continuous, the crack grows at a constant load P_c as shown in figure 5.2. However, if the crack propagates by a stick-slip mode the load-displacement curves take on a saw-tooth appearance as in figure 5.6(a). P_i is the load at initiation and P_a the load at arrest. Linear-compliance analysis of the load behaviour has provided the background for the determination of $K_c(v)$ curves in the past. In the present work this technique has been extended both experimentally and analytically to deal with the problem of unstable fast fracture.

6.2 Analysis of unstable crack propagation in double-torsion tests

The double-torsion test piece analysis presented in Chapter 4 showed three main properties

(1) Compliance C is linearly related to crack length "a"

$$C = Ba + C_o \tag{6.1}$$

where B and C_o are constants.

(2) Stress intensity K is independent of crack length and proportional to the applied load P

$$K = AP \tag{6.2}$$

where A is a constant depending on the test piece dimensions equation (4.6).

(3) Crack speed is simply related to the time rate of change of compliance

$$\frac{da}{dt} = \left(\frac{1}{B}\right)\left(\frac{dC}{dt}\right) \tag{6.3}$$

In turn the quantity $\frac{dC}{dt}$ can be readily measured in tests performed on a stiff tensile testing machine such as an Instron, where both the load P and the load point displacement y can be recorded.

By definition $$C = \frac{y}{P} \qquad (6.4)$$

$$\therefore \quad \frac{dC}{dt} = \frac{P\frac{dy}{dt} - y\frac{dP}{dt}}{P^2} \qquad (6.5)$$

Hence equation (6.3) may be written as

$$\frac{da}{dt} = \left(\frac{1}{BP^2}\right)\left(P\frac{dy}{dt} - y\frac{dP}{dt}\right) \qquad (6.6)$$

The crack front velocity is proportional to $\frac{da}{dt}$, the constant of proportionality depending upon the shape of the crack front (appendix 2).

Crack propagation in double torsion test pieces under different load conditions was examined by different authors using different forms of equation (6.6).

McKinney and Smith studying crack propagation in glass (66) performed dead-load tests i.e. $\frac{dP}{dt} = 0$ in equation (6.6). The crack speed is therefore expressed as

$$\frac{da}{dt} = \left(\frac{1}{BP^2}\right) P \frac{dy}{dt} = \left(\frac{1}{BP}\right)\frac{dy}{dt} \qquad (6.7)$$

Evans working with sintered alumina (64) used a load relaxation method, where load P_i and displacement y_i were achieved and then the machine cross-head was arrested i.e. $\frac{dy}{dt} = 0$.

For the condition $\frac{dy}{dt} = 0$ equation (6.6) becomes

$$\frac{da}{dt} = -\left(\frac{1}{BP^2}\right) y \frac{dP}{dt} \qquad (6.8)$$

But $$y = CP = C_i P_i$$

Hence $$\frac{da}{dt} = -\frac{C_i P_i}{BP^2} \frac{dP}{dt} = -P_i \frac{(Ba_i + C_o)}{BP^2} \frac{dP}{dt} \qquad (6.9)$$

The crack velocity was thus obtained directly from the rate of load relaxation followed on the recorder at constant displacement and the initial crack length a_i. The maximum crack velocity obtained was 2×10^{-2} msec^{-1}.

D. C. Phillips and J. M. Scott (71) used equation (6.6) to analyse crack propagation behaviour which occurs in epoxies. They performed tests under constant displacement rate conditions i.e. $\frac{dy}{dt}$ = constant.

Under these conditions it is necessary to evaluate y, the instantaneous value of load-point displacement corresponding to a given crack length. Phillips and Scott estimated values of "a" from the closely spaced arrest markings on the fracture surfaces of their specimens. Using the corresponding value of P they wrote

$$y = P(Ba + C) \qquad (6.10)$$

Hence, substituting in equation (6.6) :

$$\frac{da}{dt} = \frac{1}{BP}\left[\frac{dy}{dt} - \frac{dP}{dt}\left[Ba + C\right]\right] \qquad (6.11)$$

The quantity $\frac{dP}{dt}$ in equation (6.11) was obtained from the slope of the load time curve shown in figure 6.1, and achieved by increasing the chart speed of the testing machine.

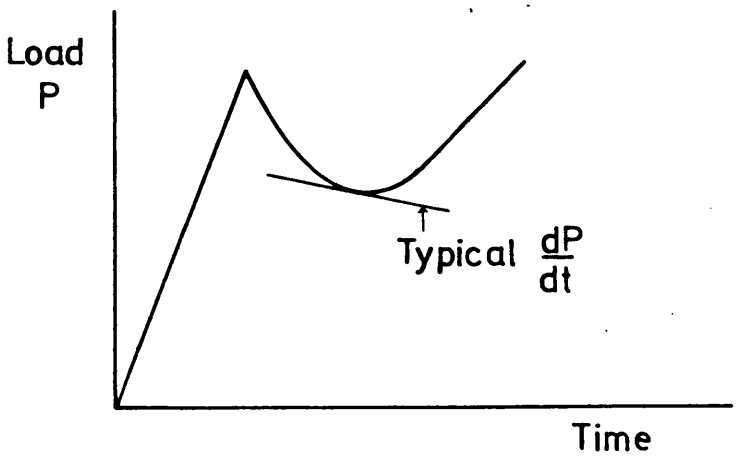

Figure 6.1 Schematic load-time curve during stick-slip propagation. The curve is obtained by running the recording chart at high rate and expanding the load scale (after Phillips & Scott (71)).

This method is questionable since the response time in conventional chart recorders is at least of the order of 0.1 seconds, and it is doubtful whether rapid jumps could be followed accurately. This was proved to be the case in this work, and another technique has to be adopted to overcome this problem, see section 7.2. The maximum apparent crack velocity achieved by Phillips and Scott was 5×10^{-3} m sec^{-1}.

The solution adopted in the current programme was to eliminate the variable y from equation (6.6) making the substitution

$$y = Zt \tag{6.12}$$

$$\text{and} \quad \frac{dy}{dt} = Z \tag{6.13}$$

where Z is the constant cross-head speed of the testing machine and t is the time measured from the commencement of the test.

This gives

$$\frac{da}{dt} = \frac{Z}{B}\left[\frac{1}{P} - \frac{t}{P^2}\frac{dP}{dt}\right] \tag{6.14}$$

This equation represents the relationship between load, crack length and time for a material under the specified conditions whether crack propagation be stable or unstable as will be shown in Chapter 8.

6.3 K(ȧ) determination during a crack jump

To determine K and ȧ values during the unstable crack jump represented by the sudden load drop shown in figure 5.5(a), the constants A and B in equations (6.2) and (6.14) respectively must be evaluated, together with the shape of load/time curve during a transient. The latter is the subject of the next chapter.

The evaluation of A and B:

The constant A can be obtained from the specimen dimensions as shown by equation (4.6). The value of B however is dependent on both dimensions and material modulus equation (4.7). Polymer modulus is known to be strain rate dependent (72, 73), therefore the value of B is not constant over all cross-head speeds and its value must be evaluated for a given strain rate.

For dry specimens this was achieved from the compliance analysis calibration curve where the compliance C is a function of crack length "a" equation (6.1) and the value of B is given by the slope $\frac{dC}{da}$ (see section 5.1.3).

In environmental tests with slip-stick behaviour, similar compliance/crack length curves are obtained with the compliance measured from the deflection and load at initiation and the corresponding crack length measured on the fracture surface. The compliance equation was arranged such that the change in specimen dimensions were allowed for.

Hence equation (4.2) becomes

$$C_i bh^3 = \left[\frac{6(1+\nu)\rho^2}{E}\right] a_i + C_o bh^3$$

where C_i = compliance at initiation

a_i = crack length at initiation

Plots of $C_i bh^3$ vs a_i are shown in figure 6.2 over a range of cross-head speeds.

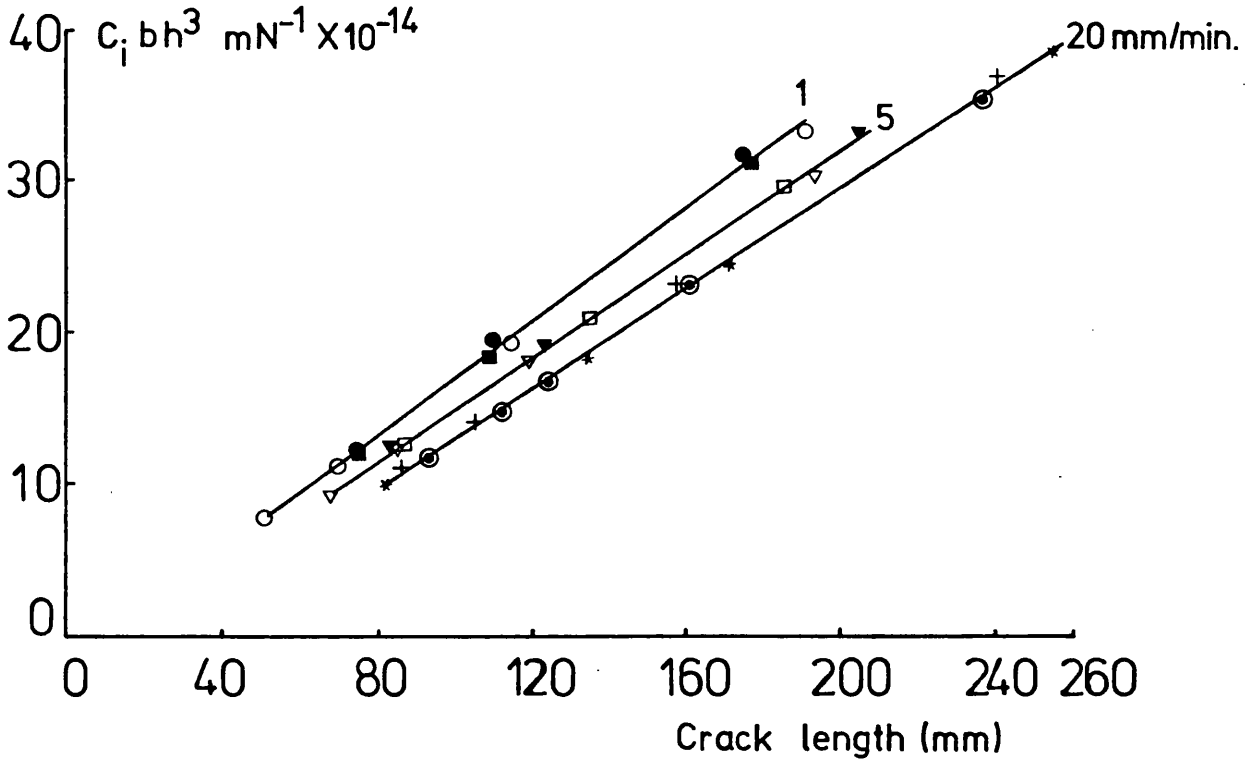

Figure 6.2 $C_i bh^3$ as a function of crack length (methanol tests) at cross-head speeds of 1, 5 and 20 mm/min.

The number of points on the curve represent number of jumps that occurred during the test. The slope of these straight lines gives the value of $\frac{6(1+\nu)\rho^2}{E}$ and as $6(1+\nu)\rho^2$ is a constant, these plots clearly indicate that with an increase in cross-head speed higher moduli are obtained. The corresponding value of B for a given strain rate could be determined from the slope of the line and the specimen dimensions since

$$B = \text{slope} \times \frac{1}{bh^3}$$

CHAPTER 7 CAPTURE OF LOAD TRANSIENTS

7.1 Introduction

Catastrophic failure in brittle materials has been the concern of many. The fracture mechanics is used to recognize the condition which causes such failure by studying how the growth of an inherent defect in the material is influenced by conditions of stress and environment. A particularly useful experimental method is to measure the relationship between crack propagation speed ($\dot{a}$) and stress intensity factor (K) using pre-cracked test pieces of simple geometry. Previously these measurements called for methods such as high speed cinematography which are laborious and expensive. This section deals with a technique developed by the author for rapid crack propagation measurements where no appreciable running costs are encountered and the system does not interfere with conditions in the crack tip region, so it is especially suitable for work in controlled environments. Using the analysis adopted for this technique, a mathematical model for crack initiation and arrest in a Polymer/environment system has been proposed.

7.2 Technique developed for retrieving transients

This section describes the technique adopted, using equation (6.14) to determine crack speed and hence (K/å) information during the crack jumps, by recording the load transients obtained from unstable behaviour. The rate of such load drops is much too rapid to be determined from the Instron chart recorder (figure 5.6(a)), thus other possibilities are investigated to retrieve these fast dropping load signals with the aid of a transient recorder.

7.2.1 Apparatus

The DL 905 transient recorder (Data Laboratories Limited) is a digital instrument designed to capture single shot or low repetition events and present them for continuous display on a CRO. Readout to a YT plotter is also available. It was applied in this work to record unique signals.

The input waveform is digested to a resolution of 8 bits and stored in a 1k word memory which is continuously updated at a chosen sweep frequency until a trigger signal is received. Updating then stops, and the sample remains in store until the unit is re-armed, i.e. instructed to take a fresh record. The pre-trigger recording mode on this instrument makes it possible to see the waveform both before and after the trigger, with precise control over the amount of pre and post trigger information recorded.

Triggering arrangements:

The DL 905 transient recorder can be triggered either internally or externally.

Internally the sweep trigger is derived from the signal input via the input amplifier, and requires the value and direction of the signal at which triggering will occur to be predetermined. This procedure was found to be unreliable since the trigger level could not be accurately determined, and in many cases the absolute value of the input signal was too small. Hence the external mode was used instead. This called for a pulse of height 0 to +5v, of 100 ns minimum width, with rise/fall times less than 100 ns.

In the present programme, the pulse was supplied by a crystal microphone connected via a decoupling capacitor at the external trigger input of the transient recorder. The triggering level of the transient recorder was preset to give optimum results.

7.2.2 Experimental arrangement

Figure 7.1 is a block diagram of the equipment. The encircled numbers indicate the different positions which were successively used in the attempt to obtain a satisfactory load signal output.

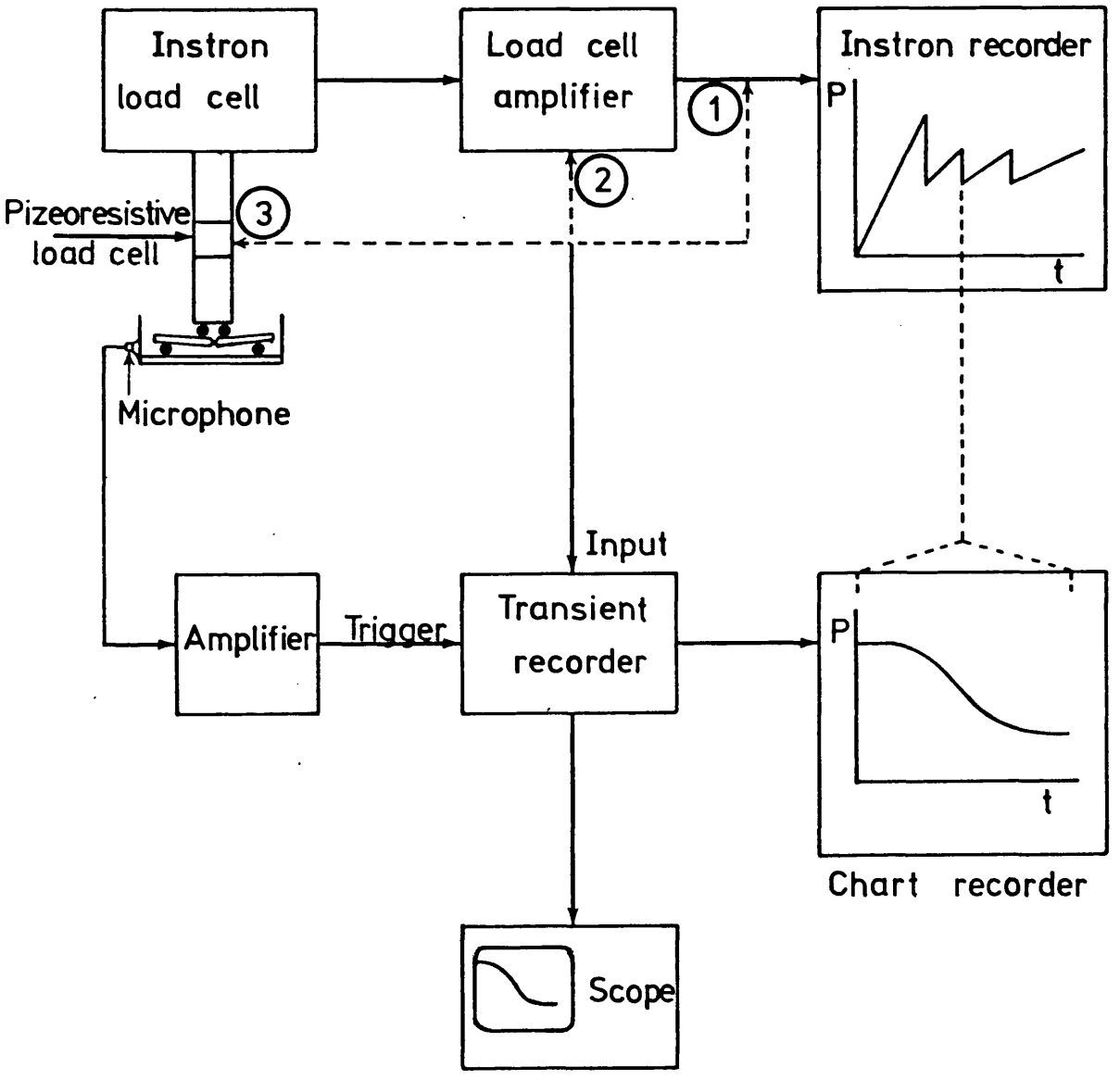

Figure 7.1 Equipment block diagram.

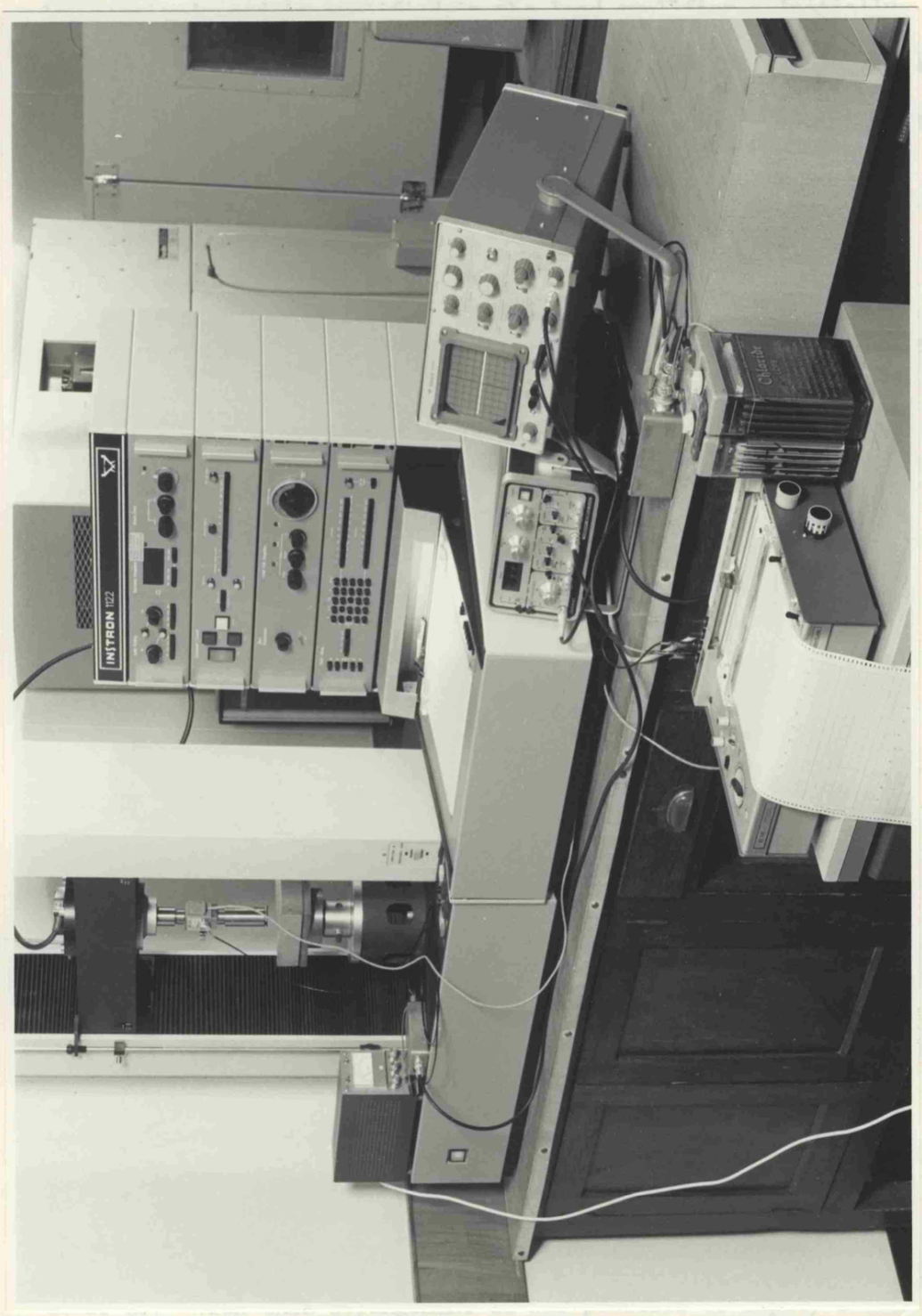

Figure 7.2 Apparatus for detecting transient events.

In the diagram, the Instron load cell consists of strain gauges which are arranged in a bridge circuit and excited by a stabilised oscillator. The resultant output load signal from the cell is of low magnitude and is amplified in the load amplifier. Initially load signals were taken from the output of this amplifier position 1. However, investigation showed that these signals are heavily damped for controlling the pen servo system of the recorder, so that the response time was of the order 0.1 seconds, see Section 7.3.

In order to achieve faster response times, attempts were next made to extract signals from before the demodulator stage position 2. Here the energising frequency of 375 Hz gave a waveform signal with four relevant information points, see figure 7.4, which were not sufficient in analysing the load/time transient.

Finally the signal was obtained from the output of a specially installed load cell mounted in tandem with the Instron cell at position 3, see also the photograph, figure 7.2. The cell is of the type J.P. 500 (supplied by Data Instrument Inc.). It is a transducer which uses the pizeoresistive characteristics of semiconductors to perform physical measurements. In addition to its high response rate which makes it capable of following fast rates of load drop during rapid fracture, it also offers a unique combination of high signal level and low impedence which enables it to drive indicating and control meters without the need for amplification. The energising voltage of the cell is 6 volts ac or dc. With this arrangement it was possible to employ a

sweep time of 20 milliseconds on the transient recorder.

When a crack jump occurs the microphone which is attached to the tank sends a trigger signal which causes the input signal to be retained. It can then be output to a chart recorder during a period of 20 seconds. At moderate cross-head speeds this can be completed before the next transient comes along.

7.3 Retrieved Signals

The output of the Instron load amplifier was connected to the transient recorder input and with a sweeptime setting of 2 seconds, the load/time characteristic obtained during a crack jump event was of the form shown in figure 7.3. However, load signals retrieved in the same manner for a number of jumps produced identical curves, regardless of height, of load peak or length of jumps. When tests were made on entirely different material, i.e. glass microscope slides, and identical curves were obtained, it became apparent that the above signal was false and was damped in order to allow for the slow response of the Instron pen recorder.

To by pass the filter of the Instron recorder for achieving faster response times, attempts were made to extract signals from before the demodulator stage. The signal retrieved here was of an ac form shown in figure 7.4. In the diagram it is evident that the energising frequency of the load cell 375 Hz, gave only $10 \times 10^{-3} S \times 375\ S^{-1}$ 4 cycles during the desired sweep time of the transient recorder, providing insufficient relevant information points. So that accurate load behaviour could not be recorded.

The final solution adopted was to retrieve signals with the aid of a separate load cell. When a mains powered dc supply was used to energise the cell, the extracted signal was rather noisy as shown in figure 7.5. This problem was overcome when dry cell batteries 6 volts total excitation voltage were employed as the energising source, see figure 7.6(a).

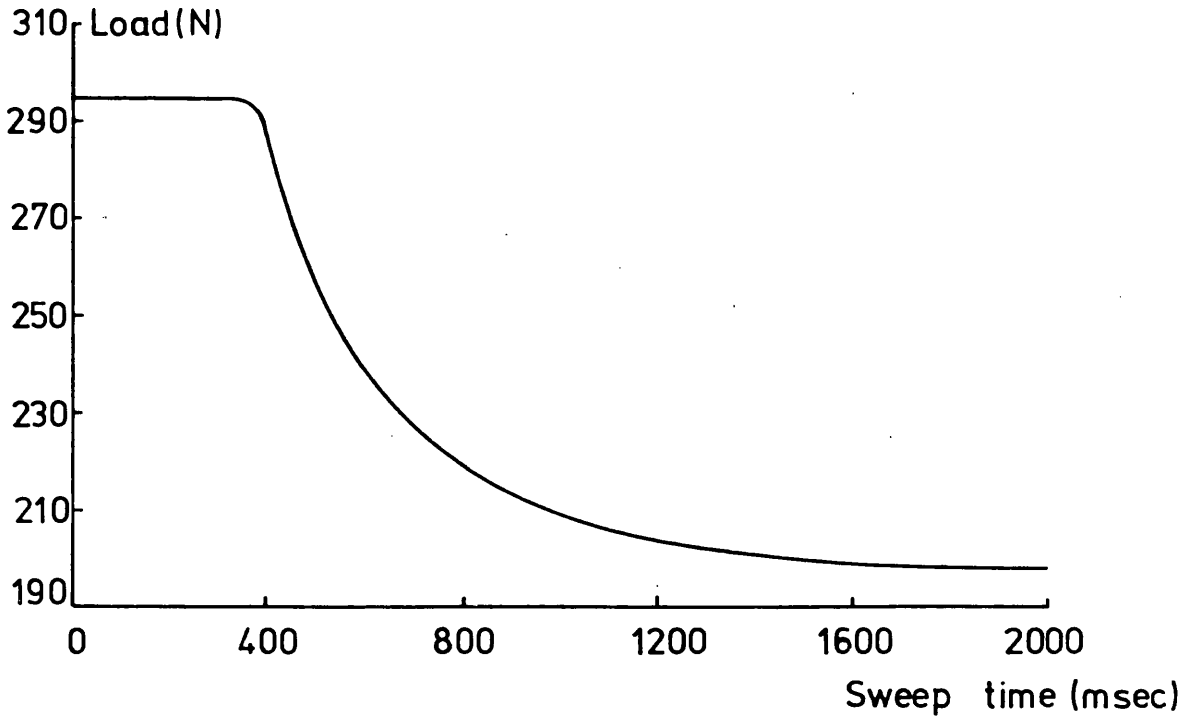

Figure 7.3 Load transient signal (signal retrieved from the output of the Instron load amplifier).

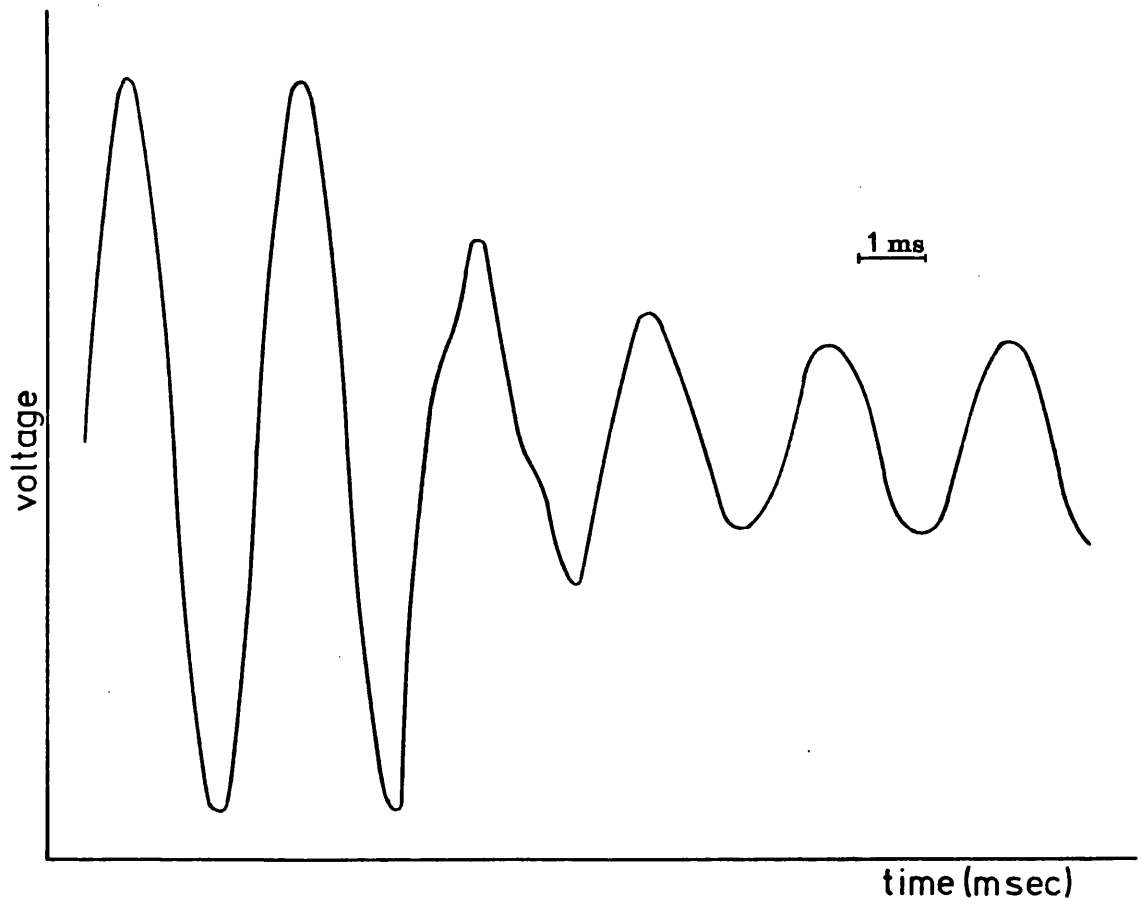

Figure 7.4 Load transient signal (signal from before the demodulator stage)

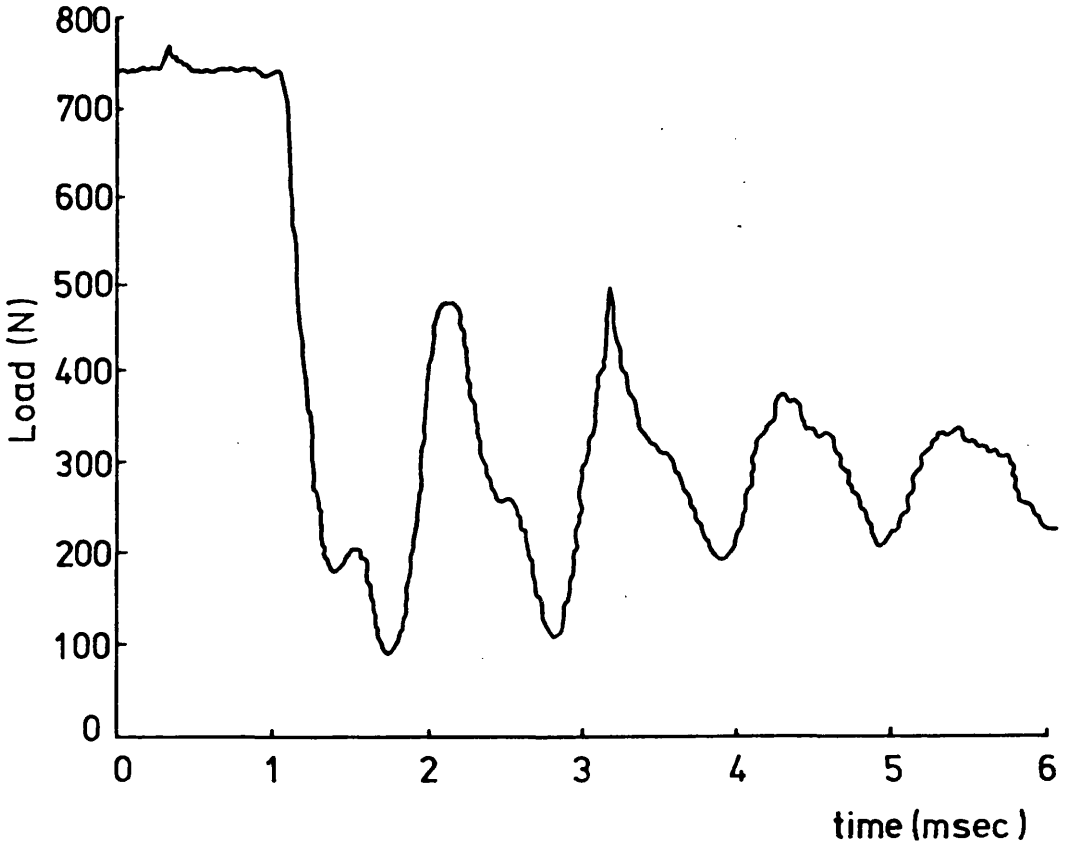

Figure 7.5 Load signal retrieved from JP load cell with main as energising source.

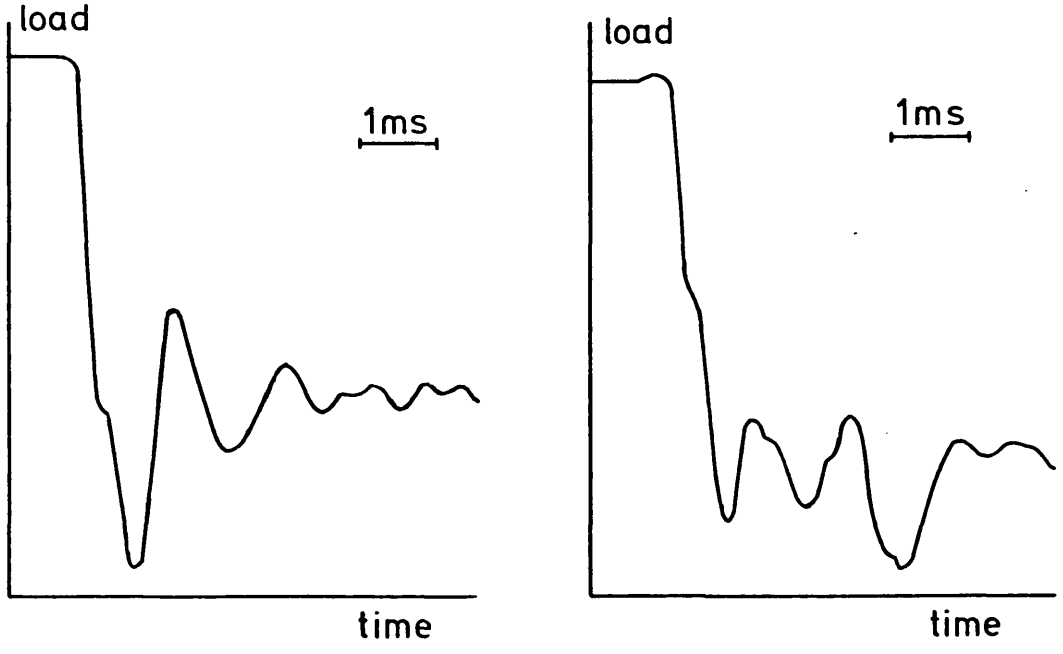

(a) Initial jump (b) Subsequent jump

Figure 7.6 Load signals for crack jumps.

The other distinctive feature in figure 7.5 was the presence of sine waves. These were attributed to vibrations in the specimen arms, induced by the crack jump. Over a number of tested samples, the quality of the signal was best for the initial transient and became poorer for subsequent jumps as the fractured arms got longer and vibration effects were more severe, as demonstrated in figure 7.6(b).

As indicated in section 5.2.3, the initial transient varied markedly from sample to sample influenced by the quality of the starter crack, therefore its behaviour could not be taken to represent a typical jump in the stick-slip propagation. To achieve the same quality of load signal as the initial transient, but with crack tip condition identical to those in the subsequent jumps, this procedure was adopted:

Using the double torsion test a crack was initiated in a dry sample and propagated to a length of about 5 cm. The sample top was then sawed off allowing for a crack tip 5 mm long which had a geometrical condition identical to those before the point of arrest in the presence of methanol. Coated with vaseline and immersed in methanol, the above sample was monotonically loaded and the load transient for the crack jump was recorded, see figure 7.7. A point of interest to be noted here was that the sweep time was of magnitude 5 milli-seconds. If this curve in turn is taken as the lowest estimate of crack speed during a jump, the speed is now established as being the fastest obtained from these signals i.e. in excess of 20 $msec^{-1}$.

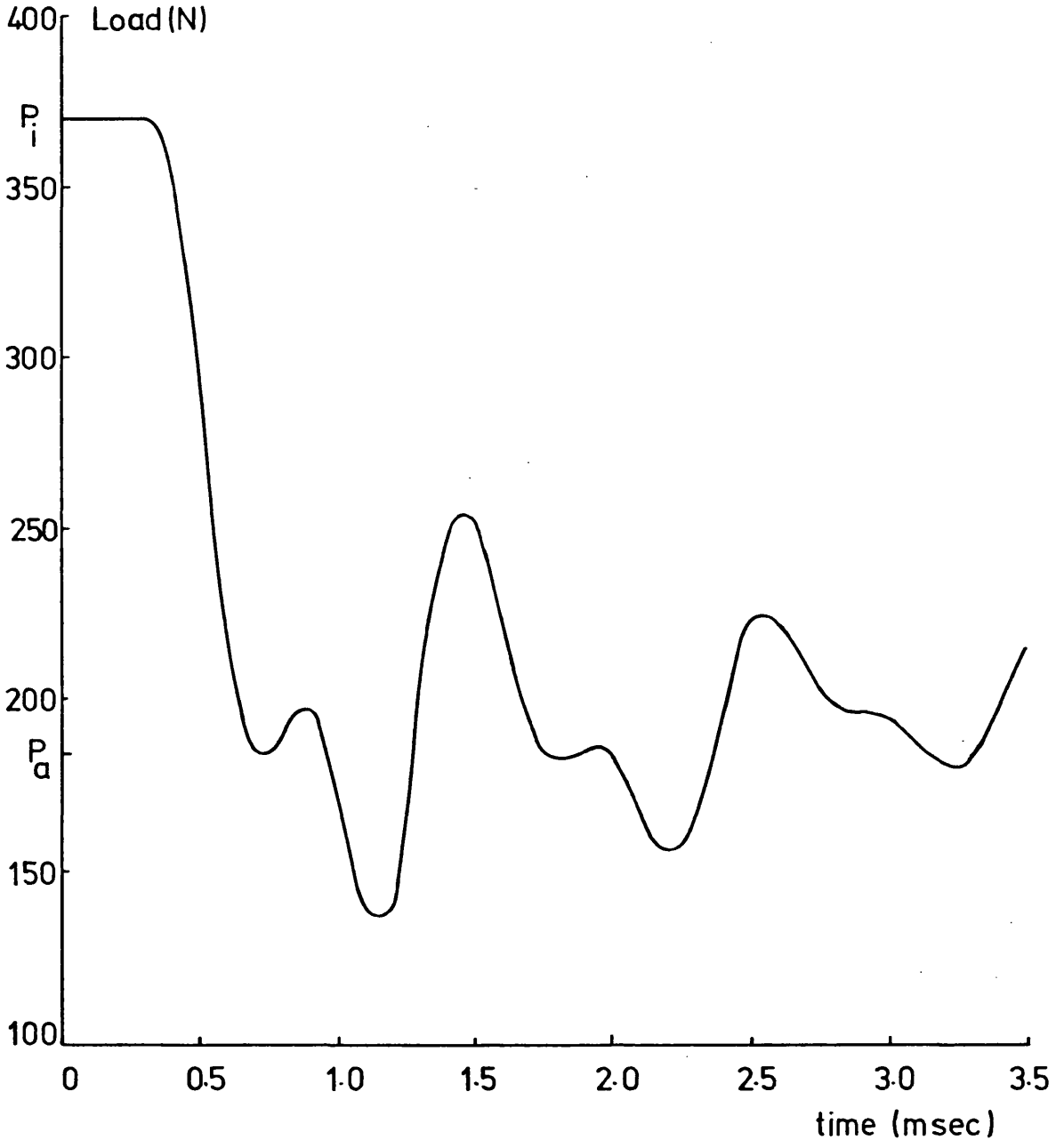

Figure 7.7 Load signal for a crack jump in methanol environment .

The corresponding values of P_i and P_a in figure 7.7 were evaluated from the voltage setting on the transient recorder, and were found identical to those measured by the Instron chart recorder.

In the analysis of K/v determination, the initial part of the curve was taken as the load behaviour in a jump event, omitting the vibration signal which was assumed to occur after the jump has taken place. Figure 7.8 in the next section shows the appropriate diagram of a load time curve during a jump achieved at a cross-head speed of 1 mm/min.

7.4 Determination of (K,v) Curve During a Crack Jump

The fastest load transient obtained which is shown in figure 7.8, gives the change of load during a crack jump. To process these results the values of P and t were manually interpolated at the cosine points and fed to a curve fitting programme (see appendix 3). A polynomial of P as a function of t, i.e. f(t) and its differential f'(t) were obtained. The programme is then designed to use these functions f(t) and f'(t) together with the constants A, B and ϕ in determining the values of K and v at any time t during the crack jump.

Figure 7.9 shows the curve of stress intensity vs crack front velocity derived from figure 7.8 via equations (6.2) and (6.14). Points of interest which should be considered here are:

(i) The curve shows two values of K for a given value of v. A similar effect has recently been reported by Kobayashi (74) who distinguished between a driven crack (high K) and a decelerating crack (low K). In the present case, the two K values presumably apply to different states of the material, ductile and brittle. For initiation of the crack tip through a heavily crazed region, a high stress intensity value is required. Once initiation occurs the stored elastic energy is released driving the crack through the virgin material. As a result the crack accelerates while the stress intensity value decreases. Ultimately this stored energy is exhausted and the crack slows to a constant velocity driven only by the energy supplied from the moving cross-head.

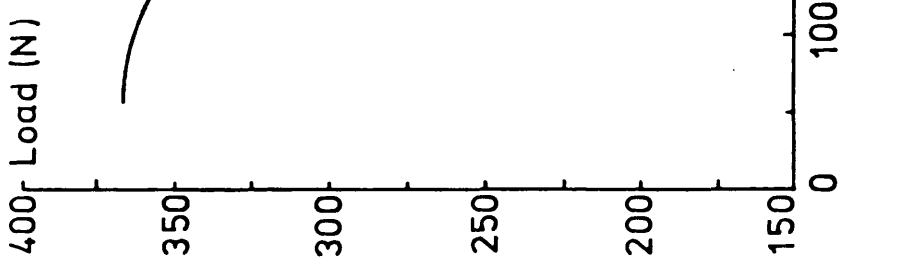

Figure 7.8 Load transient for a crack jump.

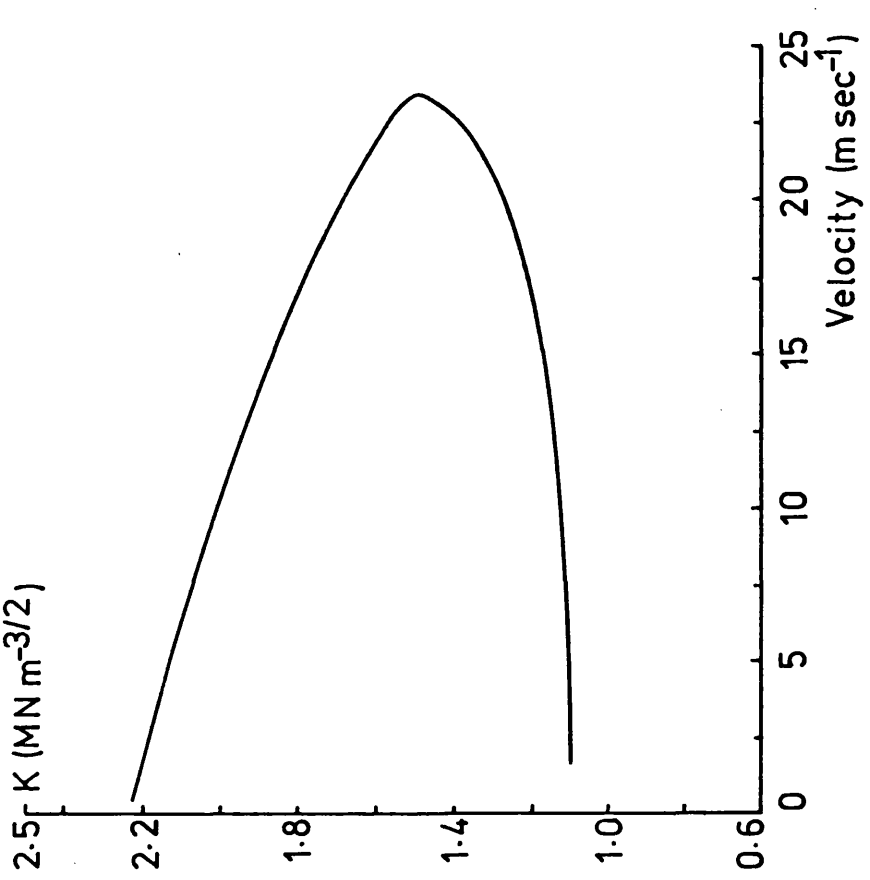

Figure 7.9 (K,v) curve for a crack jump.

(ii) The absolute value of crack speed observed are in the range of 1 to 24 $msec^{-1}$ on the same order of magnitude as the speed in impact tests on dry PMMA (38).

In determining their position, they were interpolated on the K(v) curve derived from air results, as shown in figure 7.10. From the diagram it is clearly evident that in the methanol case, higher crack initiation stress intensity value is required. With the crack running out of the methanol crazed zone, instability takes place and as a result the increase in v with a decrease in K, a behaviour identical to the air case although there is a shift towards higher values caused by the stored strain energy in the plasticized zone. However, with the strain energy exhausted, the decelerating crack speed with corresponding stress intensity values fitted in with the rest of the air results.

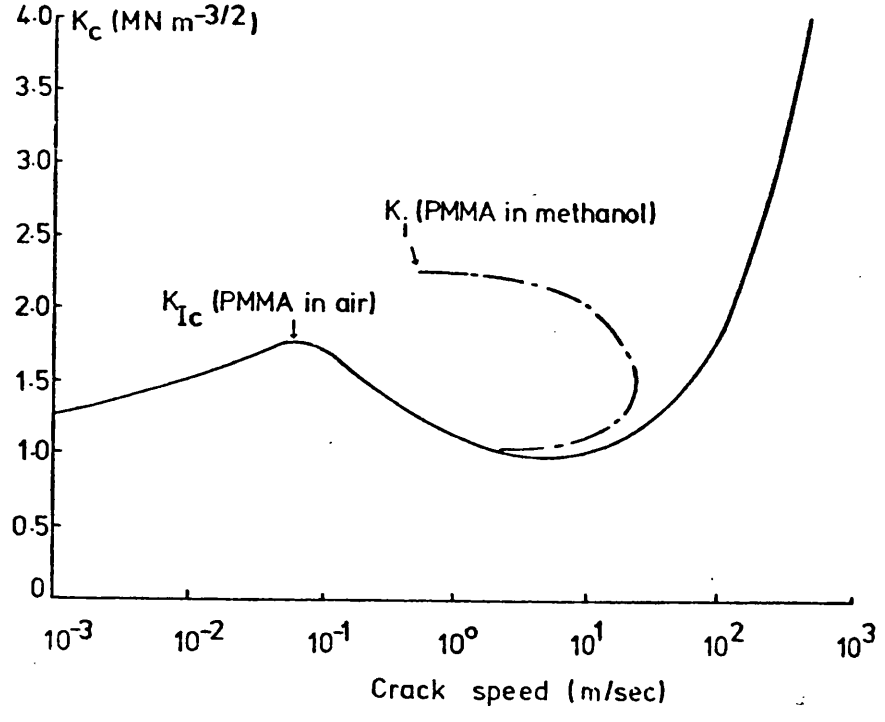

Figure 7.10 Stress intensity vs crack speed - PMMA.
—— after Marshall (92).
—·— present work.

PHASE IV

AN ANALYSIS OF CRACK PROPAGATION

CHAPTER 8: PROPOSED MODEL OF INITIATION AND ARREST EVENTS

CHAPTER 9: FRACTOGRAPHIC EVIDENCE

CHAPTER 10: ACOUSTIC EMISSION MEASUREMENTS

CHAPTER 11: TESTS PERFORMED IN DISTILLED WATER

PHASE IV AN ANALYSIS OF CRACK PROPAGATION

CHAPTER 8 PROPOSED MODEL OF INITIATION AND ARREST EVENTS

The model proposes an identification of the different events which occur during the fracture of PMMA both dry and in a liquid environment. This is achieved with reference to

(i) The load-time relationships retrieved either from the Instron chart recorder or in the case of load transients, using a transient recorder.

(ii) A fractographic study of the fractured samples, reported in Chapter 9, where the characteristic markings accompanying crack propagation are investigated.

It was stated earlier in section 6.2 that the relationship between load, crack length and time for a material under the test conditions employed can be expressed by equation (6.14) where

$$\frac{da}{dt} = \left[\frac{Z}{BP}\right]\left[1 - \frac{t}{P}\frac{dP}{dt}\right]$$

This will now be illustrated with the aid of the load/time curves obtained for the continuous and slip-stick behaviour.

For the initial rising load curve figure 8.1 (a, b) with stationary crack front

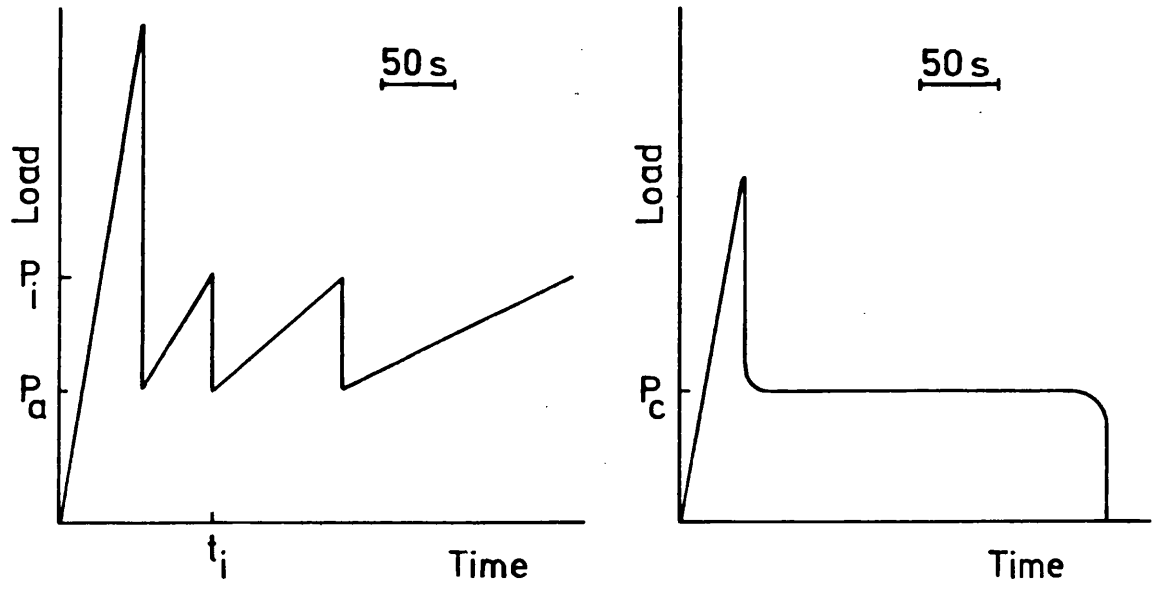

(a) Unstable, stick-slip propagation.

(b) Stable, continuous propagation.

Figure 8.1 Schematic load-time curves for crack propagation.

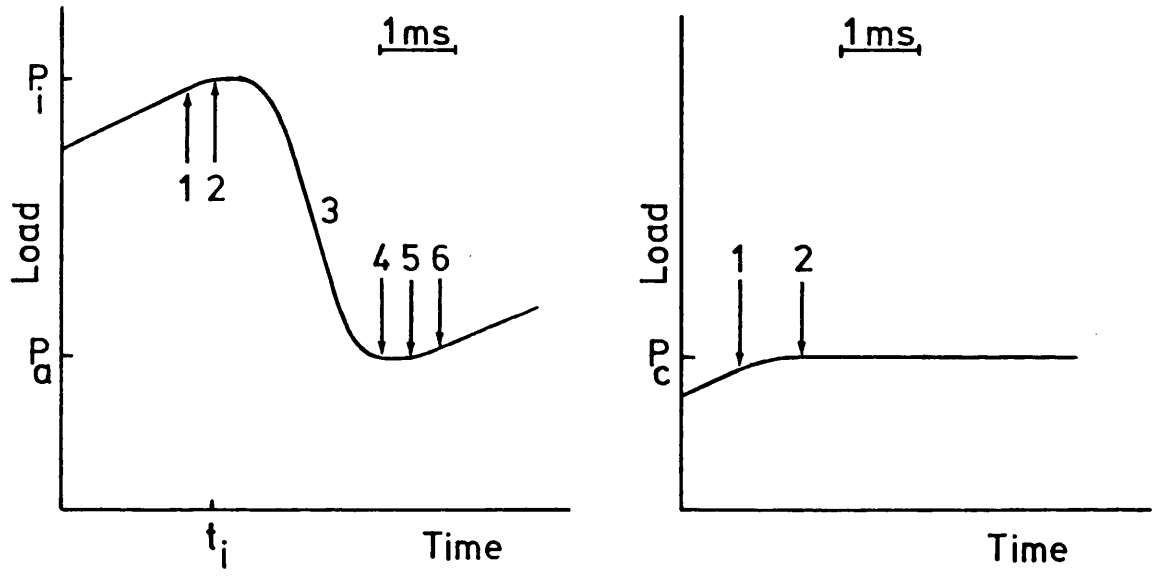

Figure 8.2(a) Transient curve (schematic).

Figure 8.2(b) Load-time curve at initiation for stable propagation.

$$\frac{da}{dt} = 0 \qquad (8.1)$$

so that equation (6.14) gives

$$\frac{dP}{dt} = \frac{P}{t} \qquad (8.2)$$

If the initial crack length is a_i then the compliance

$$C_i = Ba_i + C_o \qquad (8.3)$$

but $$C_i = \frac{Y}{P} = \frac{Zt}{P} \qquad (8.4)$$

$$\therefore \quad P = \frac{Zt}{C_i} = \frac{Zt}{Ba_i+C_o} \qquad (8.5)$$

and $$\frac{dP}{dt} = \frac{Z}{Ba_i+C_o} \qquad (8.6)$$

For constant cross-head speed Z, the slope of the rising load curve is determined by the instantaneous crack length. The value of $\frac{dP}{dt}$ for a stationary crack is of course the highest which can be achieved. By the same token, any slope below this value must represent an advancing crack front if visco-elastic effects are ignored.

The point at which crack growth commences can be identified when the relevant part of the load time graph is plotted on an extended

timescale, figure 8.2 (a, b). Evidently this is point 1 where the curve deviates from linear behaviour. Two cases to be distinguished:

(a) For stable propagation conditions and an ideally sharp starter crack the (P,t) curve, plotted on the extended timescale, will be as shown in figure 8.2 (b). The region of accelerating crack growth is seen to cover the range 1 to 2 where

$$\frac{Z}{(Ba_i+C_o)} > \frac{dP}{dt} \geqslant 0 \qquad \text{and correspondingly}$$

$$0 < \frac{da}{dt} \leqslant \frac{Z}{BP_c}$$

At point 2 defined by $\frac{dP}{dt} = 0$ equation (6.14) gives

$$\frac{da}{dt} = \frac{Z}{BP_c} \qquad (8.7)$$

while P_c remain constant, $\frac{da}{dt}$ is constant, as required.

(b) Next consider that the crack tip is either blunt or surrounded by a small zone of "plasticized" material or both such that the critical stress intensity factor is raised to a value K_i. Initiation of cracking occurs as before at point 1 (figure 8.2 (a))

The crack accelerates to a value

$$\frac{da}{dt} = \frac{Z}{BP_i} \qquad (8.8)$$

corresponding to equation (8.7) (point 2 figure 8.2 (a)).

But point 2 is merely a turning value in load after which $\frac{dP}{dt}$ increases in a negative sense and the crack accelerates continuously to a maximum velocity at point 3 which is near, but not identical to, a point of inflection of the (P,t) curve.

In the range 3 to 4 in figure 8.2 (a), $\frac{dP}{dt}$ becomes less negative and the crack decelerates. For the test situation specified, where the machine cross-head is moving at constant speed, the condition $\frac{dP}{dt} = 0$ (reached at 4), does not correspond to crack arrest, but to stable crack propagation at a speed given by

$$\frac{da}{dt} = \frac{Z}{BP_a} \qquad (8.9)$$

For PMMA/methanol where access of the liquid is restricted to flow along the length of the crack, a measurable length of stable crack growth occurs during the time taken by the liquid to "catch up" with the crack front (4 to 5 figure 8.2 (a)). This can be identified by characteristic markings on the fracture surface, as described in the next chapter.

Point number 5 can be identified as the point at which the liquid environment again begins to influence the crack tip. If, as normally assumed, the effect is one of "plasticization" and crack blunting, then K_a (or K_c) will no longer be adequate to sustain crack growth at constant speed. The crack will therefore decelerate further,

causing a rise in load, and if crack blunting is sufficient the crack will arrest, point 6. The conditions in this region are expressed by

$$\frac{Z}{BP_a} > \frac{da}{dt} \geqslant 0 \qquad \text{and correspondingly}$$

$$0 < \frac{dP}{dt} \leqslant \frac{Z}{(Ba_f + C_o)}$$

where a_f is the new crack length on completion of the jump.

The features of this proposed model may be summarised as follows:

(i) It presents the phenomena of crack initiation and arrest as a fast but continuous process, rather than as discontinuous processes, which seems inherently reasonable.

(ii) Crack velocity and the corresponding stress intensity can be traced throughout a load transient.

(iii) Certain aspects of the fracture appearance of test pieces can be satisfactorily explained.

CHAPTER 9 FRACTOGRAPHIC EVIDENCE

9.1 Introduction

The process involved in the fracture of solids are reflected in the appearance of the fracture surface. The individual events involved in failure are sculptured in the fracture surface and a proper interpretation of these markings yields valuable information to supplement theoretical studies and provide additional insight into the failure mecahnism. The fracture surface study is usually concerned with fracture behaviour, its origin, in which direction it has travelled and what has been its general nature.

This section discusses the characteristic markings accompanying the different stages of fracture for both stable and unstable propagation, then identifies the different phases of stick-slip propagation by uniting the fractographic study with the mathematical model of the process.

9.2 Identification of the Fracture Markings

The double torsion PMMA specimens fractured in both dry and methanol environments have shown distinctive fracture markings which can be identified with each condition.

Stable crack propagation in the dry specimen was accompanied by formation of very clear and characteristic fracture markings which will be referred to as "rib marks" (figure 9.1).

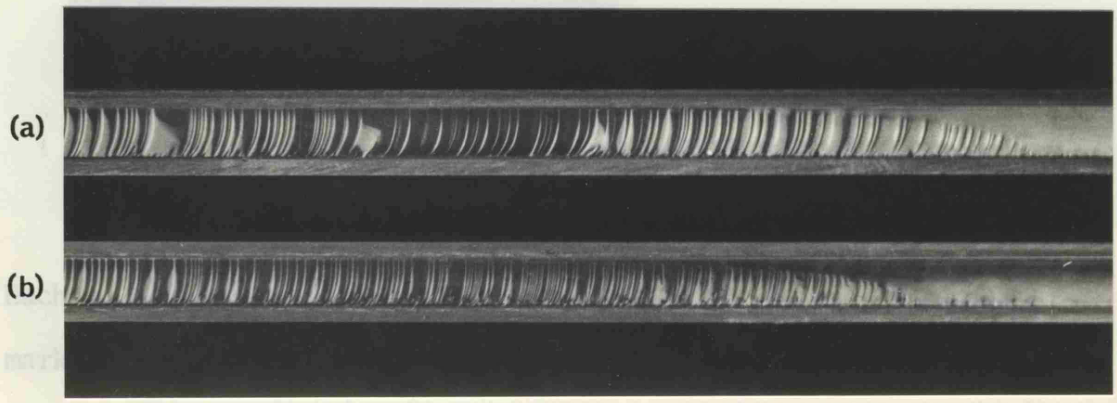

Figure 9.1 Fracture surfaces : PMMA in air.
Cross-head speeds (a) 1 (b) 20 mm/min.

The right hand end of this photograph also shows the smooth, relatively featureless surface associated with fast fracture as the crack is running out of material at the end of the specimen. The curved boundary between ribbed and smooth zones shows the form of crack front invariably observed in double torsion tests.

The rib marks observed, shown magnified in figure 9.2, appeared to correspond to those reported by several authors, for example Atkins, Lee and Cadell (75).

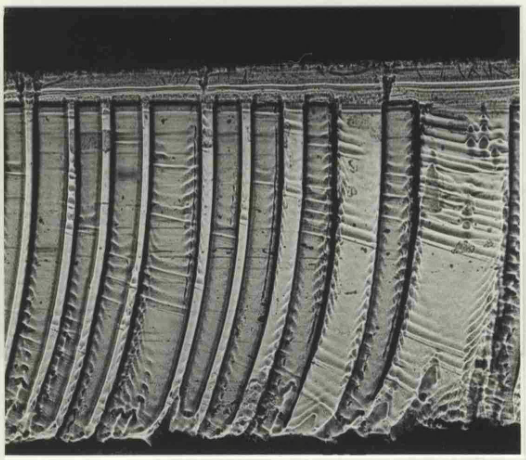

Figure 9.2 Rib marks on dry tested samples. X13.

Each "rib" is the locus of a point on the crack front. Whereas the marks are almost straight or slightly divergent on samples of the SEN and DCB type, they here take on a relatively complex curvature imposed by the test piece geometry. The observation of rib markings on double-torsion test pieces in PMMA does not appear to have been reported prior to this investigation (76), but it is interesting to note the similarity between figure 9.1 and the illustration of a stable fracture in epoxy resin by R. J. Young and P. W. Beaumont (figure 3b of reference 31).

For those samples tested under methanol, but previously coated with vaseline, such that the liquid has access to the crack tip only by flow along the length of the crack, a different type of cracking

behaviour was observed. This has been referred to as unstable or "stick-slip" behaviour and on examining the fracture surface of these specimens, three fracture zones have been identified (figure 9.3).

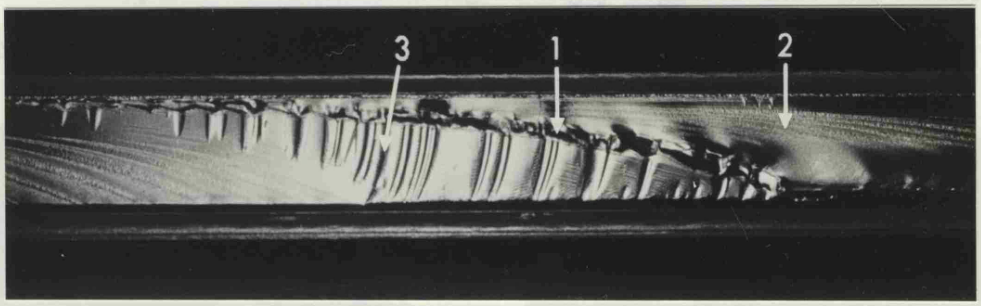

Figure 9.3 Fracture surface of PMMA sample tested in methanol showing fracture zones (X4).

(1) Heavily crazed zone.

(2) Smooth surface zone.

(3) Rib marked zone.

The following sections deal with the above regions, examining their physical extent as a function of test conditions, such as change in cross-head speeds and the presence or absence of vaseline coating.

9.2.1 Heavily crazed zone

This is identified as the region in which arrest of one crack propagation stage and initiation of the next jump occur. Inspection at high magnification (figure 9.4) shows it to be a region of heavy deformation, with much surface roughening, which is attributed to the combined action of local stress and methanol at the crack tip.

Evidence for its association with crack arrest is obtained by comparing this zone with the transition from stable to unstable propagation in a dry sample, figure 9.5, where no arrest occurs. In this case, no "crazed zone" is observed, and, taken together, the two types of fracture marking strongly suggests that the formation of crazes by the action of the methanol causes the crack to arrest.

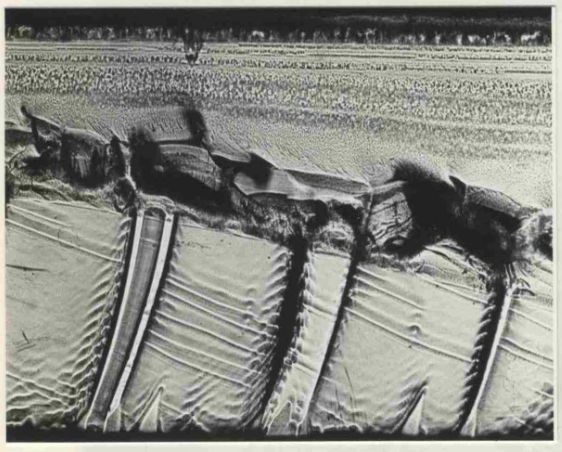

Figure 9.4 Rib marks with crazed zone on immersed (stick-slip) sample. X13.

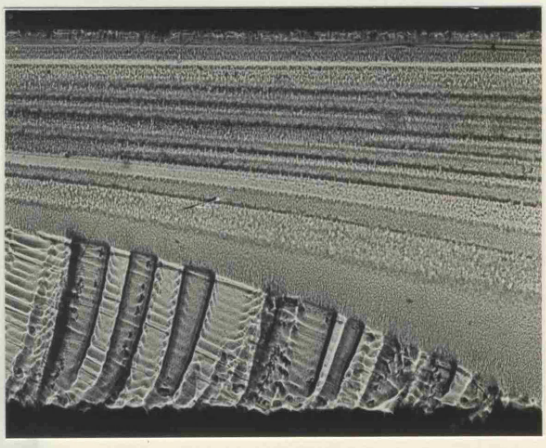

Figure 9.5 Rib marks on dry (all-stable) sample. X13.

Initiation of new growth and quasi-stable propagation through the crazed material occurs when a critical stress intensity value $K_i >> K_c$. The size of growth in the crazed zone is later showed to be machine speed dependent. At the point of initiation further increase in the strain energy drives the crack tip away from the plasticized region to the virgin material in condition where $\frac{dK}{dv} < 0$. The transition from stable to unstable must be defined by a border line which represents the point of instability.

Using a technique where the fracture surface is coated with gold before micrographic examination, see figure 9.6, the transition from stable growth in the crazed zone (mark A) to unstable failure identified with smooth surface (mark C) was observed to contain a narrow region of a shiny nature (mark B). This can represent a zone where crack sharpening processes commence, and

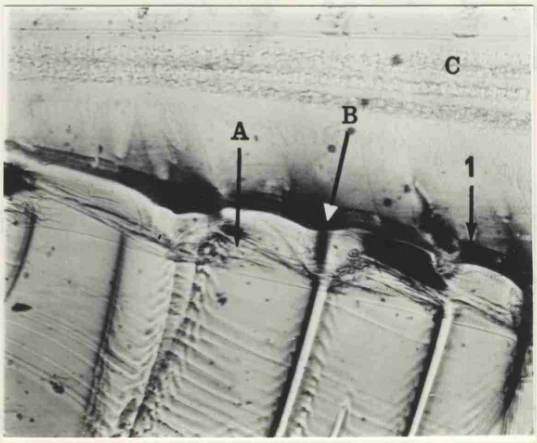

Figure 9.6 Identification of arrest and initiation zone. X16.

instability should then follow at the border line marked 1 in figure 9.6, where the sharp crack tip is driven rapidly by the released stored energy. From this figure it also appears that the arrest line between crack arrest and initiation in the crazed zone (region A) can not be defined.

Investigation into the effect of cross-head speed has shown that with the decrease in cross-head speed there was a progressive increase in the crazed zone, figure 9.7.

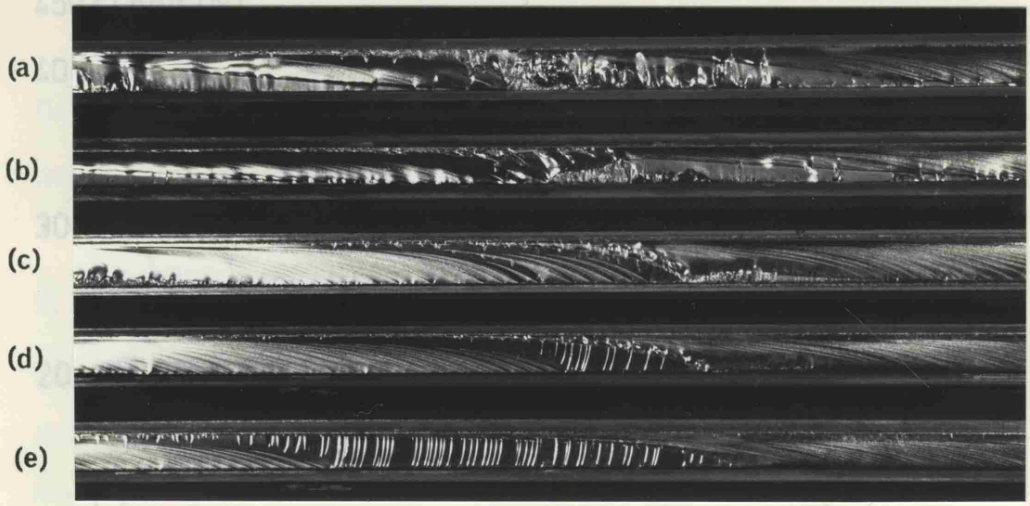

Figure 9.7 Fracture surfaces : grease coated PMMA samples in methanol. Cross-head speeds (a) 0.05 (b) 0.2 (c) 1.0 (d) 5.0 and (e) 20.0 mm/min.

This can be attributed to the prolonged presence of methanol at the crack tip. It was also assumed that the arrival of the environment at the crack tip changed the character of the material in that region, i.e. plasticized it, which causes the crack to decelerate and finally arrest. At low cross-head speeds, the time of contact between environment and crack tip is increased, because the rate of energy supplied to drive the crack through the plastic region into the virgin material is decreased. There is therefore opportunity for further diffusion of methanol. Both these features lead to further development of crazing at the crack tip before a jump is initiated.

The load-displacement curve obtained at low cross-head speed (e.g. 0.05 mm/min.) provides further evidence (figure 9.8).

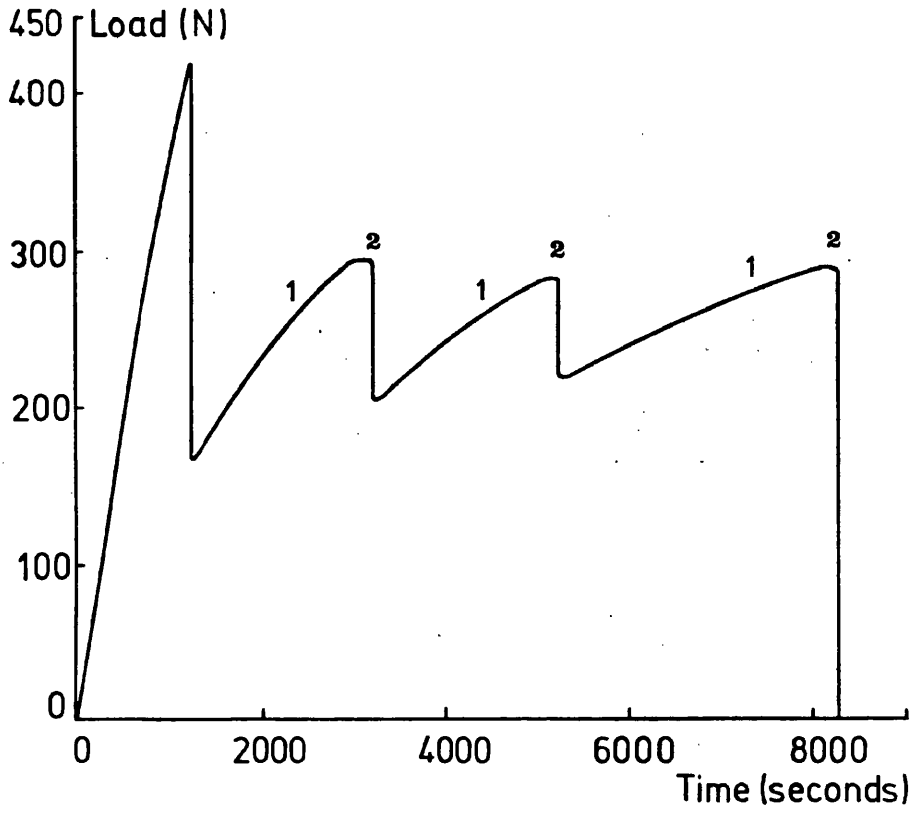

Figure 9.8 Load time (or displacement) curve for methanol test, cross-head speed 0.05 mm/min.

This figure clearly indicates that the compliance (i.e. $\frac{Y}{P}$) is not constant in the region 1 – 2, but has considerably increased before the load drop. In a double torsion test piece the compliance "C" is proportional to "a" therefore any change in compliance means a change in crack length. For the above condition this is a result of considerable growth in the crazed zone.

Further to the effect of cross-head speed, it was postulated above that at lower displacement rates:

(a) The methanol diffuses further into the crack tip and causes further plasticization.

(b) The rate of strain energy supplied to drive the crack out of the plasticized region is low.

In simple terms this means that the rate of swelling increases with the decrease in strain rate, a criterion for the apparent increase in K_i as shown in section 5.2.3. Ultimately however the value of K_i is found to level out and remains constant even with further reduction in the cross-head speed (figure 5.9). Presumably under this condition the crazed zone cannot maintain any further increase in the strain energy supplied by the Instron and crack growth commences.

9.2.2 Smooth Surface Zone

Fracture surfaces formed during unstable crack jumps were observed to have glassy smooth appearance with a sequence of parabolic marks identical with the crack profile (refer to figure 9.3).

The shiny surface is associated with the sudden failure as a result of rapid crack growth and has been reported before by Williams et al (38) and Atkins et al (75). Higher magnification has shown that the parabolic marks figure 9.9 comprise a densely populated region of conical marks identical to those of Atkins (75), reported for unstable behaviour.

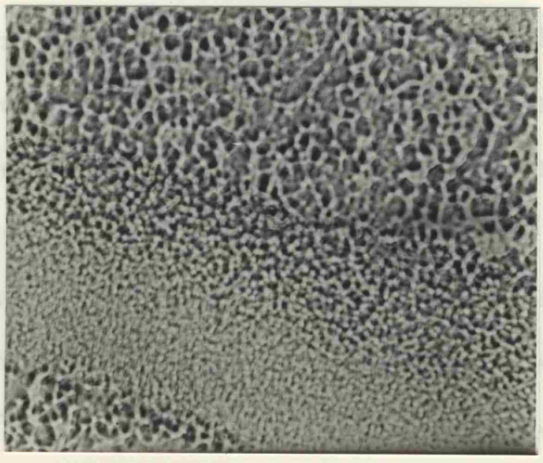

Figure 9.9 Smooth surface at high magnification. X130.

The coalescence of the voids in the crazed material at the crack tip is the prime factor for fracture markings, and the degree of coalesce is a function of the fracture toughness as discussed by Cotterall (77) and Lednicky and Pelzbauer (78). In the unstable region when the crack initiation toughness is high, crack speed is rapid and therefore limited time is available for the voids to

coalesce. Thus the total number of the effective secondary fracture nuclei increases producing a higher density of conical markings on the surface.

Regarding the parabolic marks, these could be what is referred to in the literature as Wallner lines (79). They are lines caused by travelling stress waves which are generated as the fracture originates, by the sudden release of elastic energy. The travelling waves magnify and distort the stress distribution at the crack front which produces the periodicity in the fracture surface.

In homogeneous materials, for example glass, a technique was developed to produce an evenly rippled surface by irradiating the specimen by ultrasonic waves generated externally throughout the duration of fracture (80, 81). The periodicity and orientation of the ripples provided a measure of the fracture velocity in terms of the known frequency of irradiation. Therefore the parabolic marks shown in figure 9.3, which in this case are due to self-generated stress waves, could reflect on the crack speed in that region; but since the frequency of the stress waves is unknown, there is no possibility of using this as a measuring technique.

The pattern of smooth surface zones on a test piece could be related to the load vs time behaviour. Where K_i and K_a are constant within a single test as normally observed (figure 5.6 (a)), these successive crack jumps are noted to increase in length in a manner predictable from the test piece geometry, as illustrated in the following analysis:-

By definition the compliance $C = \frac{y}{P}$.

Therefore on the load-time curve shown in the adjacent diagram

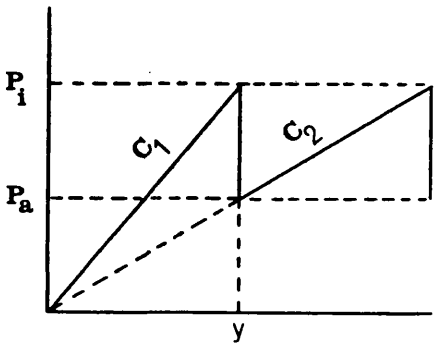

$$C_1 = \frac{y}{P_i} \quad \text{i.e.} \quad Ba_1 + C_o = \frac{y}{P_i} \qquad (9.1)$$

$$C_2 = \frac{y}{P_a} \quad \text{i.e.} \quad Ba_2 + C_o = \frac{y}{P_a} \qquad (9.2)$$

Equation (9.1) from (9.2) gives

$$B(a_2 - a_1) = y\left[\frac{1}{P_a} - \frac{1}{P_i}\right]$$

$$\Delta a = \frac{y}{B}\left[\frac{1}{P_a} - \frac{1}{P_i}\right] \qquad (9.3)$$

Where Δa = crack jump.

Therefore for tests where P_i and P_a remain constant, Δa is proportional to the deflection y. Within a test since y increases with time, the successive crack jumps will therefore increase.

The experimental results for the crack jumps are given in table 9.10 for three cross-head speed conditions. The initial jump (transient 0) was omitted since it usually has a high value reflecting the bluntness of the precracked tip and the consequent build up of elastic energy. With the successive transients, the general trends as expected shows an increase in the length of the jump within the same test.

It also appears from table 9.10 that the size of the jump for corresponding transient number had lower values at higher cross-head speeds. There was consequently an increase in the number of transients at the higher speeds. This effect is the result of the reduction in K_i (see section 5.2.3), which reduces the stored strain energy available to drive the crack forward.

Transient No.	Cross-head speed 0.5 mm/min	Cross-head speed 5 mm/min	Cross-head speed 20 mm/min
	Length of jumps (mm)	Length of jumps (mm)	Length of jumps (mm)
1	45	42	12
2	68	66	42
3	-	-	60
4			-
1	37	37	28
2	85	42	24
3	-	-	51
4			-
1	38	34	9
2	63	66	4
3	-	-	16
4			34
5			-
1	55	46	28
2	76	73	13
3	-	-	83
4			-

Table 9.10 Length of crack jumps for grease coated specimens immersed in methanol over a range of cross-head speeds.

9.2.3 Rib Marked Zone

Rib markings are seen to lie between the smooth fast fracture zone and the heavily crazed region (see figure 9.3).

Optical macrophotography at magnifications of up to 16X (figures 9.4 and 9.5) reveals no difference in detail between these rib marks formed on immersed (stick-slip) samples and those formed on dry (all-stable) samples. They may therefore be taken as an indication of stable growth following the crack jump. Much of the evidence for the proposed model of crack propagation comes from observations on the extent of stable "after growth".

Figure 9.11 shows influence of testing machine cross-head speed upon the fracture appearance of grease coated samples immersed in methanol.

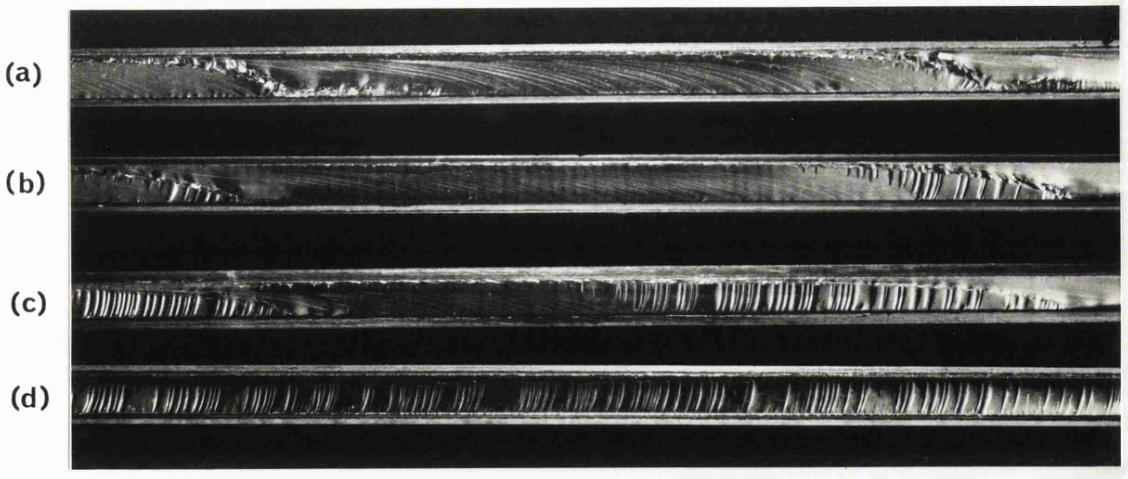

Figure 9.11 Fracture surfaces : grease coated PMMA samples in methanol. Cross-head speeds (a) 1 (b) 5 (c) 20 and (d) 50 mm/min.

For cross-head speeds 1, 5 and 20 mm/min. (figures 9.11(a), (b) and (c) respectively), a progressive increase in the length of the rib mark regions following a given crack jump is observed.

Following the above observation, a theory was postulated to try to predict the extent of stable growth identified by the length of the rib marks. As previously stated in section 5.2.3, there occurs over this range of cross-head speeds a negligible variation in K_a and small, but consistent decrease in K_i with increasing testing rate. The broad pattern is therefore the same throughout with about four crack jumps prior to final failure. During a crack jump the "total growth" S is measured from A to C as shown in the diagram below:

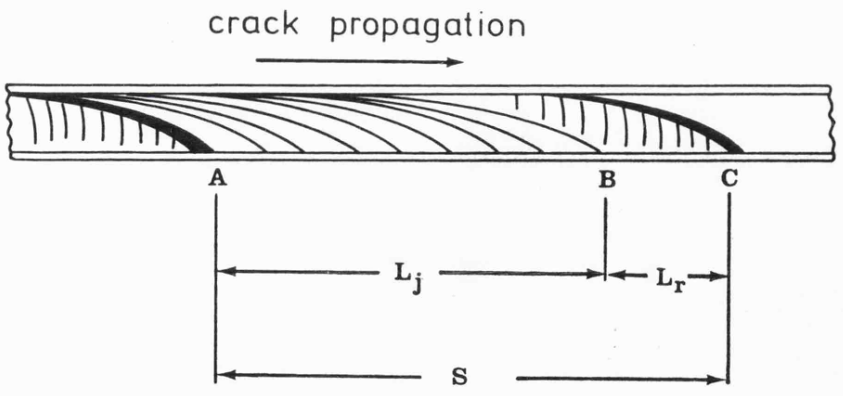

Schematic diagram of a crack jump

Assuming that the rate of flow of liquid methanol (v_L) along newly opened crack of similar profile is roughly constant then the time available for stable "after growth" identified with rib marks i.e. B ⟶ C is given by $\frac{S}{v_L}$ since the fast fracture is almost instantaneous.

The velocity of stable crack growth is given by

$$v = \phi \frac{da}{dt} = \frac{\phi Z}{BP_a} \quad \text{(refer to section 5.1.3)}$$

Where Z is the machine cross-head speed and B is the constant rate of change of compliance with crack length. Therefore the length of stable growth L_r is given as

$$L_r = \frac{\phi Z}{BP_a} \frac{S}{v_L} \qquad (9.4)$$

From the previous diagram $S = L_j + L_r$

where L_j length of the jump A ⟶ B

∴ equation (9.4) can be written as

$$L_r = \frac{\phi Z}{BP_a v_L} (L_j + L_r) \qquad (9.5)$$

rearranging (9.5)

$$\frac{L_j}{L_r} = \left[\frac{BP_a v_L}{\phi Z} - 1 \right] \qquad (9.6)$$

The theory therefore predicts the following:

(a) For crack jump of equal length, L_r should be proportional to the testing rate Z as demonstrated in figure 9.11.

(b) Within the same test, the length of rib marks (L_r) will be proportional to length of the jump (L_j), assuming v_L is constant.

i.e. $\frac{L_j}{L_r}$ = constant

In the double torsion test following the initial jump, successive jumps within the same test have shown an increase in length (table 9.11 in the previous section). Therefore for these same specimens, measured L_r values should follow in the same manner. These values are reported in table 9.12. At first sight the general trend seems to support the theory, however, when $\frac{L_j}{L_r}$ was evaluated for these conditions, the result was not constant as predicted by the theory, and a large scatter was observed. The discrepancy could be due to v_L which for the sake of simplicity was assumed constant. Methanol flow towards the advancing crack front could be of a complex nature, with certain aspects such as vibration in the specimen and vaseline squeezed through the crack surface, having an influencing effect.

In order to obtain a general idea about the effect of machine speed on the extent of stable growth, an average length of rib marks over the length of each sample was evaluated and is given in table 9.12,

Transient No.	Cross-head speed 0.5 mm/min	Cross-head speed 5 mm/min	Cross-head speed 20 mm/min
	Length of rib marks (mm)	Length of rib marks (mm)	Length of rib marks (mm)
1	7.2	3.2	7.2
2	10.0	9.1	8.1
3	-	-	22.8
4			-
1	4.4	12.0	9.2
2	8.5	8.0	13.1
3	-	-	16.0
4			-
1	12	7.2	10
2	1	14.5	5
3	-	-	20
4			42
5			-
1	4.0	8.0	25.5
2	6.5	14.3	24.9
3	-	-	-
Average No.	18.3	25.8	65.7

Table 9.12 Length of rib marks for same specimens given in table 9.10

for three cross-head values. It is clearly evident from the results that the overall size of rib marks (or stable growth) has considerably increased as the cross-head speed increased to 20 mm/min..

The onset of fully stable crack growth at a cross-head speed of 50 mm/min. with otherwise identical conditions (figure 9.11(d)) provides further corroboration. In this case rib marks were present over the whole length of the specimen. It can be supposed that the velocity of stable propagation under these conditions ($v = 8.7 \times 10^{-3}$ $msec^{-1}$) is sufficient for the crack front to remain ahead of the advancing liquid.

In this test rib marks are associated with stable growth and not for example with vibrations of the crack front accompanying rapid deceleration. This was proved when tests were performed under identical conditions on immersed grease-coated samples and on samples left uncoated so that the liquid should have immediate access to the crack tip. The tests were carried at two cross-head speeds:

(a) 20 mm/min (figure 9.13). Values of K_i and K_a and the duration of the load transients were such that the velocity/time history of the unstable propagation may be supposed identical. Rib markings however were entirely absent in the uncoated sample (magnified in figure 9.14), as would be expected if stable growth were suppressed by the environment.

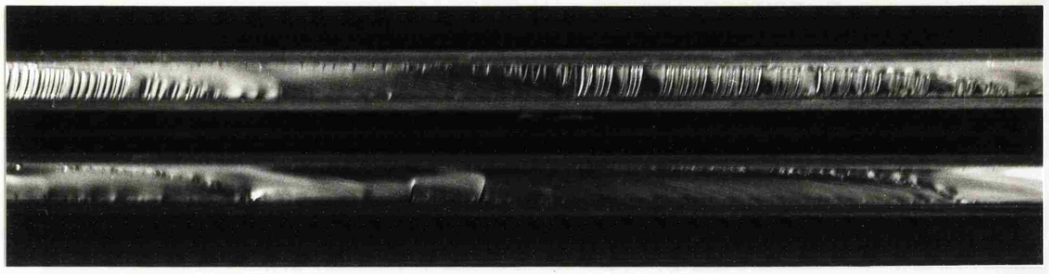

Figure 9.13 Fracture surface of immersed samples, cross-head speed 20 mm/min.
(a) Sample coated with grease.
(b) Sample free of grease.

Figure 9.14 As figure 9.13 magnification 16X.

(b) 50 mm/min. cross-head speed test, the fully stable crack propagation identified earlier with rib marks on the coated specimen figure 9.11 (d), totally changed to unstable behaviour with the absence of any rib marks on the surface for the uncoated specimen figure 9.15. Where we have in the former case the crack front remaining ahead of the advancing liquid, in the latter the liquid has immediate access to the crack tip and causes immediate bluntness.

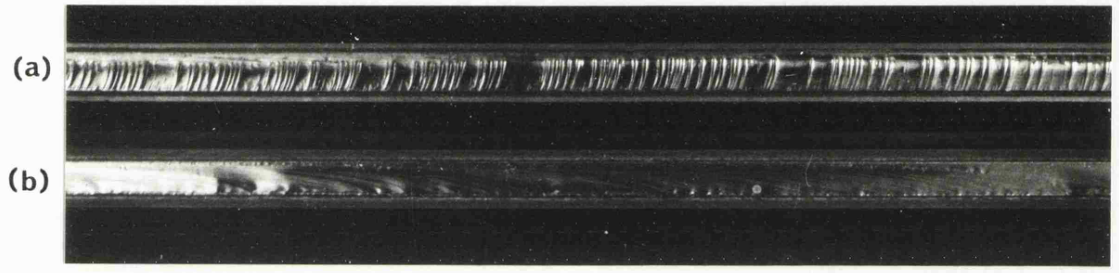

Figure 9.15 Fracture surfaces of immersed samples, cross-head speed 50 mm/min.
(a) Sample coated with grease.
(b) Sample free of grease.

Values of K_i and K_a for both coated and uncoated specimens are shown in table 9.16. The K values are more scattered for the uncoated samples since fluid flow is not controlled, and K_a values are statistically higher for the uncoated samples because fluid flow is from all sides. This gives a faster response time in blunting the crack tip, such that stable propagation with a sharp crack tip is never encountered.

Cross-head speed mm/min	Samples free of vaseline		Samples coated with vaseline	
	K_i $MNm^{-3/2}$	K_a $MNm^{-3/2}$	K_i $MNm^{-3/2}$	K_a $MNm^{-3/2}$
20	1.74 ± 0.15	1.39 ± 0.17	1.59 ± 0.12	1.23 ± 0.04
50	1.51 ± 0.06	1.27 ± 0.03	K_c = 1.32 ± 0.01 $MNm^{-3/2}$	

Table 9.16 Tests in methanol (free and coated specimens).

Finally fresh fracture surfaces of PMMA samples were found to exhibit bright colours. Initially these colours were thought to be the effect of light on methanol or vaseline left on the surface. However, dry and vaseline free specimens showed the same fracture surface colouration. This was also reported in papers by Higuchi (82) and Wolock (83). Broutman et al (30) have indicated that the observed colours vary with the angle of incidence of the light, and therefore an interference phenomenon is assumed responsible for this colour production, which is due to the difference in index of refraction of the oriented layer caused by fracture and the bulk polymer.

9.3 Correlation between fracture markings and the mathematical model

A summary of the mechanism of unstable crack propagation in the presence of liquid environment is presented in this section using an overall correlation between load-time curve and fracture markings.

In section 8, a single load drop corresponding to a crack jump was presented on a much extended time scale, together with the feature of fracture this is shown in figure 9.17.

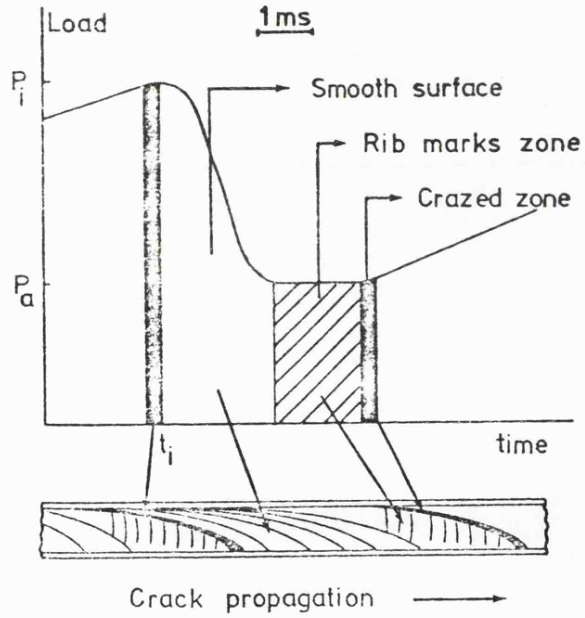

Figure 9.17 Relation of load transient to features of fracture.

It can be deduced from this figure that during a crack jump, the fast moving unstable crack decelerates progressively not immediately to rest, but to a constant velocity v_c corresponding to the value of stress intensity factor K_a and the rib marks after the jump represent this region.

The implication is that the crack does not simply stop because of the exhaustion of elastic energy. In the type of test described, elastic energy is being continuously supplied by the testing machine. For the crack to arrest some new phenomenon must intervene such that K_a ($\equiv K_c$) is no longer adequate to maintain the velocity v_c. The crack therefore decelerates (shown in figure 9.17 as the crazed zone), and under these test conditions an inevitable consequence is that the load rises. The point of true crack arrest therefore lies slightly above the minimum point of the load time curve of figure 9.17, being defined by the condition

$$\frac{dP}{dt} = \frac{P}{t} \qquad \text{(equation (8.2))}$$

with further supply of strain energy by the machine, further growth in the crazed zone commences at higher stress intensity value K_i as shown in the figure.

For PMMA in an aggressive liquid environment, it was deduced that the arrival at the crack tip of liquid left behind during the fast propagation phase, causes the crack to arrest.

CHAPTER 10 ACOUSTIC EMISSION MEASUREMENTS

In materials irreversible phenomena such as plastic deformation and the initiation and growth of cracks release minute quantities of strain energy, part of which is emitted as an elastic wave sometimes called a stress wave. Acoustic emission is the term used to describe these stress waves produced as a result of the application of stress to the material. In this project the technique is used to correlate acoustic emission with the type of observed crack propagation.

10.1 Introduction

Acoustic emission testing is now well established as a technique for the prediction of failure in materials. The principal concept is that opening flaws and moving cracks in the bulk or on the surface of deforming materials generate elastic stress waves which can be detected by a probe (or transducer) attached to the sample surface. The transducer which is mechanically driven by these stress waves sends out electrical signals which are magnified and can be processed with respect to their amplitude and rate of generation. The information obtained is used in connection with fracture processes and failure prediction.

The principle and application of acoustic detection in a variety of materials are well described in the literature by two ASTM (84, 85) publications. It was adopted by Evans et al (86, 87) for the analysis of crack propagation in polycrystalline alumina, and by

Fuwa et al (88, 89), Becht et al (90) and Sims et al (91) in the field of fibre-reinforced composite materials.

In this work acoustic emission technique was applied to the identification of crack propagation behaviour in association with load displacement curves and fracture surface markings.

10.2 Acoustic Emission Detection System

Acoustic emission measurements were made during fracture mechanics testing using double torsion test specimen in dry and immersed conditions.

The apparatus lay out for detection of the acoustic signals is shown in figure 10.1. The signal is detected by a P.Z.t-5 (lead Zirconate titanate) piezo electric transducer coupled firmly to the specimen surface with a layer of silicone grease. This prevented loss of acoustic signal at the transducer sample interface. In environmental tests the transducer was sealed in a fine rubber sheath before being attached to the sample. The detected signal is passed through a Dunegan 3000 series equipment for amplification and processing. In the Dunegan an S/D - 60P pre-amplifier boosted the signal from the transducer by 1000 X (60 dB), and contained a band pass filter where low frequency electrical noise in the laboratory of magnitude < 100 KHz was eliminated. The main amplifier was set for a further gain of 10 X (20 dB) giving an overall gain of 10000 X (80 dB). The amplified signal was then passed to a discriminator with adjustable triggering level, where a procedure known as ring down counting takes place. Rising electrical pulses which exceed a given threshold voltage are counted as individual events (refer to figure 10.2). These pulses or events were displayed cumulatively on a digital counter and plotted as a function of time on a chart recorder.

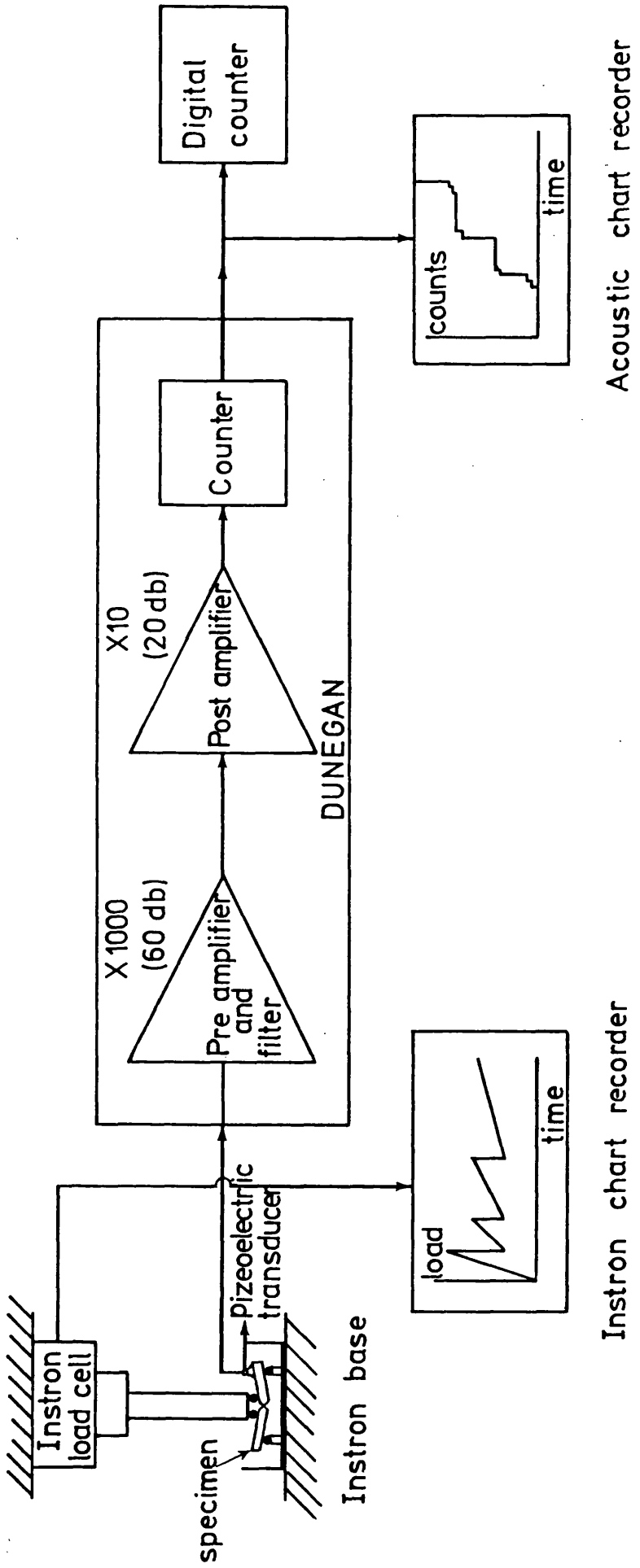

Figure 10.1 Acoustic emission system.

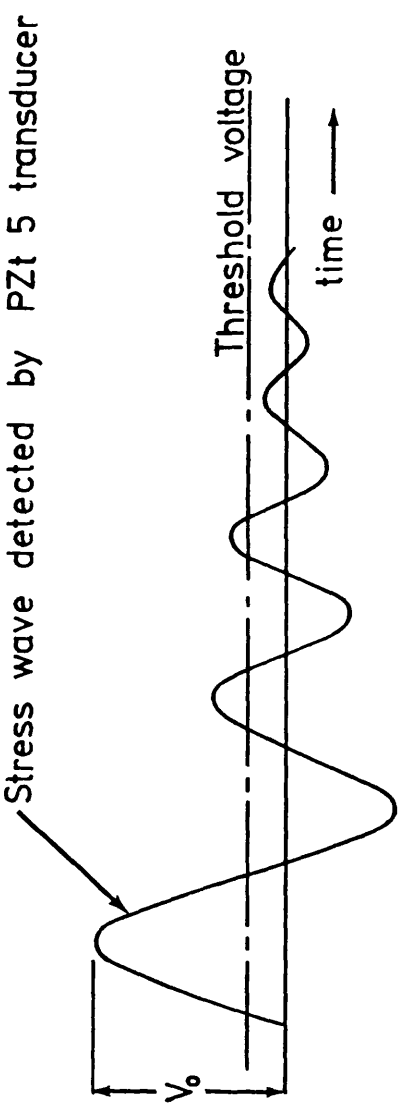

Figure10.2 Ring down signal.

10.3 Results and Discussion

Acoustic emission measurements during crack growth:

Stable crack propagation identified earlier with stress intensity factor K_c and the crack velocity v provided an acoustic emission curve shown in figure 10.3 with the corresponding load/time curve. From the figure the initiation of the blunt pre-starter crack at a load P_i gave a burst of acoustic emission. As the test proceeded, stable crack propagation occurred maintaining the load constant at P_c, while the total acoustic counts progressively increased. At failure the crack accelerated rapidly emitting a burst of counts.

The unstable crack propagation obtained in methanol tests showed bursts of acoustic energy during crack jumping only - on the load-time curve P_i falls to P_a, see figure 10.4. However, a few acoustic counts were sometimes recorded at initiation and immediately following a crack jump. The latter may be taken to represent the final movements before arrest.

Discussion:

In the process of stable crack propagation, slow growth of relatively small fracture - initiating flaws shown in the fracture surface within rib-like marks (figure 9.1, page 127) generate bursts of emission of relatively low amplitude (as may be deduced from the small number of counts generated (figure 10.3). In crack jumping

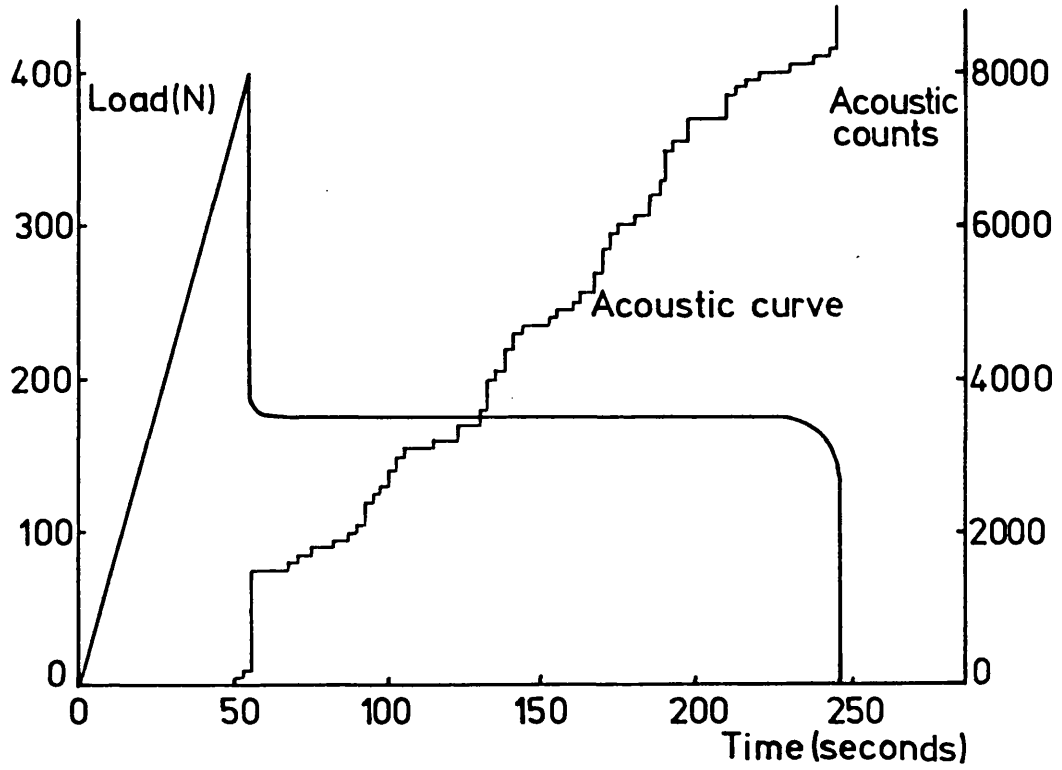

Figure 10.3 Stable crack propagation .

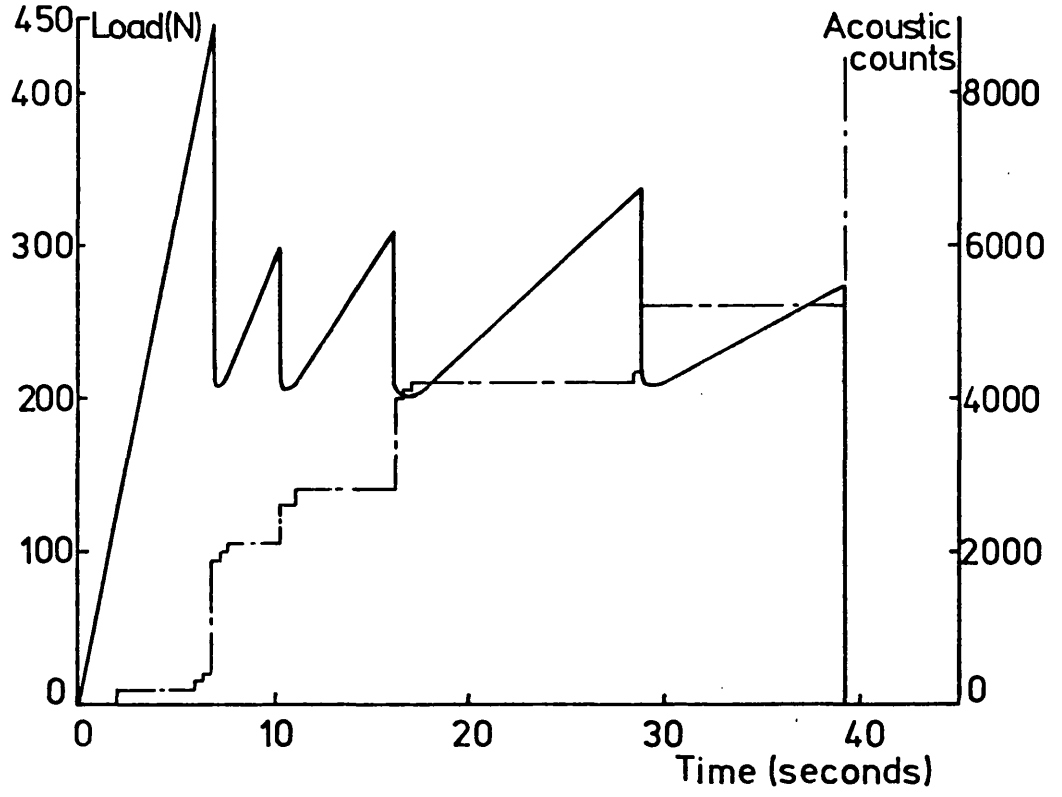

Figure 10.4 Unstable crack propagation .
—— load-time curve .
—·— acoustic curve .

behaviour, however, rapid crack growth occurs and substantial emission is obtained following the jump, figure 10.4.

The few counts observed at initiation and pre arrest in the latter case are as a result of slow growth at initiation and stable growth after the jump. These are identified earlier on the fracture surface with crazed zone and rib marks zone respectively.

CHAPTER 11 TESTS PERFORMED IN DISTILLED WATER

These tests are carried out to establish whether stick-slip propagation observed in PMMA samples is unique to the presence of methanol. Water is chosen as the control environment since it is chemically less aggressive than methanol, and therefore can be regarded as one which probably will have a less effect in altering the polymer behaviour. Identical testing techniques and procedures are adopted in order to carry out a comparison of results obtained in the two environments. This can provide further understanding in the mechanism of environmental fracture.

11.1 Experimental results

(a) Preliminary tests.

Double torsion tests were performed on sharply notched specimens immersed in distilled water. Since water does not cause surface crazing in PMMA, no grease coating was required.

The crack jumping behaviour reported for methanol was again the distinctive feature, with a similar mechanism of environmental attack i.e. plasticization of the material at the crack tip and effectively more energy required for crack initiation. However, the behaviour of these jumps in the water environment seemed to be influenced by the condition of the pre starter cracks, judged from the initiation load.

Where the starter crack was "sharp" enough to give initiation load P_i < 50 kgf, the load drop was much less sudden, and quasi-stable propagation was observed. On the load/time curve figure 11.1(a) irregular saw tooth behaviour was observed. By contrast rapid jumps followed by sudden arrest followed in specimens with induced cracks for which P_i > 50 kgf. The characteristic load/time curve can be seen in figure 11.1(b), and it demonstrates regular jumping.

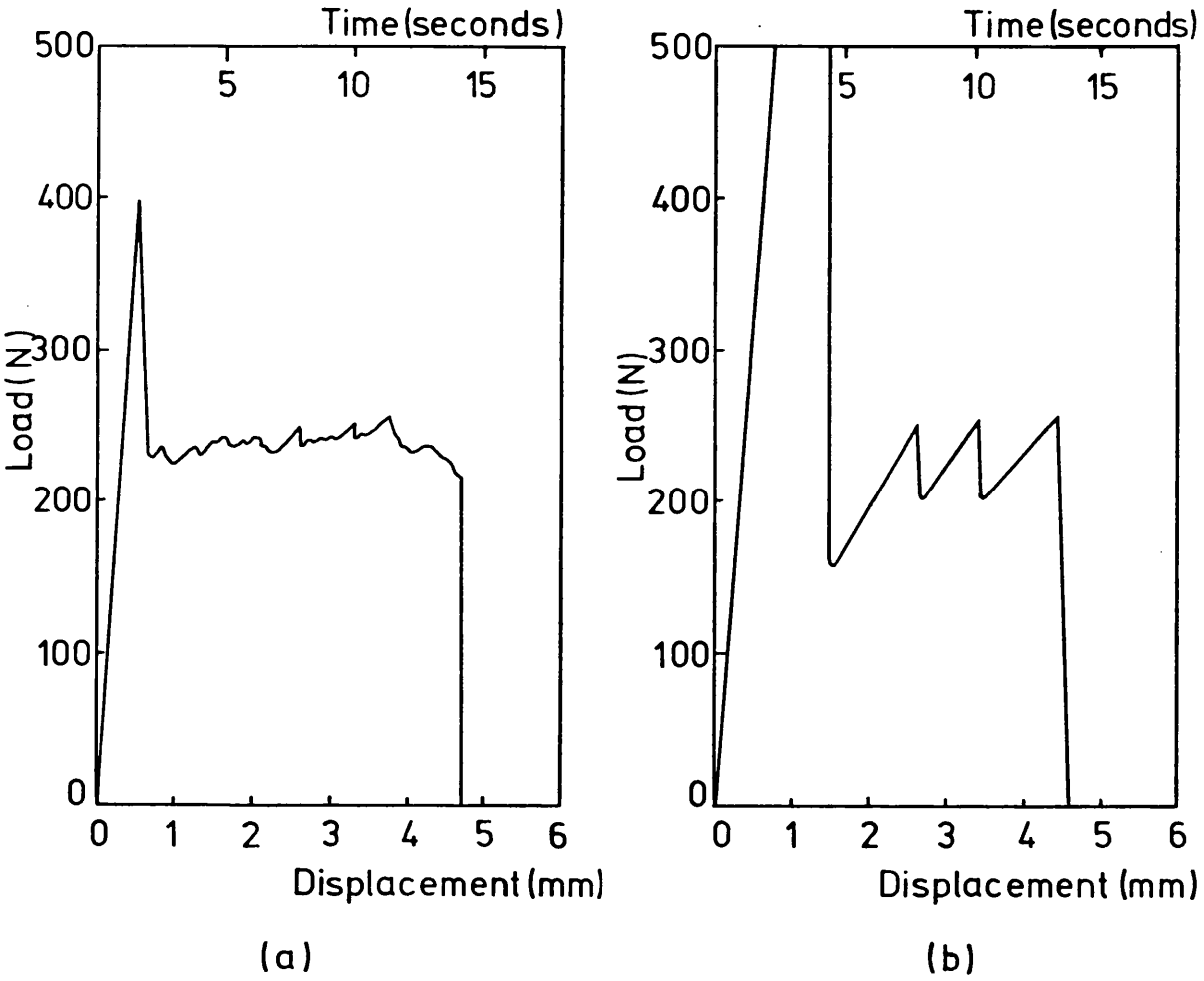

Figure 11.1 Load-time (or Load-displacement) curves for PMMA specimens in distilled water. Cross-head speed 20 mm/min.
(a) Starter crack with P_i < 50 Kgf.
(b) Starter crack with P_i > 50 Kgf.

The value of P_i reflects the condition of the crack tip with higher values for the more blunt ones. Consequently blunt starter cracks which term will refer to those with P_i > 50 kgf, provide regular jumping behaviour. In establishing this phenomena, specimens without sharp cracks were used in water tests. The results showed consistency in the regularity of jumping within a test and over a range of cross-head speeds. The explanation could lie in the mobility of the fluid. It was apparent that water flow towards a moving crack was too slow to cause an immediate and effective wetting at the crack tip. However, using specimens with blunt starter cracks provided initial jumps with high energy release rate, and as rapid fracture occurred, a sudden vacuum was created which aided the transport of the water environment. For a regular sequence of these type of jumps to occur will ultimately rely on the initial event.

Specimens with regular jumps, the stress intensity values at initiation arrest were evaluated and shown in table 11.2, with the corresponding cross-head speeds. The scatter in these values must be attributed to the testing conditions since fluid flow was not controlled.

Number of Samples	Cross-head Speed mm/min	K_i $MNm^{-3/2}$	K_a $MNm^{-3/2}$
5	0.5	1.67 ± 0.06	1.23 ± 0.03
3	2.0	1.57 ± 0.08	1.25 ± 0.02
4	5.0	1.61 ± 0.09	1.23 ± 0.03
3	20.0	1.66 ± 0.10	1.25 ± 0.06

Table 11.2 Tests in distilled water, specimens free of vaseline and with a blunt starter crack.

In identical conditions, i.e. free of vaseline samples and a cross-head speed of 20 mm/min, methanol results have shown higher K_i and K_a values, (see table 9.16 page 147). K_i and K_a represent stress intensity values at crack initiation and arrest respectively. With the absence of vaseline, the liquid has immediate access to the crack tip, therefore higher K_a obtained in methanol environment reflects on the rapid speed of methanol in comparison with water to suppress a crack jump and causes arrest.

With respect to K_i, for the same contact time between crack tip and environment, methanol compared to water diffuses further into the material at the tip. The result is a larger crazed zone in the case of methanol leading to higher K_i values.

(b) Investigation of end flow effect.

Fracture of PMMA in methanol and water provided a crack arrest mechanism, where the liquid is capable of catching up a running crack front and altering its tip condition. The degree of mobility and effectiveness of these liquids for immediate arrest action is assessed and compared by controlling the flow mechanism of environment during fracture.

Vaseline coated specimens (uncracked), provided this condition where liquid flow was restricted through the crack end.

The results with the water as liquid environment given in table 11.3 have shown (a) stick-slip propagation over cross-head speeds of 0.2 and 0.5 mm/min. and (b) stable growth with a constant K_c and crack speed at cross-head speed of 1.0 mm/min.. Under the same condition methanol tests showed continuous cracking at a high speed of 50 mm/min..

Cross-head Speed mm/min	K_i $MNm^{-3/2}$	K_a $MNm^{-3/2}$
0.2	1.31 ± 0.08	1.14 ± 0.05
0.5	1.40 ± 0.08	1.20 ± 0.05
1.0	K_c = 1.13 $MNm^{-3/2}$	

Table 11.3 Tests in distilled water, specimens coated with vaseline and with a blunt starter crack.

The jumping behaviour in water environment was similar to that observed in methanol where the jump was followed by a period of stable growth before arrest. The duration of steady growth increased with the increase in cross-head speed until fracture in the specimen was entirely continuous. This was more evident from the fracture surface of these specimens (see section 11.2).

Continuous cracking achieved in the presence of methanol or water is a result of the liquid being entirely left behind by the steady speed running crack. An effect which can be attributed to the chemical nature of the liquid such as viscosity. Methanol with the lower viscosity is more mobile and therefore high crack velocity is necessary to prevent tip plasticization. This is confirmed when crack speeds are obtained using cross-head speed values, equation (4.9), and correlated with the corresponding viscosity of the liquids, table 11.4. These results suggest that a small change in viscosity leads to a larger difference in crack speed to maintain continuous cracking.

Environment	Viscosity Nsm^{-2}	Crack speed $msec^{-1}$
Methanol	0.594	87×10^{-4}
Water	1.00	1.8×10^{-4}

Table 11.4 Viscosity of Environment with crack speed value.

Stick-slip propagation under the controlled flow conditions has shown K_i higher in methanol than in water, whereas K_a in both water and methanol are of the same magnitude. (Compare results in table 11.4 and 5.8.) The higher K_i values again reflect on the size of the crazed zone due to methanol as discussed in the previous section.

The similarity in K_a is due to the test conditions. Since in a vaseline coated specimen liquid flow occurs mainly during the steady state region, therefore a change of environment is likely to alter the duration of stable growth as shown before, rather than change the arrest intensity value K_a which follows the steady state.

11.2 Fracture appearance

Following the fractographic work on the PMMA/methanol system, a similar study was conducted on specimens fractured in water. Examination of the fractured surfaces obtained in the two conditions (i.e. methanol and water) have shown identical marks, therefore in conjunction with the previous identification of fracture marks (see section 9.2), the type of crack growth in water tests was demonstrated.

The condition of the pre-starter crack was reported in the previous section to influence growth behaviour, this was clearly shown on the surface, figure 11.5.

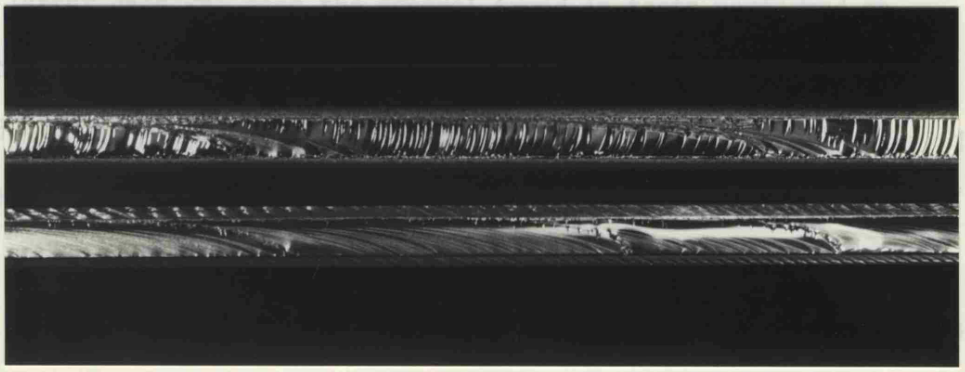

Figure 11.5 Fracture surface of PMMA samples tested in distilled water.
(a) Initial transient P_i < 50 kgf.
(b) Initial transient P_i > 50 kgf.

Although the two specimens in the above figure were tested under the same conditions except for the induced crack, the surface marks clearly illustrate a difference in crack propagation behaviour.

In the former figure 11.5(a), the sample with a non-blunt initial crack had smooth surfaces (characteristic of rapid failure) in small areas within large regions of rib marks (reminiscent of continuous cracking). Whereas the specimen with a blunt starter crack, figure 11.5(b), the smooth surface was of a longer length with the absence of rib marks. This clearly indicates that:

During crack propagation in specimen (a) the liquid environment was left behind during most times of the test, while in (b) instant wetting of the crack tip by the environment lead to immediate arrest (on the load/time curve figure 11.1(b), a sharp rise in the curve).

The latter case was also the general trend in tests performed on specimens without initial cracks, over a range of machine speeds as demonstrated in figure 11.6. Under these conditions the following observations were made:-

(1) The length of the jumps within each sample progressively increased as shown from the results in table 11.7. This is predicted from the test piece geometry as discussed in section 9.2.2.

(2) The absence of rib marks at all ranges of machine speeds, see figure 11.6, a phenomena by now accepted as instant wetting of crack tip.

(3) The plasticized zone showed a tendency to decrease in length with the increase in cross-head speed, results reported in table 11.7. This behaviour is in agreement with the methanol type tests (see section 9.2.1).

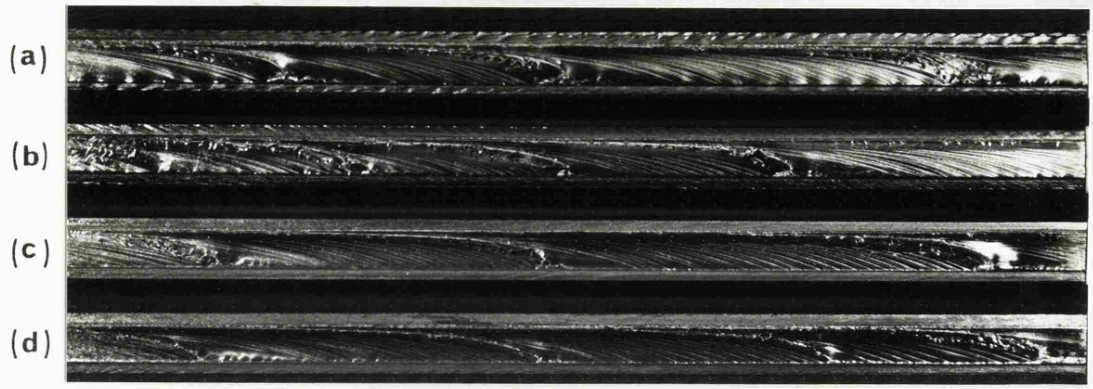

Figure 11.6 Fracture surfaces. Free of grease PMMA specimens with a blunt starter crack, immersed in distilled water. Cross-head speeds (a) 0.2 (b) 0.5 (c) 5.0 and (d) 20 mm/min.

Transient No.	Cross-head speed 0.5 mm/min.		Cross-head speed 5.0 mm/min.	
	Length of jumps (mm)	Length of crazed zone (mm)	Length of jumps (mm)	Length of crazed zone (mm)
1	24.5	2.5	17	0.5
2	38.5	4.0	26.5	0.5
3	75.0	1.5	46.0	0.7
4	-	-	-	-
1	33	2.5	46.5	0.3
2	58.1	2.1	67.0	0.5
3	-	-	-	-
1	18	2.0	84	0.8
2	28	2.0	61	0.5
3	36.5	2.5	-	-
4	76.5	2.5		
5	-	-		

Table 11.7 Length of crack jumps for PMMA specimens immersed in distilled water.

Fractographic evidence of end flow effect:

Fracture surfaces for specimens with controlled flow mechanism (i.e. with vaseline coating) are shown in figure 11.8(a), (b) and (c).

The presence of rib marks clearly indicates stable growth in conditions where the water flowing between the created surface is left behind. With the arrival of water at the crack front, propagation ceases and a jump identified with smooth surface follows.

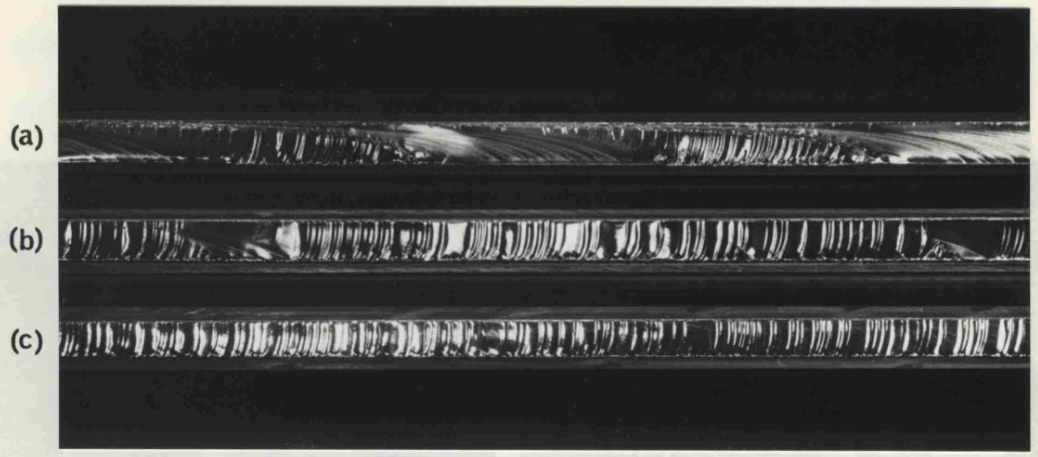

Figure 11.8 Fracture surfaces : grease coated PMMA samples with a blunt starter crack, immersed in distilled water. Cross-head speeds (a) 0.2 (b) 0.5 (c) 1.0 mm/min.

The effect of increasing the cross-head speed is an increase of continuous growth, as a result more rib marks are observed on the surface (compare figure 11.8(a) and (b)). Consequently full stable growth can be obtained at a speed where the rate of strain energy supplied is enough to keep the crack running ahead of the fluid. In water tests, this is achieved at a cross-head speed of 1 mm/min.,

and the specimen surface showed a continuous line of rib marks (see figure 11.8(c)). Whereas in methanol environment, due to the higher mobility of methanol, a cross-head speed of 50 mm/min. is required to give the same effect. (Compare figures 11.8(c) and 9.11(d).)

It is also worth comparing here the crazed zone which was caused by the presence of each environment at the crack front, figure 11.9. For the same testing conditions the crazed zone due to methanol shows a rougher surface than that due to distilled water.

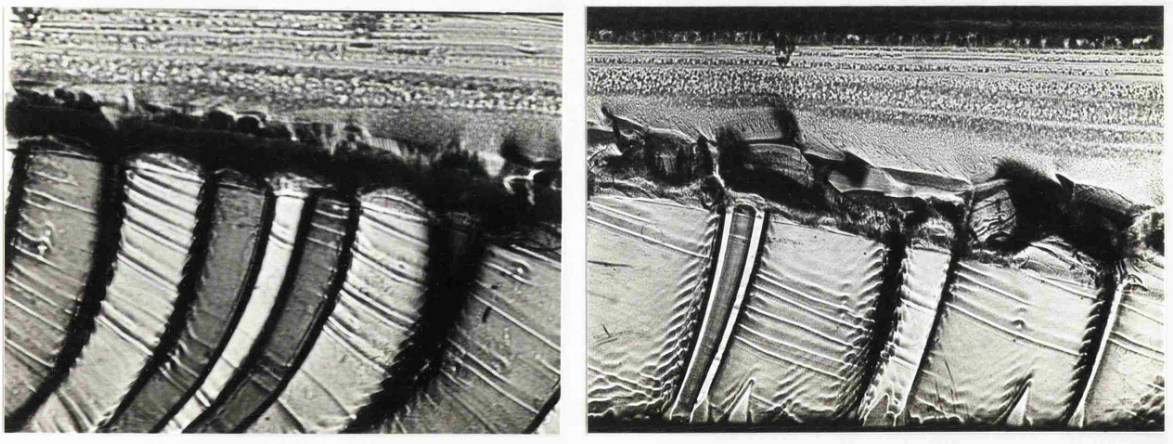

(a) (b)

Figure 11.9 Crack arrest zone.

(a) As in water test.
(b) As in methanol test.

CONCLUSION

Investigation into the environmental fracture of PMMA under the influence of constant cross-head speed conditions was primarily performed in the presence of methanol.

The experimental results have shown that Outwater PMMA specimens which exhibit stable crack propagation in dry conditions have developed unstable crack behaviour when they are coated with grease and immersed in the methanol. Grease coating applied to prevent surface crazing provided control flow conditions for these experiments where the liquid has access only through the fracture surface.

The observed unstable failure comprised of a sequence of crack jumps, each with initiation and arrest event. For these jumps it is found that:

(a) The stress intensity value required to initiate the crack K_i is greater than K_c (stress intensity for stable crack propagation).

(b) The rapidly moving crack decelerates to a steady state condition and arrest at a stress intensity value K_a comparable with K_c.

The determination of K/v relationship in an event of a jump together with a fractographic study provided an explanation to the various stages of stick-slip propagation. The results have shown that crack initiation at high K in methanol is due to a crazed zone in the

vicinity of the crack tip. Crack jumping involves breaking out of this blunted region into the dry material driven rapidly by the released stored elastic energy and reaches a maximum speed of about 24 m/sec. With the exhaustion of strain energy the crack decelerates not to rest, but to conditions of steady growth, with the energy being provided for by the machine cross-head. The duration of steady growth, identified with characteristic rib marks on the fracture surface, indicates the delayed arrival of the environment which is left behind during the jump. In an event of the environment catching up with the advancing crack, growth ceases and additional strain energy is supplied to cause further cracking.

In establishing whether this stick-slip mechanism applies to the presence of other liquids, tests are performed in distilled water. The tests results have shown similarity in the fracture behaviour to that of methanol, however variable, such as the condition of the starter crack seems to influence the water results. Also under identical conditions, crack arrest is rapid for the less viscous and more mobile liquid, i.e. methanol. K_i values are also higher for methanol tests reflecting on the size of the crazed zone.

In summing up, the author believes that in addition to the study of environmental fracture of PMMA, this investigation has provided the outlines and procedures to be taken in future work for similar systems. These systems may include other polymers in other environments, or even cases where the unstable behaviour is common

in materials in dry conditions, such as epoxies and polyesters. The purpose of the exercise as shown in PMMA, is to obtain a further understanding into the fracture behaviour of these materials and the environmental effects when they are applied.

APPENDIX 1

Outwater test piece analysis :

The Outwater-Jerry double torsion fracture specimen is illustrated in figure A-1.

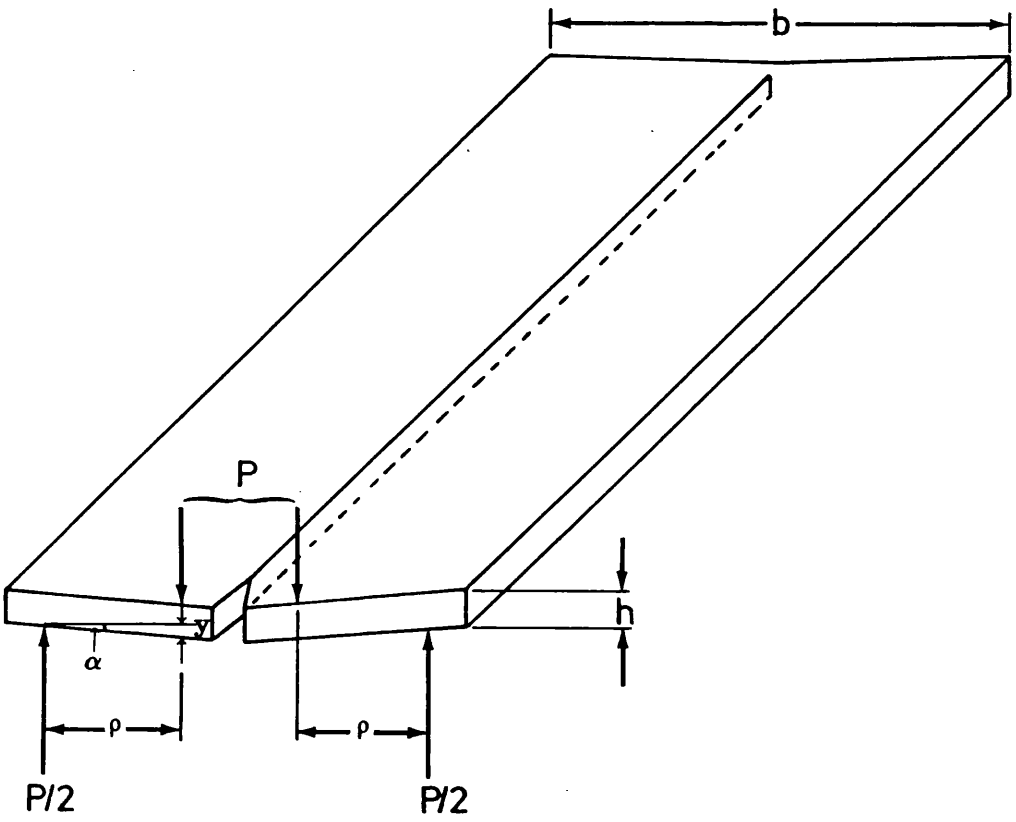

Figure A-1 Outwater double torsion specimen.

where α = angle of twist

ρ = moment arm

b = width of specimen

h = thickness of specimen

y = load point deflection

P = applied load

From basic analysis of a bar of non-circular uniform section under pure torsion, the following relations are obtained (67).

$$\alpha = \frac{Ma}{K'G^*} \qquad \text{(A-1)}$$

$$M = \frac{P\rho}{2} \qquad \text{(A-2)}$$

$$\text{and} \quad K' = \frac{bh^3}{32}\left[\left(\frac{16}{3}\right) - 6.72\left(\frac{h}{b}\right)\left[1 - \left(\frac{4h^4}{3b^4}\right)\right]\right] \qquad \text{(A-3)}$$

where M = the twisting moment resulting from load $\frac{P}{2}$ acting on half the specimen at a length ρ.

K' = a factor dependent on the form and dimensions of the cross-section.

a = crack length.

G^* = shear modulus.

Since for the usual specimen dimensions the second term in the parentheses of equation (A-3) is relatively insignificant, it will be dropped giving

$$K' = \frac{bh^3}{6} \qquad \text{(A-4)}$$

Using the small-angle relation

$$\alpha = \sin\alpha = \tan\alpha \qquad \text{(A-5)}$$

and substituting the value of M and K' from equations (A-2) and (A-4) in equation (A-1), the value of α can be given as

$$\alpha = \frac{y}{\rho} = \frac{3P\rho a}{bh^3G^*} \qquad \text{(A-6)}$$

which in turn yields

$$y = \frac{3P\rho^2 a}{bh^3G^*} \qquad \text{(A-7)}$$

By definition the compliance $C = \frac{y}{P}$ (A-8)

$$\text{Then } C = \frac{3P\rho^2 a}{bh^3G^*} \times \frac{1}{P} = \frac{3\rho^2 a}{bh^3G^*} \qquad \text{(A-9)}$$

$$\text{and } \frac{dC}{da} = \frac{3\rho^2}{bh^3G^*} \qquad \text{(A-10)}$$

Using the fracture toughness relation of Irwin, Kies and Smith (93)

$$G = \frac{P^2}{2b_c}\frac{dC}{da} \qquad \text{(A-11)}$$

$$\text{and } K_c^2 = GE = \left(\frac{P^2}{2b_c}\right)\left(E\,\frac{dC}{da}\right) \qquad \text{(A-12)}$$

where b_c = crack width i.e. specimen thickness minus notch depth if grooving is provided for the crack to follow.

G = The energy/unit fracture area required for crack growth.

E = Young's modulus of material.

K_c = Stress intensity factor for stable growth.

By substituting the value of $\frac{dC}{da}$ from equation (A-10) in equation (A-11) the following relation is obtained

$$G = \frac{P^2}{2b_c} \frac{3\rho^2}{bh^3G^*} = \frac{3}{2} \frac{P^2\rho^2}{b_c bh^3G^*} \qquad \text{(A-13)}$$

In turn the value of G from equation (A-13) is substituted in equation (A-12) yields

$$K_c = P\sqrt{\frac{3}{2}\frac{E}{b_c}\rho^2 \frac{1}{bh^3G^*}} \qquad \text{(A-14)}$$

but the shear modulus $G^* = \frac{E}{2(1+\nu)}$ (A-15)

where ν = Poisson's ratio

Hence substituting the value of G^* in equation (A-14) gives

$$K_c = P \sqrt{\frac{3}{2} \frac{E}{b_c} \rho^2 \frac{2(1+\nu)}{bh^3 E}}$$

$$K_c = P \sqrt{\frac{3}{b_c} \frac{(1+\nu)\,\rho^2}{h^3 b}} \qquad \text{(A-16)}$$

APPENDIX 2

Crack front profile and crack velocity correction factor :

During crack propagation in the double torsion test piece, the crack front profile is of a parabolic shape as shown in figure A-2.

At various stages during propagation the crack extends further along the lower face than the upper face, as a result the crack front velocity taken at midway is usually smaller than the measured crack tip speed.

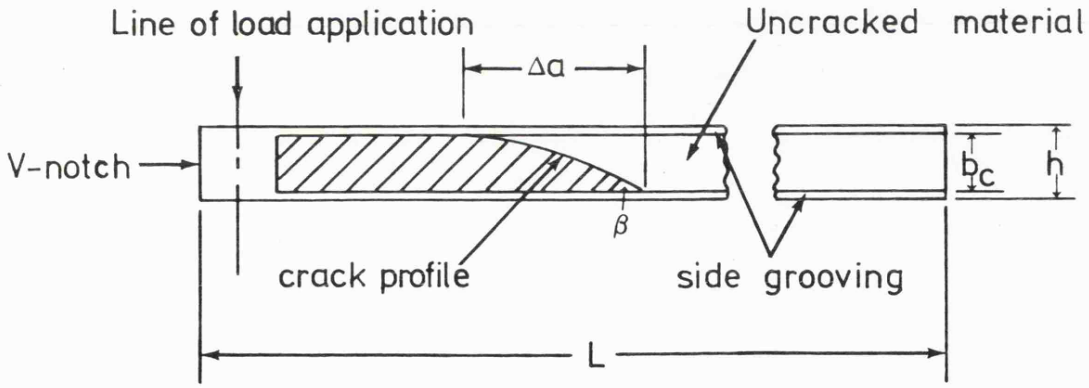

Figure A-2 The crack front in a double torsion test specimen.

A. G. Evans (64) has shown that a correction factor can be determined from Δa and b_c (refer to figure A-2), where Δa is the difference between the crack length measured along the top and bottom faces of the double torsion specimen and b_c is the width of the crack.

The factor which is usually given the symbol ϕ is known as the crack velocity correction factor and its value is equal to sin β. β is the angle between the specimen length and the tangent at the midpoint of the crack front.

Therefore $$\phi = \sin\beta = \frac{b_c}{(\Delta a^2 + b_c^2)^{\frac{1}{2}}} \qquad \text{(A-17)}$$

Hence the velocity of the crack front is not given directly by $\frac{da}{dt}$ as assumed in the analysis of section 4.3, but it is smaller by an amount determined by ϕ. Therefore the truecrack velocity can be expressed as

$$v = \phi \frac{da}{dt} \qquad \text{(A-18)}$$

$\frac{da}{dt}$ = crack tip speed

ϕ = correction factor = $\frac{b_c}{(\Delta a^2 + b_c^2)^{\frac{1}{2}}}$

i.e. Observations of the crack profile is required to obtain accurate velocity data.

In the present work for PMMA specimens

Δa = 20 mm

b_c = 4 mm

$\therefore$ $\phi \approx 0.2$

APPENDIX 3

The load time behaviour during a crack jump was expressed as a polynomial which interpolates points on the P vs t curve.

The procedure is based on the Chebyshev series (47) where the general form is given as

$$\frac{1}{2} A(1)\ To(X) + A(2)\ T_1(X) + A(3)\ T_2(X) + \text{-----} A(n+1)\ T_n(X) \quad \text{(A-19)}$$

A(1), A(2), ----- A(n+1) are coefficients and To(X), $T_1(X)$, ----- $T_n(X)$ denotes the Chebyshev polynomials defined by the relation

$$T_n(X) = \cos\ (n \text{ arc cos } X) \quad \text{(A-20)}$$

and the common form is given as

$$T_{n+1}(X) = 2X\ T_n(X) - T_{n-1}(X) \quad \text{(A-21)}$$

Since $To(X) = 1$

and $T_1(X) = X$ from equation (A-20)

Then all $T_n(X)$ can be computed from equation (A-21), and the first polynomials are:

$$To(X) = 1$$

$$T_1(X) = X$$

$$T_2(X) = 2X^2-1$$

$$T_3(X) = 4X^3-3X$$

$$T_4(X) = 8X^4-8X^2+1$$

$$T_5(X) = 16X^5-20X^3+5X$$

The coefficient terms in the Chebyshev series were evaluated using a NAG (numerical algorithemic group) library routine program.

The routine requirements are X and Y values at the cosine points. The X values are determined by the expression:

$$X(R) = \frac{1}{2}\left[X_{max} - X_{min}\right]\left[\cos\frac{\pi(R-1)}{n}\right] + \frac{1}{2}\left(X_{max} - X_{min}\right) \qquad \text{(A-22)}$$

$$(R = 1, 2, 3, \text{----}, n + 1)$$

where X_{max} and X_{min} are respectively the upper and lower ends of the range of X to be interpolated and n is an arbitary number.

The required Y points are obtained from the curve (see figure A-3).

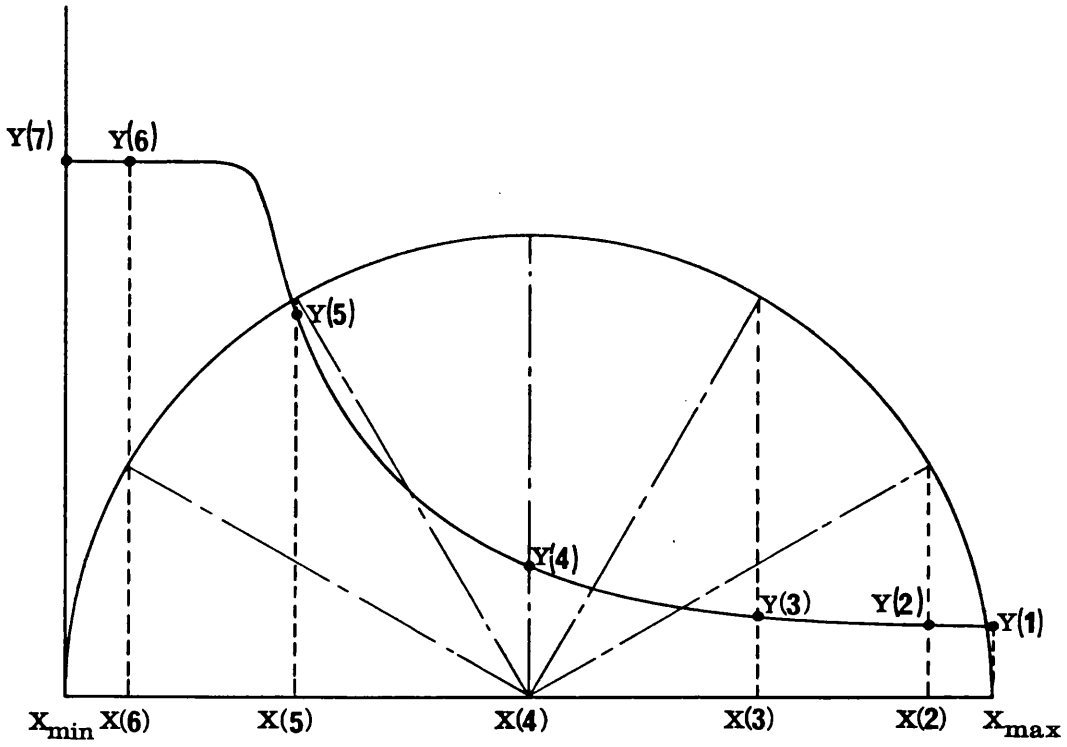

Figure A-3 Determination of Y values at the X cosine points for n=6.

On the evaluation of the coefficients, the program is then designed to evaluate the product of the coefficients with their corresponding polynomials equation (A-19), and to add all the terms to produce a continuous polynomial of the form:

$$B_o + B_1X + B_2X^2 + \text{-----} B_nX^n$$

where B_o, B_1, B_2, ----- , B_n are constants.

REFERENCES

1. ASTM Designation D883 - 62T.

2. DE COSTE, J. B.; MALM, F. S.; and WALLDER, V. T. - Ind. Eng. Chem., 43, 117, (1951).

3. OUGHTON, C. D. - Glass Ind., 26, 72, (1945).

4. HOWARD, J. B. : "Stress cracking (in Thermoplastics)." - Engineering Design for Plastics, (Baer, E.ed.), Reinhold, N. Y. (1964).

5. SPURR, O. K.; and NIEGISCH, W. D. : "Stress crazing of some amorphous thermoplastics." - Journal of Applied Polymer Science, 6, 23, pp. 585 - 599, (1962).

6. SAUER, J. A.; MARIN, J.; and HSIAO, C. C. : "Creep and damping properties of polystyrene." - J. App. Physics, vol. 20, pp. 507 - 517, (1949).

7. WARBURTON HALL, H.; and RUSSELL, E. W. : "PMMA: Crazing, thermal and mechanical properties." - A.R.C. Tech. Report., R. & M. No. 2764, (1953).

8. MAXWELL, B.; and RAHM, L. F. - Ind. Eng. Chem. 41, 1988, (1949).

9. NIELSEN, L. E. : "The apparent domain structure of Polystyrene as revealed by liquid vapour crazing." - Journal of Applied Polymer Science, 1, p. 24, (1959).

10. BERNIER, G. A.; AND KAMBOUR, R. P. : "The role of organic agents in the stress crazing and cracking of Poly (2, 6 - dimethyl - 1, 4 - phenylene oxide)." - Macromolecules, 1, 5, pp. 393 - 400, (1968).

11. ANDREWS, E. H.; and BEVAN, L. : "Fracture mechanics approach to corrosion stress cracking in glassy plastics." - Physical Basis of Yield and Fracture Conference, pp. 209 - 213, Oxford (1966).

12. KELLY, A. : "Strong solids", Clarendon press Oxford, 1966.

13. GRIFFITH, A. A. : "The phenomena of rupture and flow in solids." - Phil. Trans. Roy. Soc., A 221, 163, (1920).

14. BERRY, J. P. : "The surface energy of PMMA." - J. Pol. Sci., 50, 107, (1961).

15. BERRY, J. P. : "The tensile strength of Polystyrene." - J. Pol. Sci., 50, 313, (1961).

16. OROWAN, E. : "Energy criteria of fracture." - Welding J. Res. Suppl., 34, pp. 157 - 160, (1955).

17. IRWIN, G. R. : "Fracture dynamics in fracturing of metals." - ASMS, Cleveland (1948).

18. OROWAN, E. : "Fracture and strength of solids." - Rep. Prog. Phys., 12, 185, (1949).

19. IRWIN, G. R. : "Analysis of stress and strain near the end of a crack traversing a plate." - J. App. Mech., 24, p. 361, (1957).

20. IRWIN, G. R.; and KIES, J. A. : "Fracture and fracture dynamics." - Welding J. Res. Suppl., 17, 95 S, (1952).

21. IRWIN, G. R.: and KIES, J. A. _ "Critical energy rate analysis of fracture strength." - Welding J. Res. Suppl., 33, 4, pp. 193 - 198, April (1954).

22. DAY, E. E. : "Strain energy release rate determination for some perforated structural members." - Welding, J. Res. Suppl., 21, 60s, (1956).

23. SRAWLEY, J. E.; JONES, M. H.; and GROSS, B. : "Experimental determination of the dependence of crack extension force on crack length for a single-edge notch tension specimen." - NASA, TND - 2396, (1964).

24. WESTERGAARD, H. M. : "Bearing pressures and cracks." - J. Appl. Mech., 61, A 49 - A 53, (1939).

25. KNOTT, J. F.; and ELLIOT, D. : "Worked examples in fracture mechanics." - The Institution of Metallurgists, Monograph No. 4, (1979).

26. PARIS, P. C.; and SIH, G. : "Stress analysis of cracks." - A.S.T.M., S.T.P. 381, (1965).

27. BROWN, H. F.; and SRAWLEY, J. E. : "Fracture toughness testing." ; A.S.T.M., S.T.P. 410, (1966).

28. OBREIMOFF, J. W. : "The splitting strength of Mica." - Proc. Roy. Soc. A., Vol. 127, p. 290, (1930).

29. BENBOW, J. J.; and ROESLER, F. C. : "Experiments on controlled fractures." - Proc. Phys. Soc. B.70, pp. 201 - 211, (1957).

30. BROUTMAN, L. J.; and Mc GARRY, F. J. : "Fracture surface work measurements on glassy polymers by a cleavage technique I. Effects of temperature." - Journal of Applied Polymer Science, vol. 9, pp. 589 - 608, (1965).

31. YOUNG, R. J.; and BEAUMONT, P. W. R. : "Crack propagation and arrest in epoxy resins." - Journal of Materials Science, 11, p. 776, (1976).

32. YAMINI, S.; and YOUNG, R. J. : "Stability of crack propagation in epoxy resins." - Polymer, vol. 18, pp. 1075 - 1080, (1977).

33. PHILLIPS, D. C.; SCOTT, J. M.; and JONES, M. : "Crack propagation in an amine-cured epoxide resin." - Journal of Materials Science, vol. 13, p. 311, (1978).

34. YAMINI, S.; and YOUNG, R. J. : "Crack propagation in and fractography of epoxy resins." - J. of Materials Science, vol. 14, pp. 1609 - 1618, (1979).

35. GLEDHILL, R. A.; KINLOCH, A. J.; YAMINI, S.; and YOUNG, R. J. : "Relationship between mecahnical properties of and crack propagation in epoxy resin adhesives." - Polymer, vol. 19, p. 574, (1978).

36. YOUNG, R. J. : "Fracture of thermosetting resins." - p. 183 - Developments in Polymer Fracture - 1, Book edited by ANDREWS, E. H..

37. MARSHALL, G. P.; CULVER, L. E.; and WILLIAMS, J. G. : "Crack and craze propagation in polymers - a fracture mechanics approach, 1 - Crack growth in PMMA in air." - Plastics and Polymers, 37, pp. 75 - 81, (1969).

38. WILLIAMS, J. G.; RADON, J. C.; and TURNER, C. E. : "Designing against fracture in brittle plastics." - Polymer Engineering and Science, pp. 130-141, (1968).

39. BEAUMONT, P. W. R.; and YOUNG, R. J. : "Failure of brittle polymers by slow crack growth - Part 1 Crack propagation in PMMA and time-to-failure predictions." - Journal of Materials Science, 10, pp. 1334 - 1342, (1975).

40. MAI, Y. W. : "On the environmental fracture of PMMA." - Journal of Materials Science, vol. 10, pp. 943 - 954, (1975).

41. MAI, Y. W.; and ATKINS, A. G. : "On the velocity-dependent fracture toughness of epoxy resins." - Journal of Materials Science, vol. 10, p. 2000, (1975).

42. MAI, Y. W.; ATKINS, A. G.; and CADDELL, R. M. : "On the stability of cracking in tapered DCB testpieces." - Int. J. of Fracture, vol. 11, p. 939, (1975).

43. MARSHALL, G. P.; and WILLIAMS, J. G. : "The correlation of fracture data for PMMA." - Journal of Materials Science, vol. 8, pp. 138 - 140, (1973).

44. GREEN, A. : "The fracture of PMMA." - Ph.D. Thesis, Imperial College (London), (1971).

45. COTTERELL, B. : "Velocity effects in fracture propagation." - Appl. Mtls. Res., 4, p. 227, Oct. (1965).

46. STUART, H. A.; MARKOWSKI, G.; and JASCHKE, D. - Kinstoffe, 54, pp. 618 - 625, (1964).

47. FRÖBERG, CARL-ERIK. : "Introduction to Numerical Analysis." - Addison - Wesley Publishing Company, Inc. p. 290.

48. MARSHALL, G. P.; CULVER, L. E.; and WILLIAMS, J. G. : "Craze growth in PMMA : A fracture mechanics approach." - Proc. Roy. Soc. London A, 319, pp. 165 - 187, (1970).

49. KRAMER, E. J.; and BUBECK, R. A. : "Growth kinetics of solvent crazes in glassy polymers." - Journal of Polymer Science, Polymer Physics Edition, vol. 16, pp. 1195 - 1217, (1978).

50. ANDREWS, E. H.; and LEVY, G. M. : "Solvent stress crazing in PMMA. 1 - Geometrical effects." - Polymer, vol. 15, pp. 599 - 607, (1974).

51. WILLIAMS, J. G.; and MARSHALL, G. P. : "Environmental crack and craze growth phenomena in polymers." - Proc. Roy. Soc. London A, 342, pp. 55 - 77, (1975).

52. NICOLE VERHEULPEN-HEYMANS; and BAUWENS, J. C. : "Effect of stress and temperature on dry craze growth kinetics during low-stress creep of polycarbonate." - Journal of Materials Science, vol. 11, pp. 7 - 16, (1976).

53. KAMBOUR, R. P. : "A review of crazing and fracture in thermoplastics." - J. Polymer Science, Macromolecular reviews, vol. 7, p. 1, (1973).

54. GRAHAM, I. D.; WILLIAMS, J. G.; and ZICHY, E. L. : "Craze kinetics for PMMA in liquids." - Polymer, vol. 17, p. 439, (1976).

55. DUGDALE, D. S. : "Yielding of steel sheets containing slits." - J. Mech. Phys. Solids, 8, pp. 100 - 104, (1960).

56. ANDREWS, E. H.; and BEVAN, L. : "Mechanics and mechanism of environmental crazing in a polymeric glass." - Polymer, vol. 13, pp. 337 - 346, (1972).

57. KRAMER, E. J.; HEIDER, G. K.; and DIETER, G. : "Growth criteria for solvent crazes." - Journal of Materials Science, 13, pp. 1093 - 1098, (1978).

58. BORDUAS, H. F.; CULVER, L. E.; and BURNS, D. J. : "Fracture mechanics analysis of fatigue crack propagation in PMMA." _ J. Strain Anal., vol. 3, No. 3, (1968).

59. TADA, H.; PARIS, P.; and IRWIN, G. : "The stress analysis of cracks handbook." - Del. Research Corporation, Hellertown, Pennsylvania, (1973).

60. WIEDERHORN, S. M.; and BOLZ, L. H. : "Stress corrosion and static fatigue of glass." - J. of American Ceramic Society, vol. 53, No. 10, pp. 543 - 548, (1970).

61. ATKINS, A. G.; LEE, C. S.; and CADDELL. R. M. : "Time-temperature dependent fracture toughness of PMMA - Part 1." - Journal of Materials Science, vol. 10, pp. 1381 - 1393, (1975).

62. OUTWATER, J. O.; and JERRY, D. J. : "On the fracture energy of glass." - Interim Report, University of Vermont, Burlington, August (1966).

63. KIES, J. A.; and CLARK, A. B. J. : "Fracture propagation rates and times to fail following proof stress in bulk glass." - Proceedings of the Second International Conference on Fracture, Brighton, paper 42, (1969).

64. EVANS, A. G. : "A method for evaluating the time-dependent failure characteristics of brittle materials - and its application to polycrystalline alumina." - J. of Materials Science, 7, pp. 1137 - 1146, (1972).

65. MARSHALL, G. P.; COUTTS, L. H.; and WILLIAMS, J. G. : "Temperature effects in the fracture of PMMA." - J. of Materials Science, vol. 9, pp. 1409 - 1419, (1974).

66. McKINNEY, K. R.; and SMITH, H. L. : "Method of studying subcritical cracking of opaque materials." - J. of American Ceramic Society, vol. 56 (1), pp. 30 - 32, (1973).

67. ROARK, R. J. : "Formulas for stress and strain." - 3rd ed., pp. 171 - 174, McGraw-Hill Book Co., New York (1954).

68. MAI, Y. W.; and LEETE, N. B. : "Discussion of "Effect of environment on stability of cracking in brittle polymers." - J. of Materials Science, vol. 14, pp. 2264 - 2267, (1979).

69. GURNEY, C.; and HUNT, J. : "Quasi-static crack propagation." - Proc. Roy. Soc. London A299, p. 508, (1967).

70. HAKEEM, M. I.; and PHILLIPS, M. G. : "Effect of environment on stability of cracking in brittle polymers." - Journal of Materials Science, 13, pp. 2284 - 2287, (1978).

71. PHILLIPS, D. C.; and SCOTT, J. M. : "Determination of the K,v diagram of epoxide resins." - Journal of Materials Science, vol. 9, pp. 1202 - 1205, (1974).

72. WILLIAMS, J. G. : "Visco-elastic effects on crack growth in PMMA." - Int. J. of Fracture Mechanics, vol. 8, p. 393, (1972).

73. YOUNG, R. J.; and BEAUMONT, P. W. R. : "Time-dependent failure of poly (methylmethacrylate)." - Polymer, vol. 17, pp. 717 - 722, (1976).

74. KOBAYASHI, T. : "Fracture dynamics of variable fracture toughness epoxies." - National Technical Conference, Society of Plastic Engineering, "High performance plastics", 9 - 13, (1976).

75. ATKINS, A. G.; LEE, C. S.; and CADELL, R. M. : "Time-temperature dependent fracture toughness of PMMA." - J. of Materials Science, vol. 10, Part 1 pp. 1381 - 1393, Part 2 pp. 1394 - 1404, (1975).

76. HAKEEM, M. I.; and PHILLIPS, M. G. : "Unstable crack propagation - a fractographic study using PMMA in liquid environments." - J. of Materials Science, vol. 14, pp. 2901 - 2905, (1979).

77. COTTERAL, B. : "Fracture propagation in organic glasses." - Int. J. of Fracture Mechanics, vol. 4, p. 209, (1968).

78. LEDNICKY, F.; and PELZBAUER. : "Morphology of the fracture surface layer of poly (methylmethacrylate) and the fracture mechanism." - J. of Polymer Science, Part C, Polymer Symposia, no. 38, pp. 375 - 386, (1972).

79. WALLNER, H. Z. - Physik, 114, 368, (1939).

80. KERKHOF, F. - Naturwissenschaften, 40, 478, (1953).

81. SCHARDIN, H. - Fracture (ed. B. L. Averbach), p. 298, John Wiley and Sons, Inc., (1959).

82. HIGUCHI, M. - Repts. Res. Inst. Appl. Mech, Kyrushu University, 6, 173, (1958).

83. NEWMAN, S. B.; and WOLOCK, I. - in Adhesion and Cohesion, Elsevier, Amsterdam, p. 218, (1962).

84. ASTM, Acoustic emission, STP 505, (1972).

85. ASTM, Monitoring structural integrity by acoustic emission, STP 571, (1975).

86. EVANS, A. G.; LINZER, M.; and RUSELL, L. R. : "Acoustic emission and crack propagation in polycrystalline alumina." - Materials Science and Engineering, 15, pp. 253 - 261, (1974).

87. EVANS, A. G.; and LINZER, M. : "Failure prediction in structural ceramics using acoustic emission." - J. American Ceramic Society, vol. 56, p. 575, (1973).

88. FUWA, M.; HARRIS, B.; and BUNSELL, A. R. : "Acoustic emission during cyclic loading of carbon-fibre-reinforced plastics." - J. Phys. D : Appl. Phys., 8, pp. 1460 - 1471, (1975).

89. FUWA, M.; BUNSELL, A. R.; and HARRIS, B. : "An evaluation of acoustic emission techniques applied to carbon-fibre composites." - J. Phys. D : Appl. Phys., 9, pp. 353 - 364, (1976).

90. BECHT, J.; SCHWALBE, H. J.; and EISENBLAETTER, J. : "Acoustic emission as an aid for investigating the deformation and fracture of composite materials." - Composites, 7, pp. 245 - 248, (1976).

91. SIMS, G. D.; DEAN, G. D.; READ, B. E.; and WESTERN, B. C. : "Assessment of damage in GRP laminates by stress waves emission and dynamic mechanical measurements." - J. of Materials Science, 12, pp. 2329 - 2342, (1977).

92. MARSHALL, G. P. : "The growth of cracks and crazes in polymers - A fracture mechanics approach." - Ph.D. Thesis, Imperial College (London), (1972).

93. IRWIN, G. R.; KIES, J. A.; and SMITH, H. L. : "Fracture strength relative to onset and arrest of crack propagation." - Amer. Soc. Test. Mater., Proc. 58, pp. 640 - 660, (1958).

94. BERRY, J. P. : "Determination of fracture surface energies by the cleavage technique." - J. App. Phys., 34, 62, (1963).

95. VAN DEN BOOGAART, A. : "Crazing and characterization of fracture in polymers." - Physical Basis of Yield and fracture conference, p. 167, Oxford (1966).

96. Broutman, L. J.; and KOBAYASHI, T. - US Army Materials and Mechanics research centre report, AMMRC CR 71 - 14.

97. DAVIDGE, R. W.; and TAPPIN, G. : "The effective surface energy of brittle materials." - J. of Materials Science, 3, 165, (1968).

98. OLEAR, P. D.; and ERDOGAN, F. : "Time-temperature dependent brittle fracture of viscoelastic solids." - J. Appl. Pol. Sci., vol. 12, pp. 2563 - 2574, (1968).

99. KEY, P. L.; KATZ, Y.; and PARKER, E. R. : "Application of fracture mechanics to glassy plastics." - Sci. Tech. & Aero Rept., (N68 - 29464), p. 2904 - NASA (UCRL - 17911) (1968).

100. KIES, J. A. : "Aircraft glazing materials - A method for evaluating the shatter resistance of Aircraft Canopy Materials." - N. R. L. Memorandum Report No. 237. (1953).

101. SVENSSON, N. L. : "The variation of the fracture energy of brittle plastics with temperature." - Proc. Phys. Soc., 77, p. 876, (1961).

102. VINCENT, P. I.; and GOTHAM, K. V. : "Effect of crack propagation velocity on the fracture surface energy of PMMA." - Nature, 210, p. 1254, (1966).

103. FUJISHIRO, I.; MII, H.; and KATO, S. : "Fracture energy of PMMA." - Chem. Abs., 74, 32234, (1971).

104. HIGUCHI, M. : "Strain rate dependent breaking strength of PMMA." - Proc. 1st Int. Conference on Fracture, Sendai, JAPAN, p. 1211, (1965).

105. BENBOW, J. J. : "Stable crack growth in plastics." - Proc. Phys. Soc., 78, p. 970, (1961).